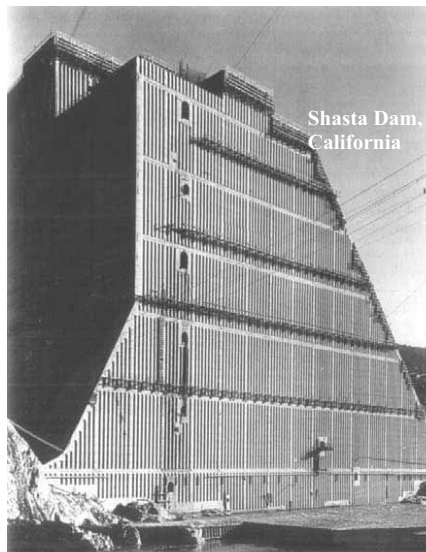
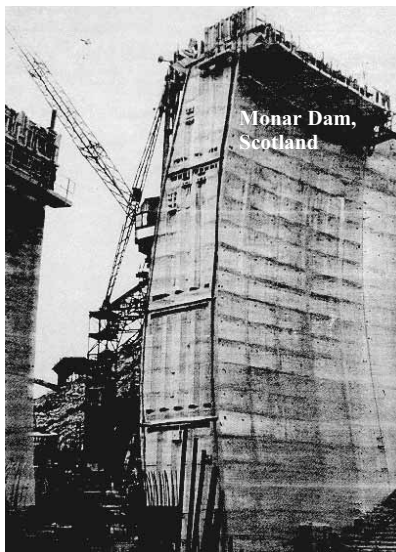


RECLAMATION

Managing Water in the West

Report DSO-07-05

Shear Key Research Project Literature Review and Finite Element Analysis



Dam Safety Technology Development Program



U.S. Department of the Interior
Bureau of Reclamation
Technical Service Center
Denver, Colorado

December 2007

REPORT DOCUMENTATION PAGE

*Form Approved
OMB No. 0704-0188*

The public reporting burden for this collection of information is estimated to average 1 hour per response, including the time for reviewing instructions, searching existing data sources, gathering and maintaining the data needed, and completing and reviewing the collection of information. Send comments regarding this burden estimate or any other aspect of this collection of information, including suggestions for reducing the burden, to Department of Defense, Washington Headquarters Services, Directorate for Information Operations and Reports (0704-0188), 1215 Jefferson Davis Highway, Suite 1204, Arlington, VA 22202-4302. Respondents should be aware that notwithstanding any other provision of law, no person shall be subject to any penalty for failing to comply with a collection of information if it does not display a currently valid OMB control number.

PLEASE DO NOT RETURN YOUR FORM TO THE ABOVE ADDRESS.


1. REPORT DATE (DD-MM-YYYY) 12-2007		2. REPORT TYPE		3. DATES COVERED (From - To)	
4. TITLE AND SUBTITLE Shear Key Research Project—Literature Review and Finite Element Analysis				5a. CONTRACT NUMBER	
				5b. GRANT NUMBER	
				5c. PROGRAM ELEMENT NUMBER	
6. AUTHOR(S) Guerra, Andres				5d. PROJECT NUMBER	
				5e. TASK NUMBER	
				5f. WORK UNIT NUMBER	
7. PERFORMING ORGANIZATION NAME(S) AND ADDRESS(ES) Bureau of Reclamation Technical Service Center Structural Analysis Group Denver, Colorado				8. PERFORMING ORGANIZATION REPORT NUMBER DSO-07-05	
9. SPONSORING/MONITORING AGENCY NAME(S) AND ADDRESS(ES) Bureau of Reclamation Denver, Colorado				10. SPONSOR/MONITOR'S ACRONYM(S)	
				11. SPONSOR/MONITOR'S REPORT NUMBER(S) DSO-07-05	
12. DISTRIBUTION/AVAILABILITY STATEMENT National Technical Information Service, 5285 Port Royal Road, Springfield, VA 22161					
13. SUPPLEMENTARY NOTES					
14. ABSTRACT					
15. SUBJECT TERMS					
16. SECURITY CLASSIFICATION OF:			17. LIMITATION OF ABSTRACT SAR	18. NUMBER OF PAGES	19a. NAME OF RESPONSIBLE PERSON
a. REPORT UL	b. ABSTRACT UL	a. THIS PAGE UL			19b. TELEPHONE NUMBER (Include area code)

BUREAU OF RECLAMATION
Technical Service Center, Denver, Colorado
Structural Analysis Group, 86-68110

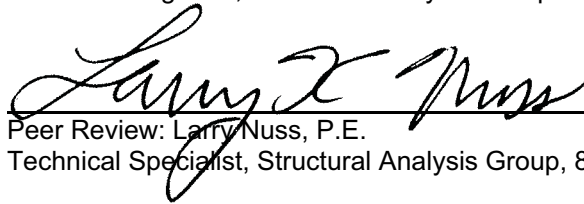
Report DSO-07-05

Shear Key Research Project Literature Review and Finite Element Analysis

Dam Safety Technology Development Program
Denver, Colorado



Prepared: Andres Guerra
Structural Engineer, Structural Analysis Group 86-68110



Peer Review: Larry Nuss, P.E.
Technical Specialist, Structural Analysis Group, 86-68110

9/5/2007
Date

REVISIONS					
Date	Description	Prepared	Checked	Technical Approval	Peer Review

Mission Statements

The mission of the Department of the Interior is to protect and provide access to our Nation's natural and cultural heritage and honor our trust responsibilities to Indian Tribes and our commitments to island communities.

The mission of the Bureau of Reclamation is to manage, develop, and protect water and related resources in an environmentally and economically sound manner in the interest of the American public.

Acknowledgments

This work was supported by Reclamation's Dam Safety Technology Development Program.

Contents

	Page
Acknowledgments.....	iii
Background.....	1
Literature Review.....	3
Strength of Shear Keys	3
Fracture Mechanics Approach for Failure of Concrete Shear Keys	3
Rock Mechanics for Potential Shear Failure Surfaces.....	6
Models that Explore the Effect of Contraction Joint Opening on the Dynamic Response of Arch Dams.....	7
Models Aimed at Capturing the Effects of Shear-Keyed Contraction Joints ...	8
Lau, Noruziaan, and Razaqpur (1998).....	8
Ahmadi, Izadinia, and Bachmann (2001)	9
Tzenkov and Lau (2002).....	10
Toyoda, Ueda, and Shiojiri (2002)	11
Lawrence Livermore National Laboratory Studies on Morrow Point Dam.....	12
Literature Review Conclusion	13
Finite Element Study.....	14
Material Properties.....	15
Contact Surfaces and Boundary Condition.....	16
Loading Conditions.....	16
Results.....	17
Analysis I—Sliding Initiation.....	17
Analysis II—Closed Joint	19
Analysis III—Partially Open Joint.....	20
Analysis IV—Degraded Material Property	21
Finite Element Study Conclusion	22
Method to Compare Known and Implemented Contraction Joint Behavior	23
Implementation of the Proposed Method.....	25
Contraction Joint Displacement Data	26
Contraction Joint Stress Data.....	27
Conclusion	30
References.....	31
Figures.....	33

Tables

No.	Page
1	Material properties for concrete in shear key study..... 16

Figures

No.	Page
1	Typical contraction joint shear key dimensions..... 35
2	Cracking sequence (after Bakhoun [1991]) (Kaneko <i>et al.</i> , 1993)..... 35
3	Shear-off fracture sequence (Kaneko <i>et al.</i> , 1993). 36
4	Band width (Kaneko <i>et al.</i> , 1993)..... 36
5	Shear vs. normal stress for plain concrete shear key based on equations from Kaneko <i>et al.</i> , 1993. 37
6	Shear stress vs. shear slip displacements from Kaneko <i>et al.</i> , 1993..... 38
7	Rock mechanics—undulating joint..... 39
8	Shear vs. normal stress in undulating rock joints. 39
9	Finite element mesh of Big Tujunga Dam (Fenves <i>et al.</i> , 1992)..... 40
10	Constitutive relations of nonlinear joint element (Lau <i>et al.</i> , 1998)..... 40
11	Relation between stresses and normal or tangential displacements (Ahmadi <i>et al.</i> , 2001). 41
12	Cracking and crushing in Morrow Point Dam (Tzenkov and Lau, 2002). ... 42
13	Effect of reservoir water level (Toyoda <i>et al.</i> , 2002)..... 42
14	Sinusoidal contraction joint from Noble and Solberg (2004)..... 43
15	Transverse displacements vs. upstream/downstream displacements (Noble and Solberg, 2004)..... 43
16	FEM model with loads and boundary conditions. 44
17	Contact surface locations in yellow. 44
18	Morrow Point Dam contraction joints keyways and grouting system. 47
19	Morrow Point Dam galleries general layout..... 48
20	Node locations for y-displacement plot in figure 21. Analysis I. 49
21	Y-displacement for nodes shown in figure 20. Analysis I..... 49
22	Sliding initiation formulation..... 50
23	Plot of shear strengths and sliding initiation..... 51
24	Deformed shape with body load of 15,000 in/s ² at end of 3 seconds. 51
25	Node locations for displacement plots..... 52
26	X-displacements. Analysis II..... 52
27	Y-displacements. Analysis II..... 53
28	Y-stress fringe plot. Analysis II..... 53
29	XY-stress fringe plot. Analysis II..... 54
30	Maximum principal stress fringe plot. Analysis II. 54

31	Regions I through IV for element stress results.....	55
32	Element locations for stress results in region I.	55
33	Y-stress: elements in region I. Analysis II.....	56
34	XY-stress: elements in region I. Analysis II.....	56
35	Maximum principal stress: elements in region I. Analysis II.	57
36	Element locations for stress results in region II.....	57
37	Y-stress: elements in region II. Analysis II.	58
38	XY-stress: elements in region II. Analysis II.....	58
39	Maximum principal stress: elements in region II. Analysis II.....	59
40	Element locations and labels for stress results in region III. Analysis II.....	59
41	Y-stress: elements in region III. Analysis II.	60
42	XY-stress: elements in region III. Analysis II.	60
43	Maximum principal stress: elements in region III. Analysis II.	61
44	Element locations and labels for stress results in region IV.	61
45	Y-stress: elements in region IV. Analysis II.....	62
46	XY-stress: elements in region IV. Analysis II.....	62
47	Maximum principal stress: elements in region IV. Analysis II.	63
48	FEM model, initial condition with-3 inch gap. Analysis III.....	63
49	Deformed shape with body load of 15,000 in/s ² at end of 3 seconds. Analysis III.....	64
50	X-displacements. Analysis III.....	64
51	Y-displacements. Analysis III.....	65
52	Y-stress fringe plot. Analysis III.....	65
53	XY-stress fringe plot for region I elements. Analysis III.	66
54	Maximum principal stress fringe plot. Analysis III.	66
55	Y-stress: elements in region I. Analysis III.	67
56	XY-stress for elements in region I. Analysis III.....	67
57	Element location and labels for XY-stress of partially open joint.....	68
58	XY-stress for elements shown in figure 56. Analysis III.....	68
59	Maximum principal stress for elements shown in figure 56. Analysis III..	69
60	Maximum principal stress for elements in region I. Analysis III.	69
61	Deformed shape with body load of 15,000 in/s ² at end of 3 seconds. Bottom part has degraded material properties (2 million lb/in ² modulus). Analysis IV.	70
62	X-displacements. Analysis IV.	70
63	Y-displacements. Analysis IV.	71
64	Y-stress fringe plot. Analysis IV.	71
65	XY-stress fringe plot. Analysis IV.....	72
66	Maximum principal stress fringe plot. Analysis IV.....	72
67	Y-stress: elements in region I. Analysis IV.	73
68	XY-stress for elements in region I. Analysis IV.....	73
69	Maximum principal stress for elements in region I. Analysis IV.....	74
70	Y-stress for elements in region II. Analysis IV.	74
71	XY-stress for elements in region II. Analysis IV.	75
72	Maximum principal stress for elements in region II. Analysis IV.....	75
73	Nambe Falls Dam dimensional layout.....	77

74 Plan view, Nambe Falls Dam 3-dimesional finite element model..... 79

75a Nambe Falls Dam $\frac{1}{50,000}$ AEP earthquake acceleration time histories and
acceleration response spectra..... 80

76 Plan view at time of large openings in the contraction joints (displacement
magnification factor of 100). 82

77 Plan view of contraction joint circled in figure 76 at time = 0 seconds..... 83

78 Relative x-displacement between adjacent nodes..... 83

79 Relative z-displacement between adjacent nodes..... 84

80 Illustration of radial and tangential components to the left and right of
crown of dam. 84

81 Relative radial displacements between adjacent nodes. 85

82 Relative tangential displacement between adjacent nodes. 85

83 Illustration of element 82080 used for stress time history data. 86

84 X-stress in the joint at element 82080..... 87

85 Z-stress in the joint at element 82080..... 87

86 ZX-stress in the joint at element 82080..... 88

87 Illustration of positive rotation from x-z axes to 1-2 axes..... 88

88 Radial stress in the joint at element 82080. 89

89 Tangential stress in the joint at element 82080..... 89

90 Shear key interaction diagram with time history shear and normal stress
pairs..... 90

91 Close up of shear key interaction diagram with time history shear and
normal stress pairs..... 90

Concrete arch dams are usually constructed of adjacent cantilever sections that are separated by vertical contraction joints. The contraction joints, typically spaced 40 to 50 feet apart, release tensile arch stresses caused by shrinkage and temperature drops in mass concrete that can otherwise create radial cracking. Shear keys in the contraction joints are an important component intended to maintain the arch shape of the dam by resisting upstream/downstream relative displacements between adjacent monoliths through the transfer of shear forces. See figure 1 for typical Bureau of Reclamation contraction joint shear key dimensions.

The objectives of this study are to determine how much strength and resistance the shear keys develop relative to the typically implemented finite element (FE) models of concrete arch dams. This study will give risk teams a more defensible basis when judging if an arch dam maintains its arch action during seismic events that move the dam upstream and open contraction joints. This study will also help risk assessment teams better estimate probabilities of failure for arch dams with and without shear keys.

This report proposes a method that assesses the behavior in the joint to provide further evaluation on the stability of arch dams with and without shear keys. Generically, the proposed method compares the behavior of the typically implemented contraction joint model with known joint behavior and geometry. The known joint behavior is based on past research on shear key failure (Kaneko *et al.*, 1993a, 1993b), sliding in rough, undulating rock surfaces (Hoek and Bray, 1981; Ladanyi and Archambault, 1970), and the behavior of an FE model of typical shear keys that was developed as part of this study. The proposed method provides a means of assessing the effects of contraction joints without changing the current methods utilized or increasing the complexity of the current methods utilized for structural evaluation of concrete arch dams.

Background

The stress distribution in a concrete arch dam is typically described in terms of arch and cantilever actions. The increased stability of an arch dam is provided by the compressive arching action in the horizontal plane that causes loads to transfer into the abutments. The transfer of loads into the abutments reduces the percentage of load carried by cantilevers. While compressive arching action utilizes the high compressive strength of concrete, cantilever actions can create tensile forces that are more likely to damage concrete with tensile strengths approximately $\frac{1}{10}$ or $\frac{1}{20}$ that of the compressive strength.

The amount of load carried by arching action and cantilever action depends on the relative stiffness of the arch, cantilevers, foundation, and abutments. In an indeterminate structure, the stiffer components carry more load and less-stiff components carry less load. During seismic events, the relative resistance provided by the arch and cantilever actions also becomes dependent on the resistance across the contraction joints as arch stiffness is reduced when inertia loads cause upstream displacements and joint opening.

Finite element methods are often used to determine the seismic behavior and response of three-dimensional models of concrete arch dams. The FE models of arch dams, generically, are defined as linear or nonlinear. Linear FE models are often employed foremost because they are more efficiently developed and analyzed. Linear FE models capture the response of a monolithic arch dam (no contraction joints) with elastic material properties. Nonlinear finite element analysis (FEA) is computationally more expensive and is typically utilized when the linear FEA results indicate the need to more accurately determine the behavior of a concrete arch dam. Nonlinear FE models most often include the effects of contraction joints and/or inelastic material properties.

A literature review regarding the effects of contraction joints on the response of concrete arch dams is presented herein. Generically, linear FEA of monolithic and homogeneous concrete arch dams results in different structural responses than FEA with contraction joints that incorporate geometric nonlinearities. Studies (Fenves, Mojtahedi, and Reimer 1992; Lau, Noruziaan, and Razaqpur, 1998; Ahmadi, Izadinia, and Bachmann, 2001; Tzenkov and Lau, 2002; Toyoda, Ueda, and Shiojiri, 2002; Noble and Solberg, 2004) have shown that (1) the fundamental vibration period of the dam lengthens with joint opening, (2) the stresses are redistributed from the arches to the cantilevers with joint opening, and (3) joint openings are typically greater in the upper extents of the dam. The FE models from these studies, which are later presented in detail, demonstrate the progression from FE models that only include joint opening to models that include a relationship between joint openings and shear displacements in the joint. These studies have implemented joint properties using apparent friction angles and apparent cohesions, nonlinear spring elements, and a sinusoidal contact surface that incorporates shear displacements with joint opening. While the implemented joint properties are intended to accurately describe the constitutive properties of a joint, there is little work that aims at comparing differences between the implemented properties and the constitutive joint properties. Rather, past studies compare results from linear and nonlinear models or provide parametric analyses of joint properties. Note that this study does not intend to develop joint constitutive properties for FEA.

An understanding of the overall structural system of a concrete arch dam is crucial to assess and utilize the results from studies. Fundamentally, the addition of contraction joints to an FE model increases the number of degrees of freedom in an indeterminate system. The stiffness of the contraction joint influences not

only the overall response of the dam but also the response in the contraction joint since an indeterminate system distributes stresses based on the relative stiffness of the structural components. For example, an FE model that includes an artificially low stiffness in a contraction joint will result in lower stresses in the contraction joint and higher stresses in other parts of the dam. On the other hand, a contraction joint with an artificially high stiffness will show higher stress in the joint and lower stress in other parts of the dam. Neither structural response would be entirely correct until the relative stiffness of all the structural components is accurately defined.

Rather than developing joint constitutive properties for FEA, this report proposes a method that compares the results from typically implemented contraction joint models with known behaviors in contraction joints. The known joint behaviors are based on studies that explore shear key and joint behavior.

Literature Review

Strength of Shear Keys

Fracture Mechanics Approach for Failure of Concrete Shear Keys

Two articles by Kaneko *et al.* (1993a; 1993b) present the theory and verification of a “Fracture Mechanics Approach for Failure of Concrete Shear Key.” The goal of the first article (1993a) is to develop a simple mathematical model for “the analysis and design of a plain or fiber reinforced concrete shear key joint” (1993a).

The article presents two different cracking mechanisms for shear key joints. An S crack is a single curvilinear crack, and M cracks are diagonal multiple cracks. Figure 2, from the article, illustrates M cracks and S cracks for a typical shear key according to a study by Bakhoun (1991).

The article presents a simple fracture sequence of shear-off failure that further explains the developments of S and M cracks based on experimental and analytical observation. Consider a single rectangular key that is subjected to shear and compressive loading, as in figure 3. In the first stage of loading, tensile stresses resulting from shear stress concentrations at the upper corner of the key cause a short S crack to develop (see figure 3(a)(1)). Development of the S crack induces rotation of the key specimen, which causes M cracks to develop along the base of the key specimen where tensile stresses increase with the rotation of the key specimen (figure 3(a)(2)). With further shear loading, the M crack opening displacements continuously increase. At the point just before failure, the shear key is held in place by compressive struts between the M cracks (figure 3(a)(3)). A reasonable model assumes that no shear stress exists along the base of the key

specimen as the compressive struts between M cracks carry all loads in compression (Kaneko *et al.*, 1993a). Failure of the key specimen occurs when the compressive struts are crushed (figure 3(a)(4)).

Based on the described failure mechanisms and sequences of shear-off failure, various models can be applied to determine the performance of shear keys. Kaneko *et al.* (1993a) implement a linear elastic fracture mechanics (LEFM) formulation for S cracking and a combination of a smeared crack and truss model to formulate M cracking. A wedge crack model (WCM) and a rotating smeared-crack-band model (RSCBM) are employed to predict S crack and M crack formation, respectively. To develop the shear slip-stress displacement behavior of the keyed joint, the two models are combined such that the WCM predicts the initial stages of loading and the RSCBM predicts all stages of loading thereafter. The point of transition between the WCM (S cracks) and the RSCBM (M cracks) is complex to define but is needed to compute the entire load-displacement relationship. Kaneko *et al.* (1993a) applied a simple model to define the point of transition. The transition point does not affect the stress-displacement relation at failure but it does affect the stress-displacement relation during and up to failure. Kaneko and Mihashi (1999) further studied the transition between M and S cracking.

The verification article (Kaneko *et al.*, 1993a) explains: the peak shear strength of a keyed joint is controlled by M cracking and thus can be predicted using the RSCBM. The mathematical characteristics of the RSCBM allow the development of a closed loop design formula for predicting shear strength of keyed joints. Equations (18a) and (18b) of this article predict the shear strength of a shear key for plain concrete:

$$\tau_{\max} = \frac{f'_c - C}{2} \sin 2 \left\{ \cos^{-1} \sqrt{\frac{\sigma_x - C}{f'_c - C}} \right\} (\text{MPa}) \quad (18a)$$

$$C = \frac{f'_c h}{568000 G_f} \left(\frac{1}{3} - 4\sqrt{f'_c} \right) + \frac{\sqrt{f'_c}}{11} (\text{MPa}) \quad (18b)$$

where:

G_f = the specific fracture energy (material property, N/m),

f'_c = the compressive strength of concrete (MPa),

σ_x = the compressive stress normal to the face of the key (MPa)

h = the bandwidth, approximated in the article as the width of the area dominated by M cracks, measured normal to the face of the key (meters) (see figure 4).

Note that this equation is only suitable when there are no normal displacements in the joint and assumes that normal and shear stresses are uniform along the base of

the key. The article also develops an iterative formulation, not defined here, to predict the shear slip displacement.

Figure 5 illustrates the shear key interaction diagram, or relationship between normal and shear stresses, based on equations (18a) and (18b) for fixed values of h , G_f , and f'_c . In reference to determining the bandwidth, the fracture mechanics article states that “. . . preliminary analysis showed that the influence of h on the shear stress-slip relation of the key joints was relatively small for the entire load-displacement history” (Kaneko *et al.*, 1993a). The value of h for the graph in figure 5 is 10 mm.

The specific fracture energy, G_f , of cement-based materials as a function of maximum aggregate size is between 300 N/m and 500 N/m for normal and dam concrete, respectively (Wittmann, 2002). A value of 400 N/m was used for the plot in figure 5. The values of h and G_f had little effect on the results in figure 5, and f'_c varied between 27.5 MPa and 49 MPa.

Figure 5 illustrates that the shear strength, or maximum shear stress, is zero when the normal stress reaches the compressive strength of concrete so the key breaks with very little shear force. The shear strength reaches a peak value of about half the concrete compressive strength when the normal stress is approximately half the concrete compressive strength.

While the fracture mechanics approach predicts that the shear strength tends towards zero for low normal stresses, this is not entirely accurate. Recall that equations (18a) and (18b) predict the peak shear strength of a shear key over a range of normal loads. The peak shear strengths for specimens with 0.69-MPa (100-lb/in²) and 2.07-MPa (300-lb/in²) normal stresses are shown in curves (a) and (b) in figure 6. To reach the peak shear strength requires that the key experiences plastic deformation. For the key to experience plastic deformations, the cohesive capacity along the base of the key must first be overcome. Even a key subjected to zero normal loads will attain the cohesive strength along the base of the key assuming no sliding occurs. Equations (18a) and (18b) do not include the effects of overcoming the cohesive strength of the concrete because the peak shear strength is based on a model that has moved into the region of plastic deformations. In this sense, equations (18a) and (18b) are accurate for shear strengths that are above the cohesive strength of concrete when normal loads approach zero. Cohesive strengths are typically about 10 percent of the concrete compressive strength. The plot in figure 5 implements this idea by maintaining that the shear strength is above 10 percent of the compressive strength of concrete when normal loads approach zero.

After developing the previously discussed theory, the same authors published a companion paper (Kaneko, *et al.*, 1993b) to verify the model for the failure of plain concrete shear keys. This article illustrates good agreement between the theoretical model results, experimental results, and nonlinear FEA results when

comparing the entire load-displacement relations and the maximum shear stress, or shear strength, of shear keys. Figure 6 illustrates the shear slip displacement versus shear stress results for laboratory experiments and for the proposed model. Experiments were carried out on individual shear key specimens with a normal prestress of 0.69 MPa (figure 6(a)) and 2.07 MPa (figure 6(b)), which is said to remain constant during experiments. The peak shear stress for the proposed model seen in figure 6 corresponds to the maximum shear stress as calculated with equation 18(a). The peak shear stresses for the proposed model are about 7.5 Mpa and 11 Mpa for normal loads of 0.69 MPa and 2.07 Mpa, respectively. The shear key implemented for finite element analysis and experiments has an asperity of $1\frac{1}{4}$ inches, a base width of $3\frac{7}{8}$ inches, and an inclination angle of 59 degrees. With this inclination angle, a friction angle of 31 degrees or less is needed to have sliding. Thus, it was not necessary to resist normal displacements during the experiments because the friction angle in concrete is typically above 31 degrees.

Additionally, the curves from the experiment test results (figure 6) indicate how friction and cohesion forces interact during loading of a shear key. The amount of residual shear stress after the specimen breaks correlates to the amount of normal loading on the specimen. In figure 6(a), there is between 1 MPa and 2 Mpa for the lower and upper limits, respectively, at a slip displacement of 2 mm. In figure 6(b), the shear stress at a slip displacement of 2 mm is approximately three times that seen in figure 6(a). This corresponds to the relative values of the normal stresses applied during the experiments, which are three times greater for the experiment results shown in figure 6(b) than those shown in figure 6(a). Since the residual stress is affected by the amount of normal loading, it is concluded that frictional forces control the shear strength in the joint after failure.

Theoretical models, experimental tests, and FEA for fiber-reinforced concrete shear keys are also presented in reference (Kaneko *et al.*, 1993b) but not discussed here.

Rock Mechanics for Potential Shear Failure Surfaces

A study on the shear strength of potential failure surfaces in rock masses can be related to the behavior of shear-keyed contraction joints in arch dams. Shear-keyed contraction joints are similar to potential failure surfaces in rock masses because they are both subjected to normal (compressive only) and shear loading. Additionally, potential failure surfaces in rock can have undulating geometries very similar to geometries of beveled keyed joints in arch dams. The main difference between contraction joints in arch dams and potential failure surfaces in rock masses is that shear keys have a large base width and key height, while rock surfaces usually have many small asperities. Additionally, contraction joints follow a specific undulating pattern while potential failure surfaces in rock masses follow a less specific pattern. However, rock mechanics approaches to determine the shear strength of potential failure surfaces are based on simplifications that reduce a complex failure surface to one that follows a predictable behavior, which is much easier for producing mathematical relationships.

A book by Hoek and Bray (1981) presents work done by Ladanyi and Archambault (1970) on the shear and normal stress relationships for an undulating rock joint as shown in figure 7 with inclination angle, i , normal stress, σ , and shear stress, τ . This interlocking geometry is very similar to that of beveled shear keys. A very important aspect of the shearing behavior of the plane shown in figure 7 is that tangential displacement can cause normal displacement in the joint.

The magnitude of the normal stress has a large influence on the shear behavior of a potential failure plane in rock as it influences normal displacements. The study shows that under lower magnitude normal loading conditions shear displacements cause normal displacements. As the normal loads become higher, normal displacements do not occur, and the shear capacity becomes that of the intact rock. Note that this has been observed in the Reclamation laboratories where shear tests with less than 25 lb/in² normal stress ride up over asperities and tests with normal stress less than 25 lb/in² shear through asperities. Figure 8 illustrates Ladanyi and Archambault's (1970) equation that accounts for the transition between dilation (normal displacements) and shearing modes for i of 20 degrees and friction angle, ϕ , of 30 degrees. Note that the initial relationship between σ and τ is defined by the sum of the inclination angle and friction angle.

Ladanyi and Archambault's (1970) equation is:

$$\frac{\tau}{\sigma_j} = \frac{\frac{\sigma}{\sigma_j} \left(1 - \frac{\sigma}{\sigma_j}\right)^{1.5} \left[\left(1 - \frac{\sigma}{\sigma_j}\right)^4 \tan i + \tan \phi\right] + 0.232 \left[1 - \left(1 - \frac{\sigma}{\sigma_j}\right)^{1.5}\right] \left(1 + 10 \frac{\sigma}{\sigma_j}\right)^{0.5}}{1 - \left[\left(1 - \frac{\sigma}{\sigma_j}\right)^{5.5} \tan i \tan \phi\right]}$$

In regards to shear-keyed contraction joints in arch dams, the rock mechanics study provides that shear displacements under lower normal loading conditions will result in normal displacements and that the shear strength becomes that of the intact concrete when normal stress prevents normal displacements. Thus, based on the discussed rock mechanics approach, high shear loading with low compressive normal loading will invoke normal displacements and avoid shear failure, while shear failure is more likely under high normal and shear loads.

Models that Explore the Effect of Contraction Joint Opening on the Dynamic Response of Arch Dams

An article by Fenves, Mojtahedi, and Reimer (1992) discusses the effects of contraction joints on the dynamic response of arch dams. The article states that a finite element model that includes contraction joints differs from a linear monolithic analysis in several ways: (1) the release of tensile arch stresses at

contraction joints causes redistribution of forces from the arches to the cantilevers, (2) loss of arch stiffness lengthens the vibration period of the dam, and (3) cyclic loading when the contraction joints open and close may cause local bearing failure of the concrete in the closed portions of the joints.

The objectives of this article were to investigate the effects of joint openings on the earthquake response of a typical arch dam. The authors illustrate (see figure 9) a finite element model (FEM) of Big Tujunga Dam, Los Angeles County, California, an arch dam modeled with nonlinear contraction joint elements, which allow joint opening, and linear shell elements for the remaining portions of the dam. The model assumes that the strength of the shear keys is large compared to the applied forces and tangential displacements are negligible. The article compares resulting stresses of a linear FEM with no contraction joints to an FEM with one and three contraction joints. The ground motions used for the analysis represent the maximum credible earthquake at the site. Static loads were applied in stages, and incompressible water was incorporated into the FEM.

This study found that allowing joint openings reduces the maximum tensile arch stresses by 50 to 60 percent, and the maximum cantilever stresses increase as the loads are transferred from the arches to the cantilevers. Even though the upstream crest displacements are only slightly increased over a linear analysis not including contraction joints, the results of the study showed that contraction joints opened 1.8 inches at the upstream face and completely separated at the crest. The authors state that large openings at the contraction joints invalidate the assumption of no tangential displacements as the shear keys of adjacent monoliths lose physical contact. The article concludes that the joint-opening behavior depends on the characteristics of the shear keys in the contraction joint.

Models Aimed at Capturing the Effects of Shear-Keyed Contraction Joints

Recent publications create models that incorporate detailed behavior of shear keys for dynamic analysis of concrete arch dams.

Lau, Noruziaan, and Razaqpur (1998)

Lau, Noruziaan, and Razaqpur (1998) presents a constitutive contraction joint model that accounts for the opening and closing, shear sliding behavior, and nonlinear shear key effects of the joint. Shear keys are modeled by specifying a limit on the relative tangential displacement between joint faces. The resistive capacity of the shear key is implemented using an apparent cohesion for the joint when the normal relative displacement is less than a predefined slip margin, which depends on the shear key geometry. This model is accurate when keys prevent slippage and is not accurate for limited slippage in a beveled joint that is partially open. The sliding behavior of the joint elements are shown in figure 10(b), which depicts perfectly plastic behavior when the shear stress (τ) reaches

a limiting apparent cohesion (c). The normal stiffness behavior in the joint provides compressive resistance only and is depicted in figure 10(a). For reference with figure 10, v is the normal displacement in the joint, u is the tangential displacement, and δ is the slip margin.

Successful implementation of the described model into an FEA demonstrates the validity of the model and the effect of keyed contraction joints on the dynamic response of arch dams. *Analysis results demonstrate that shear slippage in contraction joints can cause substantial changes in the displacement and stress fields of an arch dam.* Shear slippage occurs, in the model implemented by Lau *et al.*, when normal joint openings are more than an allowable slip margin. In reality, shear slippage can occur for a joint opening that is less than the geometric asperity of beveled shear keys. As found in the study by Fenves, Mojtahedi, and Reimer (1992) and in the study by Lau, Noruziaan, and Razaqpur (1998), the most substantial joint opening occurs in the upper parts of the dam. Thus, shear slippage occurs most in these portions as well. While it is assumed in the study by Lau, Noruziaan, and Razaqpur (1998) that shear keys prevent slippage, it is possible to have limited slippage in beveled keys when a joint opening is less than the allowable slip margin, or key asperity. This alludes to the fact that changes in the displacement and stress fields can occur before beveled shear key joints open more than the allowable slip margin.

Additionally, implementation of the described joint constitutive model in the work of Lau, Noruziaan, and Razaqpur (1998) provides information on the effects of different joint properties that affect the overall response of the arch dam. A parametric study presented in the article shows the influence of slip margin, shear key strength, and friction property on the seismic response of arch dams.

Ahmadi, Izadinia, and Bachmann (2001)

An article by Ahmadi, Izadinia, and Bachmann (2001) implements a constitutive model that incorporates partial tangential slippage of contraction joints as a function of the normal displacement in the joint. For a closed joint, Ahmadi *et al.* used elastic properties to determine tangential displacements when the shear stress is less than the shear strength of the keys, as determined from cohesion and friction properties according to Coulomb's relation. After the shear stress exceeds the shear strength of the keys, the joint is modeled as a perfectly plastic state. The model assumes zero shear strength when joint openings are larger than the height of the shear keys and incorporates elasto-plastic deformations by decreasing the tangential stiffness in steps with joint opening. Figure 11 demonstrates the relation between stresses and normal or tangential displacements. It is specifically stated that the inclusion of coupling between joint openings and joint slippage is the most important factor implemented in the model. The work by Ahmadi, Izadinia, and Bachmann (2001) demonstrates the capabilities of a model that accounts for major factors affecting the joints of arch dams.

A 20-element FEM of Morrow Point Dam is created to verify and study the results of the described model. The half-symmetrical-dam-body model of Morrow Point Dam includes three contraction joints and a 40-element reservoir mesh with hydrostatic and hydrodynamic pressures equivalent to water surface elevations at the top of the dam crest. The results of the model show, under symmetric dynamic loading in the stream direction, that joints in the middle of the arch span experience normal opening displacements, and joints on the quarter section of the arch span show shear failure. The shear strength of the keys is defined as a function of cohesion and friction coefficients, which are determined by Ahmadi, Izadina, and Bachmann (2001). For the analysis of Morrow Point Dam, the joint initial shear stiffness coefficient is 1 GPa, the initial normal stiffness is 2 GPa, the coefficient of friction is 0.9, and cohesion is 1.5 Mpa. These initial values degrade according to reduction factors defined by the authors: a reduction factor of 0.9 for the friction coefficient when shear failure occurs, a reduction factor 0.7 for shear stiffness due to joint opening, and a reduction factor of 0.2 for shear stiffness due to shear failure. Note that the shear key height of joint surface is 0.5 meters for the analysis of Morrow Point Dam, so zero shear strength is not assumed until joint openings are greater than 0.5 meters. Concluding remarks by the authors state that further studies are needed to determine appropriate values for cohesion and friction coefficients. Nonetheless, enough shear stress developed in the joint to cause the shear keys to fail for the assumed material properties.

For the model of Morrow Point Dam, because normal displacements in the joints were generally a few centimeters and did not exceed the geometric capacity of the keys, sufficient strength of shear keys is needed to ensure the stability of the dam. To reiterate, the strength of the shear keys depends on the cohesion and friction coefficients defined by Ahmadi, Izadina, and Bachmann (2001).

Tzenkov and Lau (2002)

An article by Tzenkov and Lau (2002) presents a dynamic analysis procedure for concrete arch dams that combines the effects of (1) shear key resistance to tangential displacement of the contraction joints and (2) inelastic behavior of the concrete for areas subject to tensile or compressive damage. The shear key in the contraction joint is modeled with an apparent cohesion and friction coefficient to incorporate linear-elastic behavior of the joint when the normal opening displacement between the two faces of the contraction joint is less than the displacement limit of the contraction joint, which is based on the shear key geometry. When normal opening displacement in the contraction joint exceeds the displacement limit, tangential strength is set to zero.

The nonlinear concrete model combines a bounding surface model and a smeared crack model to describe the behavior of the concrete under cyclic compression loads and tension loading, respectively. The bounding surface model is assumed to accurately describe all undamaged concrete and incorporates stiffness degradation by decreasing the yield strength level in areas of compressive failure.

For tensile failure conditions, a smeared crack model assumes a linear-elastic strain relationship up to defined tensile stress failure. A crack is assumed to begin in the plane orthogonal to the maximum tensile stress once tensile stresses exceed the failure strength. An exponential strain-softening curve is utilized to predict stresses after tensile stresses peak, and if a crack closes the bounding surface model, the curve is used to evaluate stress components in the direction of the crack. The rock foundation material is assumed to remain linear-elastic, and hydrodynamic effects are implemented with the added mass concept.

Morrow Point Dam is analyzed using the described method for an observed 15-second ground motion record with a peak ground acceleration of approximately 0.2g. Full reservoir is assumed. Large and strong shear keys are assumed for the contraction joints to eliminate the possibility of tangential shear failure in the joints even though the effects of shear key resistance to tangential displacements are included as one of the characteristics of the model. Thus, this is essentially an opening and closing model as well.

The resulting performance of the dam includes cracking and no crushing of the concrete. The first cracking occurs in a limited zone at the heel of the dam in the first 5 seconds of the ground motion record. Between 5 and 7.5 seconds, the cracking at the heel intensifies, and cracking begins on the downstream face in the upper part of the dam because stream direction displacements of the cantilevers increase where opening joints cause a reduction in support from adjacent cantilever monoliths. After 7.5 seconds, the cracking on the downstream face in the upper portions of the dam extends towards the lower part of the dam. No additional cracking occurs for the remainder of the earthquake record. Figure 12, from the article, illustrates the stages of these damages. The maximum cantilever stresses in Zone A (shown on figure 12) approaches 3 MPa, and the minimum arch stress in Zone B (also shown on figure 12) reaches -10 MPa.

Overall, the study by Tzenkov and Lau (2002) demonstrates that (1) opening of the contraction joints redistributes stresses from the arches to the cantilevers, (2) the closing of open joints and reduced load-bearing areas of partially open joints results in high compressive arch stresses, and (3) high cantilever tensile stresses cause cracking in the downstream portion of the upper part of the dam and at the heel of the dam.

Toyoda, Ueda, and Shiojiri (2002)

An article Toyoda, Ueda, and Shiojiri (2002) provides information about joint opening effects at various water levels of an existing arch dam. The arch dam model used in the study contains 22 monoliths and is a relatively thick three-centered dam in a seismically active mountain range in the middle part of Japan. The model is such that the nodes in the contraction joints are connected by three nonlinear spring elements; two springs are oriented tangentially to the joint face, and one spring is oriented in the normal direction. The resistive capacities of the springs are functions of the relative displacements of the spring elements and are

intended to provide accurate constitutive properties for the shear keys. Failure is modeled by setting the stiffness of one or more of the spring elements to zero.

Interesting concepts are developed by comparing, at a range of water surface elevations, the dam-foundation-reservoir natural frequencies of (1) the nonlinear joint model, (2) forced vibration results, (3) earthquake observation (microtremors) results, and (4) a model with no joints. In general, high water conditions eliminate a large portion of the nonlinear contraction joint effects by creating large arch compressive forces that hold the monoliths of the dam together. Low water surface conditions do not generate high enough arch compressive forces to hold the monoliths of the dam together, and the effects of the nonlinear contraction joints on the response of the dam become evident. For high water conditions, from 80 to 100 meters of water depth, a model containing no contraction joints compares very well to the nonlinear joint model results, the forced vibration results, and the observed earthquake results. As the water surface elevation drops below approximately 80 meters of water depth, the natural periods calculated from the model with no joints exceed those calculated from the nonlinear joint model (see figure 13 from this article). The computed fundamental natural frequency for the nonlinear joint model, the forced vibration, and the earthquake observation are nearly the same for all water surface elevations.

However, the study does not discuss issues related to the relative magnitudes of inertia forces that could open the contraction joints and the reservoir loads that provide restraining forces that hold the contraction joints essentially closed. Depending on the size of the monoliths, amount of entrained water, and ground motion accelerations, contraction joint nonlinear effects could occur under full reservoir head. Toyoda, Ueda, and Shiojiri (2002) found a model with performance characteristics such that the nonlinear effects of contraction joints are nonexistent for certain water level conditions and apparent for other water level conditions. So, while all dams will not have this characteristic, a dam with this characteristic validates models with contraction joints.

Lawrence Livermore National Laboratory Studies on Morrow Point Dam

Studies (Noble, 2002; Noble and Nuss, 2004; Noble and Solberg, 2004) on the nonlinear seismic analysis of Morrow Point Dam done by Lawrence Livermore National Laboratory and the Bureau of Reclamation show various structural performance differences between analyses results from sophisticated and simple concrete dam models. The basic model was of a monolithic/homogeneous dam with foundation and water elements. Other models included contraction joints, a foundation wedge, concrete damage effects, and a tier with failure slide surface at the dam/foundation interface.

Two contraction joint models were included in the analyses. The first joint model incorporates joints with no tensile capacity and tangential shear resistance in the horizontal direction based on assumed friction properties in the joint when the

faces of the joint are in contact. This first model assumes no sliding resistance when the gap opening in the joint is greater than zero. The other joint model includes the effects of the relationship between transverse and normal displacements in the contraction joints by approximating the shape of the shear keys with a sinusoidal curve whose geometry causes normal separations with tangential displacements. This modeling feature is unique in comparison to other studies presented herein. See figure 14 for a schematic of the sinusoidal key and figure 15 for the relationship between sliding and opening displacements of the sinusoidal key.

Overall, these studies found that a model with contraction joints resulted in a more flexible structure with a lower fundamental frequency as compared to a dam with no contraction joints. The two types of contraction joint models showed similar dam performances. The analyses showed that minimal damage would occur in the concrete of Morrow Point Dam during an applied $1/50,000$ annual exceedance probability (AEP) event. The analyses showed peak upstream/downstream displacements of 2.86 inches and peak gap openings of 0.91 inches (Noble and Solberg, 2004). A monolithic dam analysis results in 1,580 lb/in² and 3,810 lb/in² for the first and third maximum principal stresses, respectively. In comparison, a model that incorporates the sinusoidal key results in 2,540 lb/in² and 3,780 lb/in² for the first and third maximum principal stresses, respectively (Noble and Solberg, 2004).

Literature Review Conclusion

The literature review provides an indication of developed strength of the shear keys and insight about the assumed strength and displacement behavior of the shear keys relative to the overall concrete arch dam response.

A fracture mechanics approach to determine shear key strength (Kaneko *et al.*, 1993a, 1993b) is based on cracking and crushing of the concrete and shows that the shear strength of a key is approximately half of the concrete compressive strength when the normal stress is about half the concrete compressive strength and the shear strength diminishes to zero when the normal stress reaches the concrete compressive strength. The shear strength of the key also tends to zero for low normal stress. See the shear key interaction diagram in figure 5 for a graph of normal stress versus maximum shear stress based on the fracture mechanics model.

A rock mechanics approach (Hoek and Bray, 1981; Ladanyi and Archambault, 1970) that considers tangential and normal displacements provides that the initial relationship between shear and normal stress depends on the friction angle and the inclination angle of the asperities in the joint. See figure 8 for a graph of the relationship between normal and shear stress based on the undulating joint shown

in figure 7. The rock mechanics approach shows higher shear strengths than that predicted by the fracture mechanics approach.

The fracture and rock mechanics approach show good agreement in shear failure prediction for normal stresses up to about one-half the compressive strength of concrete. After this point, the rock mechanics approach predicts much higher shear strength than the fracture mechanics approach. The fracture mechanics approach is considered to provide a more accurate shear failure condition because it is based on the geometry of a shear key, and the rock mechanics approach is based on the geometry of small asperities in rough, undulating surfaces. However, the presented fracture mechanics approach does not incorporate normal displacements so this model cannot predict the shear strength of a partially open joint. The finite element analyses performed herein (subsequently presented) illustrate that stresses are drastically redistributed for a partially open joint. The shear strength based on the fracture mechanics model, therefore, is unknown for a partially open joint.

Some studies (Fenves, Mojtahedi, and Reimer, 1992; Lau, Noruziaan, and Razaqpur, 1998; Ahmadi, Izadnia, and Bachmann, 2001; Tzenkov and Lau, 2002; Toyoda, Ueda, and Shiojiri, 2002; Noble and Solberg, 2004) have shown that models with contraction joints capture the major changes in the response of a dam, even for those models that assume strong shear keys that prevent tangential displacements in the joint (Fenves, Mojtahedi, and Reimer, 1992; Lau, Noruziaan, and Razaqpur, 1998; Tzenkov and Lau, 2002). This suggests that joint opening, rather than joint shear, has a large influence on the response of a concrete arch dam. All the models that include contraction joints demonstrate that stresses are redistributed from the arches to the cantilevers, and the fundamental vibration period of the dam lengthens for joint opening. These studies also show that joint openings are typically greater in the upper portions of the dam and were mostly within the geometric height of the shear keys (typical shear key height is 6 inches) (Fenves, Mojtahedi, and Reimer, 1992; Ahmadi, Izadnia, and Bachmann, 2001). Joint opening causes an increase in cantilever stress and was shown to cause tensile cracking in the upper portions of the downstream face of Morrow Point Dam (Tzenkov and Lau, 2002). The results of these models indicate the importance of shear key strength for safe dynamic performance of concrete arch dams because the shear key properties have a large influence on the response of the dam.

Finite Element Study

Following the literature review, which discussed failure and performance properties of shear keys and joint behaviors of concrete arch dams during seismic events, a finite element analysis of a two-dimensional shear key joint was performed in LS-DYNA (Livermore Software Technology Corporation, 2003) to

study stress distribution during loadings that simulate possible load conditions experienced in a joint during one pulse of a seismic event. The model for the finite element analysis is shown in figure 16 and captures a section of a typical keyed joint in a concrete arch dam. The model extends, on each side of the joint centerline, 27 inches, and the keys are dimensioned to match those of most concrete arch dams in Reclamation's inventory and other similar dams (see figure 1 for typical key dimensions). Figure 18 shows contraction joint details for Morrow Point Dam, a thin arch dam, and figure 19 illustrates the location of the contraction joints where the shear keys are located. Contraction joints are spaced approximately 40 feet apart. Figure 18 shows there are locations in Morrow Point Dam that have as many as 18 keys on one face of the contraction joint and other locations towards the top of the dam that have 5 or fewer keys. Thus, the finite element model, which contains four keys on one face and three on the other, can represent either a localized region of the 18 keys or the entire upstream to downstream cross section of the upper extents of the dam. The boundary conditions are selected to closely match the conditions in a dam at the extents of the model.

Four different finite element analyses are performed to study (1) the relative magnitudes of normal and shear loads that initiate sliding for a model with boundary conditions such that dilation can occur, (2) the stress distribution for a closed joint with boundary conditions such that no dilation occurs, (3) the stress distribution for a partially open joint with boundary conditions such that no further dilation occurs, and (4) material property degradation by reducing the modulus of the bottom part by one-half for a closed joint with no dilation. These four finite element analyses will be identified as analyses I, II, III, and IV, respectively.

Material Properties

The material properties used for the analyses are detailed in table 1. Two material properties scenarios are used. The first scenario implements a model with the same material properties for both sides of the joint and is implemented for analyses I, II, and III. The second scenario studies the effects of material damage by reducing the modulus of elasticity on one side of the joint by one-half and is used for analysis IV. This damage could be caused by high compressive arch stresses.

Table 1.—Material properties for concrete in shear key study

Description	Values used in analysis
Density (lb/ft ³)	150
Compressive strength (lb/in ²)	
Static	4,000
Dynamic (1.2 x static)	4,800
Poisson's ratio	0.2
Splitting tension (parent concrete) (lb/in ²)	
Static	(1.7f _c ^{2/3}) 430
Dynamic (1.5 x static)	(2.6f _c ^{2/3}) 655
Modulus of elasticity (lb/in ²)	4,000,000
Shear properties (joint contact)	
Cohesion (lb/in ²)	0
Friction angle (degrees)	45

Contact Surfaces and Boundary Condition

A sliding surface is defined along the contact between part I and II (see figure 17). An assumed 45-degree friction angle and 0-lb/in² cohesion is assigned to this contact. For discussion purposes, part I will be designated as all elements above the shear key contact, and part II is all elements below the shear key contact.

The boundary conditions are selected to match the conditions in a dam at the extents of the model. For analysis I, dilation is allowed, and normal and shear loading is specified. Dilation is not allowed in analyses II, III, and IV so that stress distribution during an increase in shear loading only can be studied. To incorporate the affects of dilation during increased shear loading, a model of a partially open joint is considered as well.

For analyses II, III, and IV, vertical translation was fixed for both the top and bottom edges, and horizontal and vertical translation was fixed at the bottom right corner (see figure 16). The model for analysis I does not include fixities along the top horizontal edge of the top part so that dilation can occur. The described boundary conditions allow realistic transfer of forces from one side of the key to the other. The fixity at the bottom right corner creates stress concentrations that are unrealistic but are far enough away from the three left shear keys to not adversely affect the results.

Loading Conditions

In analysis I, a downward pressure is applied along the top edge, and a leftward pressure is applied on the right edge of part I. The downward pressure was

ramped to 2.5 lb/in^2 in 0.2 seconds, and the leftward pressure was ramped to 80 lb/in^2 in 1.0 seconds. This loading condition was designed to create dilation of the joint. The area of the right edge of part I is 360 in^2 , and the area of the top edge of part I is $1,872 \text{ in}^2$.

For analyses II, III, and IV, body loads were applied to part I in order to simulate inertia forces. The accelerations were linearly ramped to $15,000 \text{ in/s}^2$ over a time of 3 seconds in the direction shown on figure 16. For reference, gravity on earth is 386.4 in/s^2 . Although $15,000 \text{ in/s}^2$ may seem quite large, the mass to which this force is applied is much smaller than the mass that could move in a dam. This load is intended to encompass a range of feasible loads.

Results

Analysis I—Sliding Initiation

Analysis I provides the relative magnitudes of normal and shear forces where sliding begins. The point of sliding initiation in the finite element model can be compared to the point of sliding initiation for an analytic formulation of a block sliding on an inclined plane.

Figure 20 portrays the shear key in the center of the model and shows the two nodes whose displacement is plotted in figure 21. From figure 21, sliding begins at about 0.40 seconds, assuming that sliding begins when the displacement is 0.001 inches. At 0.40 seconds, the load on the top part reached the maximum applied value of 2.5 lb/in^2 and the side load has reached a value of 32.0 lb/in^2 . Multiplying these pressures by the area over which these pressures are applied provides resultant forces of 4,680 lb and 11,520 lb for the top and side loads, respectively. The ratio of side load to top load is 2.46 at 0.40 seconds. This ratio is similar to the ratio predicted by the analytical formulation of 2.41.

The proceeding analytic formulation of sliding initiation validates the finite element analysis for sliding initiation and can be compared to the shear strength of the joint as a means to determine if the joint will be in a sliding or shear-failure mode.

The analytic formulation to determine when sliding begins utilizes a model of a block on an inclined plane with vertical loads, F_y , and horizontal loads, F_x , as shown in figure 22. The force of friction, F_f , is shown to oppose movements up the ramp and is based on the same 45-degree friction angle used in the FEA. F_x and F_y are assumed to be analogous to the resultant forces calculated at the time when sliding was shown to initiate in the finite element analysis. The main difference between the FEM and the analytic formulation is that the FEM has sliding along multiple contacts while the analytic formulation only considers sliding along one contact. However, since friction forces are not a function of contact area, a model of a single contact captures the same behaviors as a model with multiple contacts. Thus, this model represents the sliding properties of the

finite element model presented herein and shows good agreement with the results of the finite element analysis.

To find the point of sliding for the block shown in figure 22, F_x and F_y are transposed into components that are parallel and perpendicular to the plane of sliding. The perpendicular components are $F_y \cdot \cos(i)$ and $F_x \cdot \sin(i)$, and the parallel components are $F_y \cdot \sin(i)$ and $F_x \cdot \cos(i)$ as shown in figure 22. Setting the sum of forces in the parallel and perpendicular directions to zero results in the final relationship between F_x and F_y where sliding initiates, as shown on figure 22 to be:

$$\frac{F_x}{F_y} = \frac{\sin(i) - \cos(i) \cdot \tan(\phi)}{\cos(i) - \sin(i) \cdot \tan(\phi)}$$

The shear keys studied herein have an inclination angle of 22.5 degrees and a friction angle of 45 degrees. Substituting 22.5 and 45 degrees into the above equation results in a ratio of 2.41. This value corresponds very well with the ratio of horizontal and vertical loads determined to initiate sliding in the finite element analyses. If the value of 2.46 determined in the FEA is assumed to represent when sliding begins, then there is approximately a 2-percent error between the analytic and finite element analyses. This error may be smaller depending on what amount of separation between two nodes is defined to be the point where sliding begins in the FEA.

Figure 23 shows the shear strength predicted by the fracture mechanics model (Kaneko *et al.*, 1993a, 1993b) the rock mechanics model (Hoek and Bray, 1981; Ladanyi and Archambault, 1970) and the stresses that initiate sliding based on observation from the FEA and from the analytic formulation of sliding initiation. The fracture mechanics and rock mechanics model assume that stresses are uniform along the base of the key. A reasonable assumption that normal and shear stresses both act over the same area along the base of the key allows the ratio developed in the analytical formulation to be used for stresses or forces.

Figure 23 details some very interesting concepts. The shear strength predicted by the rock mechanics model and the fracture mechanics model are nearly equal up to the point of about one-half the compressive strength. More interesting is the fact that sliding is shown to begin, for the given inclination angle and friction angle, before the strength of the keys is reached for normal stresses less than about $\frac{1}{5}$ of the compressive strength. Note that while the rock mechanics approach does incorporate dilation of the joint, the fracture mechanics model does not. The predicted shear strength for the fracture mechanics model will change when dilation occurs. The effects of joint opening on the fracture mechanics shear strength prediction are discussed later in the analysis III results section after studying the differences in stress distribution between the FEA of a closed and partially open joint.

Analysis II—Closed Joint

Analysis II represents a key that remains in contact during increased shear loading across the keyed joint. Figure 24 shows the deformed shape, magnified 400 times, after 3 seconds of run time when the body load reaches $15,000 \text{ in/s}^2$. Figures 26 and 27 illustrate x- and y-displacements for the points shown in figure 25. Note that the two middle nodes move up in the model (positive displacements), and the two outer nodes move down. This is caused by the fact that the left and right faces of the bottom part are unconstrained and are more easily deformed. The deformation at these joint faces allows the right and left sides to be squeezed out so that y-displacements, even in the top part become negative. The middle nodes experience positive displacements because they are far enough away from the effects of the boundary conditions at the vertical faces of the bottom part.

Figures 28, 29, and 30 show the fringe plots of y-stress, xy-stress, and maximum principal stress. In figure 28, the isolated areas of tension (in red) in between each shear key indicate a phenomenon similar to the failure process discussed in the fracture mechanics articles (Kaneko, *et al.*, 1993a, 1993b) in which tensile stresses initiate a single curvilinear crack. Also note that the y-stress along the top edge of the model approaches 30 to 40 lb/in^2 . This vertical stress is created when horizontal displacements cause vertical displacement, or dilation in the joint that is restrained by the boundary conditions.

In figure 29, the maximum shear stresses occur on the loaded side of each key in the bluish-green regions and approach zero on the side opposite of loading. These values approach 270 lb/in^2 when the body load reaches $15,000 \text{ in/s}^2$.

Figure 30 shows the maximum principal stresses when the body load reaches $15,000 \text{ in/s}^2$. The areas in red show stress concentrations at the locations where the fracture mechanics articles (Kaneko, *et al.*, 1993a, 1993b) predict a crack starting.

Stress time history plots for elements along the base of four shear keys, identified in figure 31 as regions I through IV, further detail stress results. Element locations for region I are shown in figure 32. Stress time histories of the y-stress, xy-stress, and maximum principal stress for these elements are shown in figures 33 through 35. The time history of y-stress shows that stresses are negative for elements on the left side of the key and are positive for element 4781 (See figure 32), on the right side and loaded side of the key. Also note that the minimum stresses occur in element 4779 and begin to become less negative in element 4780 (see figures 32 and 33). This provides that the resultant force acting on the key creates a moment about the base of the key. This is congruent with the rotation described in the fracture mechanics model.

The stress time-history plots in figures 34 and 35 shows that maximum shear and principal stresses occur on the loaded side of the key.

Time-history plots for regions II, III, and IV are included in figures 36 through 47, along with element locations and labels for regions II through IV.

Analysis III—Partially Open Joint

Analysis III studies the effects of a partially open joint during increased shear loading across the joint. As shown in figure 48, the joint is now partially open a distance of 3 inches. All boundary conditions, loads, and material properties are equivalent to those of analysis II.

The deformed shape, magnified 400 times, is shown in figure 49. Horizontal and vertical displacements for the nodes in figure 25 are shown in figures 50 and 51. The x- and y-displacements are only slightly larger for the partially open joint than for the closed joint in analysis II.

Stress fringe plots for y-stress, xy-stress, and maximum principal stress are shown in figures 52, 53, and 54. Throughout the model, the magnitudes of the stresses increase as compared to analysis II with a fully closed joint. The maximum y-stress experienced along the joint contact approaches 10 lb/in^2 for analysis II (figure 28) and 100 lb/in^2 for analysis III (figure 52). This demonstrates that joint openings greatly increase the tensile stresses along the base of the key. This is caused as the location of the resultant force moves up the key and creates a larger moment about the base of the key.

The shear stress fringe plot (figure 53) shows that the location of minimum shear stress shifts up into the portion where the keys are in contact for the partially open joint. From figures 56 and 58, the shear stress reaches a minimum value of approximately -170 lb/in^2 along the base of the key and exceeds -400 lb/in^2 for element 4802, which is about halfway up the key (figure 57). Analysis II, when the joint is closed, resulted in minimum shear stress along the base of the key of approximately -250 lb/in^2 . Generally, the maximum absolute shear stress in a key increases for a partially open joint, and the shear stresses along the base decreases as the maximum absolute shear stress shifts up the key into the portion where the keys are in contact.

Figures 59 and 60 illustrate the maximum principal stresses for the elements in region I and for the elements depicted in figure 56, respectively. The maximum principal stresses are essentially equal for region I elements and for those elements shown in figure 56. The maximum principal stresses increase from 300 lb/in^2 to 400 lb/in^2 for the partially open joint as compared to the closed joint analysis (figures 35 and 60).

The change in stress distribution between a closed joint and a partially open joint invalidates the shear strength predicted by the fracture mechanics approach.

Analysis IV—Degraded Material Property

This analysis differs from analysis II in that the modulus of elasticity of the bottom part is reduced by one-half to simulate weaker concrete. The deformed shape is shown in 15.1 and the x- and y-displacements for nodes shown in figures 62 and 63. The x displacements essentially double for the model with reduced modulus, and the y-displacements are only slightly larger. All strains, except for the compressive strains in part I, double in magnitude as well. It is perceived that compressive strains in part I decrease because the now less-stiff ($\frac{1}{2}$ modulus) part II does not resist the movements from part I as much as when part II had the same modulus as part I. The tensile strains in part I increase for the same reason that compressive strains decrease: the less-stiff bottom part allows more movements in part I.

The fringe plots for y-stress, xy-stress, and maximum principal stress are plotted over the same fringe levels for both analyses II and IV. This allows direct comparison of the fringe plots. Comparison of the fringe plots from analysis II (figures 28, 29, and 30) to fringe plots from analysis IV (figures 64, 65, and 66) shows that the overall stress distributions only slightly change for the degraded material property model. Although slight, one change in the y-stress fringe plots for the two analyses is seen in areas of tensile stresses. The tensile stress areas for the top part, depicted in red, encompass a larger area in figure 64 than in figure 28. Conversely, the tensile stress areas for the bottom part decrease from figure 28 to figure 64. This corresponds to the decreases and increases in principal strains as discussed previously.

Figure 67 illustrates y-stress time-history results for the elements along the base of the key in region I for the degraded material property model. Comparison of figures 67 and 68 shows that minimum y-stresses in the elements in region I change from approximately -72 lb/in^2 (Analysis I) to -62 lb/in^2 for the model with degraded material properties. The maximum tensile stresses in element 4781 increase slightly for the model with degraded material properties (shown on figures 33 and 67). While the magnitude of the maximum y-stress increases along the base of the keys, the shear and maximum principal stresses decrease in magnitude for the analysis with degraded material properties as compared to the results of analysis II.

To further assess the differences between the analysis II results and the analysis results with weaker material properties, figures 70, 71, and 72 illustrate the y-stress, xy-stress, and maximum principal stresses for the elements along the base of the key in region II. Note that region II elements are on the upper part, which has the same material properties as the model of analysis II. Figure 70, in comparison to figure 33 shows that the maximum y-stresses are smaller in magnitude (closer to zero for element 7826) for the weaker material property model.

Figure 71, in comparison with figure 34, illustrates that the minimum shear stress is larger in magnitude for analysis II. However, the maximum shear stress is approximately 10 lb/in² for the weaker material model and is 0 lb/in² for analysis II.

Maximum principal stresses, shown in figures 72 and 35, demonstrate that the degraded material property model results in lower stresses in the elements of the upper part.

Finite Element Study Conclusion

The presented FE models capture a contraction joint with seven shear keys representative of typical shear keys found in concrete arch dams. The finite element analyses provide information on the behavior of shear keys under loading normal and transverse to the joint. Overall, this study finds that the stresses that initiate sliding occur before the shear failure for normal stresses less than about $\frac{1}{5}$ of the concrete compressive strength (see figure 23), where shear failure is predicted by the fracture mechanics (Kaneko, *et al.*, 1993a, 1993b) and rock mechanics (Hoek and Bray, 1981; Ladanyi and Archambault, 1970) approaches. Essentially, if sliding begins before shear failure, then joints will experience dilation. Dilation allows an increase in upstream displacements, which can result in higher cantilever stresses.

For all FEA of the representative shear key, the stresses are shown to distribute similarly across the keys, but not uniformly across the base of each key. Weaker material properties ($\frac{1}{2}$ modulus of elasticity for analysis IV) do not appear to drastically change the magnitudes or stress distributions. However the displacements did double for the analysis with weaker material properties.

The finite element study demonstrated high tensile stresses normal to the joint face, and maximum principal stresses occur where the fracture mechanics predict a crack to begin—the base of the loaded side of the key. All stresses (normal, shear, and principal) match constitutive properties applied in the fracture mechanics approach (Kaneko, *et al.*, 1993a, 1993b) for a closed joint. When the joint is partially open, the stress distribution and location of stress concentrations drastically change.

The tensile stresses increased drastically, from 10 lb/in² to 100 lb/in², for the analysis with the joint partially open 3 inches as compared to the closed joint analyses.

The analysis of a partially open joint showed that joint opening essentially causes the moment arm of the resultant force pushing on a key to increase, which causes higher tensile stresses at the base of the loaded side of the key, lower shear stresses along the base of the key, and higher shear stresses in the area of the key that is still in contact with the key on the opposite side of the joint.

The results of the analysis of a partially open key showed that stress distributions drastically change for a partially open key. This means that the fracture mechanics shear strength predictions are invalid when the key is partially open. Further studies on a partially open key would aid in predicting a shear failure curve of a partially open key.

Method to Compare Known and Implemented Contraction Joint Behavior

This section develops a method to assess the response of concrete arch dams in reference to the implemented contraction joint models that are often used in practice. The proposed method utilizes stress and displacement results in the contraction joint from a typically implemented FE model of concrete arch dams along with known joint behaviors based on studies that explore shear key and joint behavior. The method evaluates the accuracy of the implemented joint model in reference to the response of the entire dam and also provides model validation by examining the behavior in the contraction joints. Additionally, the displacement and stress data indicate whether an arch dam maintains its arch action during and after an earthquake.

As discussed previously, concrete arch dams are indeterminate structures and distribute stresses based on the relative stiffness of the structural components in the dam. The stiffness, or resistance, provided by the contraction joints affects the magnitude of stress in the joints and the stress distribution in the dam; in other words, the results of an FEA with contraction joints reflect the implemented joint properties. In current practice, the influence of the joint in reference to the actual joint behavior is not examined. The proposed method aims to utilize known joint behavior based on shear key models discussed in the literature review (shear key interaction diagram from the fracture mechanics approach, shear and normal stress threshold that initiates sliding, and shear key geometry) in comparison to the joint displacement and stress results from FE analyses of three-dimensional concrete arch dams. This will provide the ability to quantify the influence of the implemented joint model on the resulting structural behavior. Note that stresses and displacements in the joint are not typically evaluated for structural analysis of concrete arch dams.

Consider a concrete arch dam that is analyzed using linear and nonlinear FE models. The linear FEA does not explicitly include contraction joints but portrays the contraction joints with a very large stiffness. While artificial tensile arch stresses can develop in a linear-monolithic FEA, the contraction joint shear stresses during compressive arch stresses can provide an indication of the

accuracy of the overall performance of the dam by comparing the implemented joint model, or in this case, lack of a joint model, with known joint behaviors. A time history of the normal and shear stresses at the location and in the plane of the contraction joints can provide points to compare with the shear key interaction diagram and threshold of stresses for sliding initiation. The linear FEA provides very large joint stiffness so the shear stresses in the joint can also be very large. If there exist many instances where the resulting normal and shear stresses lie outside the shear key interaction diagram in figure 23, then this indicates that the results could substantially change for a nonlinear model that includes contraction joints. Additionally, if many points lie above the threshold for sliding to begin, then the linear analysis has failed to capture the increase in cantilever displacements when shear displacements and joint openings occur.

On the other hand, if most shear and normal stress results lie inside the shear key interaction diagram in figure 23, then this indicates that the linear analysis may provide a reasonable indication of the structural response. If the points also lie within the threshold for sliding to begin, then the linear analysis may provide a very good indication of the structural response. Joint opening is the only aspect that cannot be evaluated when comparing the results of a linear analysis with known joint behavior. However, the nonlinear FEA results do provide information on joint opening.

Next consider a nonlinear FEA that includes contraction joints. Contraction joints are typically modeled as a flat surface with an apparent friction angle. This type of joint model implements zero shear resistance with any joint opening so it portrays contraction joints with shear keys as having a smaller stiffness. Tensile arch stresses do not develop, and the contraction joint shear and compressive stresses can be compared with a shear key interaction diagram and the threshold of stresses that initiate sliding. The nonlinear FEA results also contain contraction joint displacement data, which allows comparison of the behavior of the implemented joint model with known behaviors based on the geometry of the shear keys. The geometry of the shear keys defines the relationship between joint opening and shear slippage. For example, if joint openings are less than the geometric asperity of the keys, then shear slip in the joint is limited by the geometry of the key. If joint opening is larger than the asperity of the keys, then shear slip is not limited. In this sense, if a nonlinear FEA results in large shear slip with small joint opening, then the joint model is not providing enough resistance, and the FEA results will produce artificially large cantilever stresses. If the nonlinear FEA results indicate shear slippage and joint opening that corresponds with the geometry of the keys, then the overall dam response will be more reasonable.

Essentially, a contraction joint modeled as a flat surface with an apparent friction angle provides a lower bound on the stiffness of a contraction joint with shear keys, and a linear FEA provides the upper bound on the stiffness. A linear and a nonlinear FEA encompass the spectrum of possible joint behaviors. It is possible

that the joints will behave at either end of the spectrum, but it is also possible for the joint to behave somewhere in the middle of the spectrum. If this is the case and the linear and nonlinear analyses both demonstrate behaviors that substantially vary from the known joint behaviors, then other models may need to be implemented to determine a more accurate representation of the performance of the dam. The sinusoidal shear key is one such model shown to be successful in studies and is available in LS-DYNA (Livermore Software Technology Corporation, 2003). Other methods including apparent cohesion and nonlinear springs were also demonstrated herein and could provide an adequate joint model. Nonetheless, none of the joint models provide an exact model of a contraction joint, and the true joint behavior would preferably lie close to one of the implemented joint models. Unfortunately, an FE model of a concrete arch dam that includes the asperity of each shear key in all the contraction joints is not currently practical because of computation issues.

The proposed method provides a means of determining how close or how far the implemented joint behavior is from the actual behavior. This information aids in determining if an arch dam maintains arching action during and after an earthquake event and can be used to more accurately define probabilities of failure for concrete arch dams.

Implementation of the Proposed Method

The proposed method requires data that are readily available from FE analyses typically performed in assessing the stability of concrete arch dams. Time histories of the displacement data and shear and normal stress data at various elevations in the contraction joints provide the necessary results for an assessment of the joint behavior. The resulting stress behavior in the joint can be compared to the shear key interaction diagram and threshold of stresses for sliding initiation. The displacement behavior can be compared to the geometry of the shear keys. The fracture mechanics equation is described in detail in the literature review section along with a graph of the equation, which has been termed the shear key interaction diagram in figure 23 for this report. The rock mechanics equation and graph were also presented along with the equation and graph of the threshold for sliding initiation. The fracture mechanics, rock mechanics, and sliding threshold are all illustrated in figure 23 for concrete with a compressive strength of 27.5 MPa (4,000 lb/in²). In general, the proposed method determines if the data from a three-dimensional FEA of a concrete arch dam is above or below the curves presented in figure 23 and if the displacement is within the geometry of the shear keys. Note that the presented method assumes elastic material properties that do not account for inelastic redistribution of stress.

Many FE models of concrete arch dams are based on a three-dimensional coordinate system with the upstream component perpendicular to the crown of the dam. The resulting displacement and stress data are also typically presented in terms of this coordinate system. For contraction joints that are not at the crown of

the dam, it is necessary to transpose the results into a local coordinate system with axes parallel and perpendicular to the dam at the location and in the plane of the contraction joint being evaluated. A local coordinate system contains a radial direction that is perpendicular to the axis of the dam and a tangential direction that is parallel to the axis of the dam. A conversion to a local coordinate system will provide the radial and tangential displacement and stresses at the contraction joint being evaluated.

Consider an example from Nambe Falls Dam, a concrete arch dam designed and built with contraction joints with no shear keys. Although the dam does not contain shear keys, this study will discuss the possible effects of shear keys in Nambe Falls Dam.

Figure 73 illustrates the dimensional layout for Nambe Falls Dam, and figure 74 shows a plan view of the 3-dimensional LS-DYNA FE model of the dam. The entire three-dimensional FE model of Nambe Falls Dam includes the foundation and reservoir. Loading for the considered example includes effects from the foundation, reservoir and a $1/50,000$ annual exceedance probability (AEP) earthquake event. The upstream, cross-canyon, and vertical acceleration time history along with the acceleration response spectra for the earthquake event are illustrated in figure 75a. The deconvolved accelerations and response spectra are shown in figure 75b.

Figure 76 shows a plan view of the dam at 7.44 seconds when large displacements occur in the contraction joints. Note that the displacements are magnified 100 times for illustration purposes. Figure 76 provides a visual indication of the behavior of the dam during the 50,000-year AEP earthquake event.

Contraction Joint Displacement Data

Consider the contraction joint circled in figure 76. Relative displacement results between two adjacent nodes at the crest of the dam can be converted from the global x-y-z coordinate system into a local coordinate system. The local coordinate system will provide displacements in a coordinate system with axes parallel and perpendicular to the dam at the location of the contraction joint and thus normal and transverse to the face of the contraction joint. Figure 77 shows a closer plan view of the contraction joint. The z-coordinate is positive upstream and the x-coordinate is positive toward the right abutment. The relative x- and z-displacements between two adjacent nodes at the crest of the dam (indicated by the arrow in figure 77) along the upstream face are shown in figures 78 and 79.

The angle from the dam crown to the location of the contraction joint is needed to determine the radial and tangential components of the x- and z-displacements. For Nambe Falls Dam, the crown is at station 2+00, and the radius of curvature at the dam crest is 150.0 feet. The contraction joint being considered is at station 3+05. The angle from the dam crown to station 3+05 can be determined using the equation $s = r\theta$, where s is the arc length, r is the radius, and θ is the interior

angle for the arc length and radius specified. For this example, s is 105 feet, and r is 150 feet. Solving for θ results in a value of 40.107 degrees. Once the angle from the dam crown to the contraction joint, θ , is known, the x - and z -displacements can be transformed into radial and tangential components. The calculations in figure 80 illustrate the transformation from a global coordinate system into a local coordinate system. The radial and tangential displacements are then calculated by summing the radial and tangential components of the x - and z -displacements. The transformation equation for radial and tangential displacements is:

$$Radial = z \cos(\theta) - x \sin(\theta)$$

$$Tangential = x \cos(\theta) + z \sin(\theta)$$

Where z and x are the relative displacements in the z - and x -directions, respectively, as illustrated in figures 78 and 79. Note that the above equations are developed for contraction joints to the left of the crown of the dam and would be as follows for contraction joints to the right of the crown of the dam (see figure 80).

$$Radial = z \cos(\theta) + x \sin(\theta)$$

$$Tangential = x \cos(\theta) - z \sin(\theta)$$

Displacement data at various locations in the dam provide a means to quantitatively measure the behavior in the contraction joints. Implementing the above equation for the displacement time history data presented in figures 78 and 79 results in radial and tangential (joint opening) displacements shown in figures 81 and 82. The radial displacements are mostly less than 0.15 inches and show one point where the radial displacement is about 0.25 inches at approximately 7.5 seconds, which is the same time frame as that shown in figure 76. The joint opening displacements are predominately less than about 1 inch and illustrate a spike at about 7.5 seconds that exceeds 2.0 inches. These plots of sliding and tangential displacements provide information about the joint behavior during a seismic event and can be used to determine if the dam will retain its arch shape during and after an earthquake. While Nambe Falls Dam does not contain shear keys, it appears that the dam would not perform substantially differently if typical shear keys were implemented. For example, if typical shear keys were implemented (see figure 1) and joint openings were 2 inches, then the shear keys would prevent radial displacements of 4 inches or more. However, the radial displacements are much less than 4 inches, and thus the shear keys would not further restrict the displacements.

Contraction Joint Stress Data

Next, consider the stress data for element 82080, which is the element on the right side of the contraction joint being considered and is shown in figure 83. The x -, z -, and zx -stress time histories for this element are shown in figures 84 through 86.

The stresses based on the global coordinate system must be transposed into the local coordinate system to determine the radial and tangential stress in the joint. From elementary mechanics of materials, the transformation equation for expressing stresses in a 1-2 coordinate system in terms of stresses in a x-z coordinate system are as follows:

$$\begin{bmatrix} \sigma_1 \\ \sigma_2 \\ \tau_{12} \end{bmatrix} = \begin{bmatrix} \cos^2 \theta & \sin^2 \theta & 2 \sin \theta \cos \theta \\ \sin^2 \theta & \cos^2 \theta & -2 \sin \theta \cos \theta \\ -\sin \theta \cos \theta & \sin \theta \cos \theta & \cos^2 \theta - \sin^2 \theta \end{bmatrix} \cdot \begin{bmatrix} \sigma_x \\ \sigma_z \\ \tau_{xz} \end{bmatrix}$$

Where θ is the angle from the x-axis to the 1-axis, as shown in figure 87. Note that the direction of rotation is important and that for joints to the left of the crown of the dam the 1-axis is the radial component, and the 2-axis is the tangential component and vice-versa for joints to the right of the crown of the dam. Based on the above equation, the radial and tangential components of stress are developed for element 82080 and are shown in figures 88 and 89. Figure 88 illustrates the shear stress in the joint at the location of element 82080, and figure 89 illustrates the normal stress in the joint. Note that normal stresses are always negative indicating that no tensile loads occur in the joint.

Now, each shear and normal stress pair can be plotted to compare the stresses in the joint with those that cause sliding or shear key failure. Plots of the rock mechanics diagram, fracture mechanics diagram or shear key interaction diagram, threshold of sliding initiation, and resulting shear and normal stress pairs are shown in figure 90. Figure 91 illustrates a close up view of figure 90 near the origin, in the location of all the resulting normal and shear stress pairs from figures 88 and 89. Note that the sign convention for the normal stresses is reversed in figure 90 from those shown in figure 88. Thus, positive designates compressive stress in order to be in accordance with the same sign convention that was used in developing the shear key interaction diagram. Also, the absolute values of the shear stresses from figure 89 are used in figures 90 and 92 because the shear key interaction diagram only accounts for shear stress in one direction. Negative or positive shear stresses output from LS-DYNA signify the direction of the stress. However, the absolute magnitude of the shear stress is used because the same resistance is provided in the joint for stress in either direction. Also note that the values listed in figures 88 and 89 are in lb/in^2 , and the values listed in figure 90 are in Mpa.

The shear- and normal-stress pairs shown in figures 90 and 91 mostly fall within the threshold of sliding to begin and are mostly within the shear key interaction diagram based on the rock mechanics and entirely within the shear key interaction diagram based on the fracture mechanics model. Note that the fracture mechanics model does not approach zero shear strength with zero normal loads. Rather, the minimum shear strength for low normal loads is equal to 10 percent of the

compressive strength of concrete, which is a value representative of the cohesive strength of concrete.

The displacement and shear data presented for the contraction joint considered in this study indicate that the implemented contraction joint model accurately captures the joint behavior and provides that arching action will be maintained during and after the applied earthquake ground motions. If Nambe Falls Dam were to have shear keys, the displacement and stress data indicate that the joints are behaving in accordance with typical shear key geometry, and stresses do not approach limits for failure of the shear keys.

Based on this proposed method that observes two behavior results in the joint, namely displacement and stress data, there are four different potential scenarios:

1. Displacement data indicate joint behavior is within the geometry of the shear keys, and shear stress data are within the bounds of the interaction diagram
2. Displacement data indicate joint behavior is within the geometry of the shear keys, and shear stress data exceed the bounds of the interaction diagrams
3. Displacement data indicate joint behavior violates the geometry of the shear keys, and shear stress data are within the bounds of the interaction diagrams
4. Displacement data indicate joint behavior violates the geometry of the shear keys, and shear stress data exceed the bounds of the interaction diagram

Scenario one is the case illustrated herein for the contraction joint considered in Nambe Falls Dam and indicates the joint is stable and arching action will be maintained during and after an earthquake event.

Scenario two could indicate that the joint is too stiff and that the displacements are too small and thus the behavior of the dam is not entirely accurate. Or scenario two could indicate that the shear keys in the joint may fail. Scenario two is less likely for a contraction joint modeled as a flat surface with an apparent friction angle.

Scenario three could indicate that the stress data in the joint is artificially low, and the displacement data are artificially high as a contraction joint with shear keys would limit displacements to be within the bounds of the shear key geometry, especially when stresses are within the bounds of the interaction diagrams. Scenario three behaviors may warrant analyses with different joint models that limit displacement to be within the shear key geometry. This would most likely cause the stresses in the joint to increase.

Scenario four would be a worst case scenario and could indicate that stresses are artificially low. Implementing a contraction joint model that limits displacements

to be within the shear key geometry would increase the stress in the joint. Additionally, since the stresses would exceed the bounds of the shear key interaction diagram and would thus be susceptible to failure, the displacements would most likely be artificially low if a model limited displacements to be within the geometry of the shear keys. If scenario four is evident, the joints are most likely susceptible to damage or failure

The proposed method develops a way of assessing the behavior in the joint in reference to known joint behavior based on shear key interaction diagrams and shear key geometry. This provides an assessment of the stability in the joint and whether an arch dam maintains its arch action and shape before and after an earthquake event. Additionally, evaluation of displacement and stress data in the contraction joints provides a means of determining if the FE model is performing as expected. For example, tangential displacements in the joint can illustrate any penetration in a contact surface.

Conclusion

This report has reviewed studies that demonstrate the influence of contraction joints on the response of concrete arch dams. Essentially, the inclusion of contraction joints in an FE model of a concrete arch dam causes the fundamental period to lengthen and the stresses to be redistributed from the arches to the cantilevers. Additionally, joint openings were shown to be the most substantial in the upper portions of the dam.

The strength of shear keys is provided based on a fracture mechanics model that determines all normal and shear load combinations for failure. A rock mechanics model was also presented and shows good agreement with the fracture mechanics model when normal stresses are less than one-half the compressive strength of concrete (figure 23). Additionally, an elastic FEA of a two-dimensional contraction joint with shear keys, as performed as part of this study, validated the fracture mechanics approach and demonstrated that stresses are distributed evenly to all shear keys but not evenly across the base of each key. The two-dimensional FEA also validated an analytic approach for determining the load combinations for sliding initiation in a contraction joint with shear keys.

A new method was proposed to evaluate the response of concrete arch dams in reference to the implemented contraction joint models that are typically used in practice. The method compares the FEA resulting joint behavior with known behaviors based on the fracture mechanics model, the rock mechanics model, and threshold for sliding initiation. The method provides a better assessment of the stability of concrete arch dams and helps risk teams better estimate probabilities of failure for concrete arch dams with and without shear keys.

References

Ahmadi, M.T., M. Izadinia, and H. Bachmann, “A Discrete Crack Joint Model for Nonlinear Dynamic Analysis of Concrete Arch Dam,” *Computers and Structures*, Elsevier, 79, 403-420, 2001.

Bakhoun, M.M., *Shear behavior and design of joints in precast concrete segmental bridges*, PhD thesis, Massachusetts Institute of Technology, Cambridge, Massachusetts, 1991.

Fenves, G.L., S. Mojtahedi, and R.B. Reimer, “Effect of Contraction Joints on Earthquake Response of an Arch Dam,” *Journal of Structural Engineering*, ASCE, 118(4), 1039-1055, 1992.

Hoek, E. and J.W. Bray, *Rock Slope Engineering*, The Institution of Mining and Metallurgy, London, England, 1981.

Kaneko, Y. and H. Mihashi, “Analytical Study on the Cracking Transition of Concrete Shear Key,” *Materials and Structures*, 32(217), 196-202, 1999.

Kaneko, Y., J.J. Connor, T.C. Triantafillou, and C.K. Leung, “Fracture Mechanics Approach for Failure of Concrete Shear Key, I: Theory,” *Journal of Engineering Mechanics*, ASCE, 119(4), 681-700, 1993a.

Kaneko, Y., J.J. Connor, T.C. Triantafillou, and C.K. Leung, “Fracture Mechanics Approach for Failure of Concrete Shear Key, II: Verification,” *Journal of Engineering Mechanics*, ASCE, 119(4), 701-719, 1993b.

Ladanyi, B. and G. Archambault, “Simulation of Shear Behavior of a Jointed Rock Mass,” *Proceedings 11th Symposium on Rock Mechanics*, AIME, New York, 105-125, 1970.

Lau, D.T., B. Noruziaan, and A.G. Razaqpur, “Modelling of Contraction Joint and Shear Sliding Effects on Earthquake Response of Arch Dams,” *Earthquake Engineering and Structural Dynamics*, John Wiley and Sons, 27, 1013-1029, 1998.

Livermore Software Technology Corporation, *LS-DYNA: Keyword User's Manual*, Version 970, April 2003.

Noble, C.R. and J. Solberg, *Nonlinear Seismic Analysis of Morrow Point Dam—A Study for the United States Bureau of Reclamation*, UCRL-TR-202545, 2004.

Noble, C.R. and L.K. Nuss, *Nonlinear Seismic Analysis of Morrow Point Dam*, 13th World Conference on Earthquake Engineering, UCRL-CONF-202508, Vancouver, Canada, 2004.

Noble, C.R., *Seismic Analysis of Morrow Point Dam*, Workshop on Non-Linear Structural Analysis of Concrete Dams and Concrete Appurtenances to Dams, UCRL-ID-147993, Denver, Colorado, 2002.

Toyoda, Y., M. Ueda, and H. Shiojiri, *Study of Joint Opening Effects on the Dynamic Response of an Existing Arch Dam*, 15th ASCE Engineering Mechanics Conference, Columbia University, New York, 2002.

Tzenkov, A.D. and D.T. Lau, *Seismic Analysis of Concrete Arch Dams with Contraction Joints and Non-Linear Material Models*, 7th U.S. National Conference on Earthquake Engineering, Boston, Massachusetts, 2002.

Wittmann, F.H., "Crack Formation and Fracture Energy of Normal and High Strength Concrete," *Sadhana Academy Proceedings in Engineering Sciences*, Indian Academy of Sciences, 27(4), 413-423, 2002.

Figures

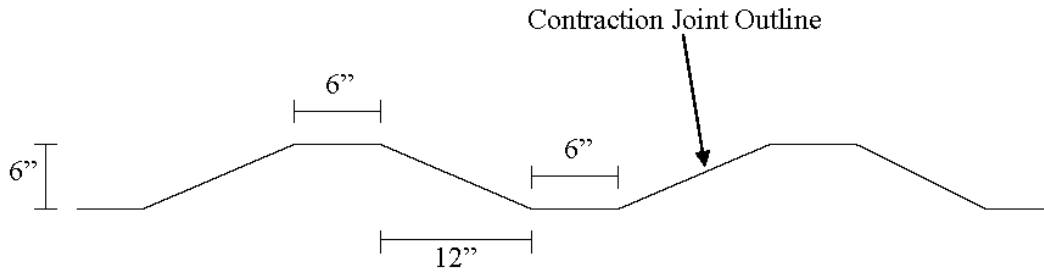


Figure 1.—Typical contraction joint shear key dimensions.

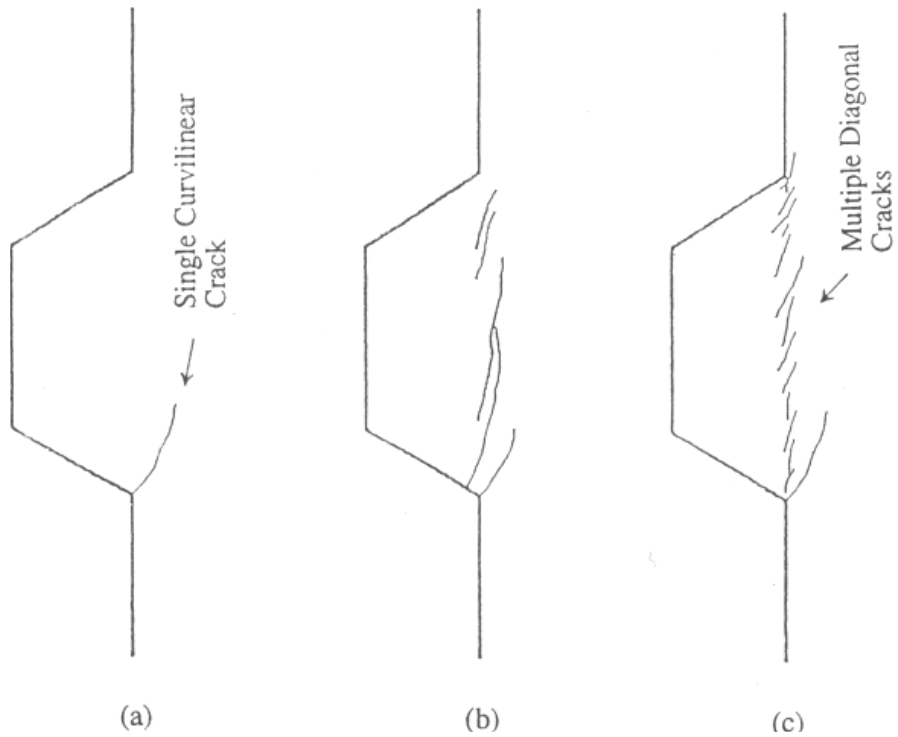


Figure 2.—Cracking sequence (after Bakhom [1991]) (Kaneko *et al.*, 1993).

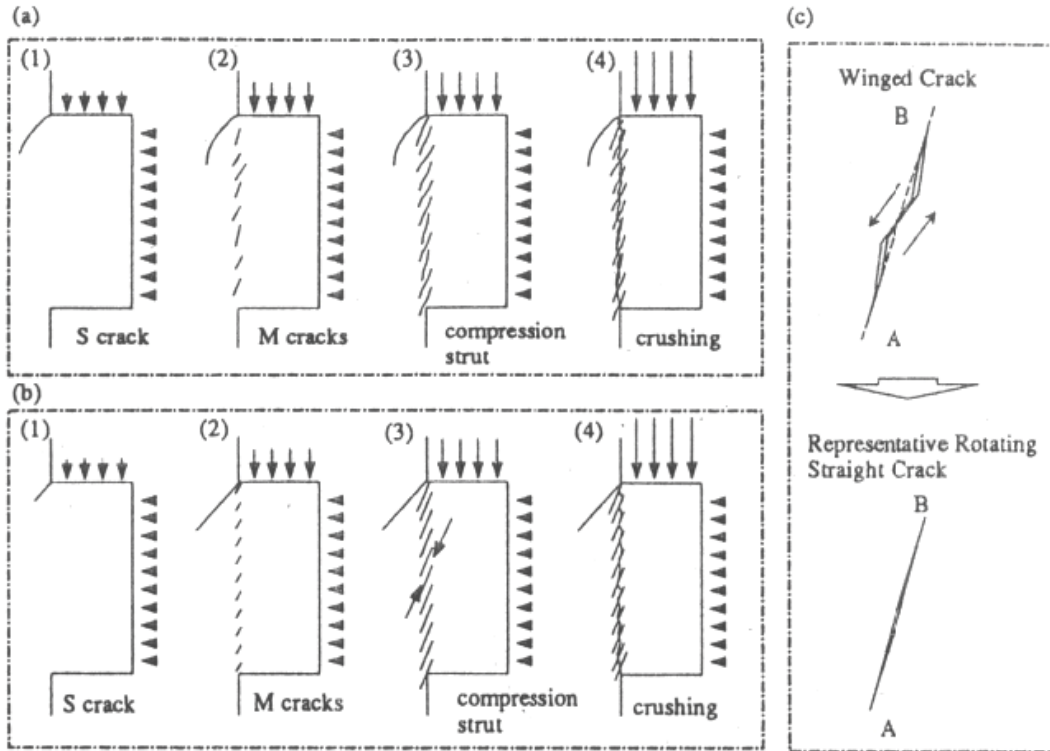


Figure 3.—Shear-off fracture sequence (Kaneko *et al.*, 1993).

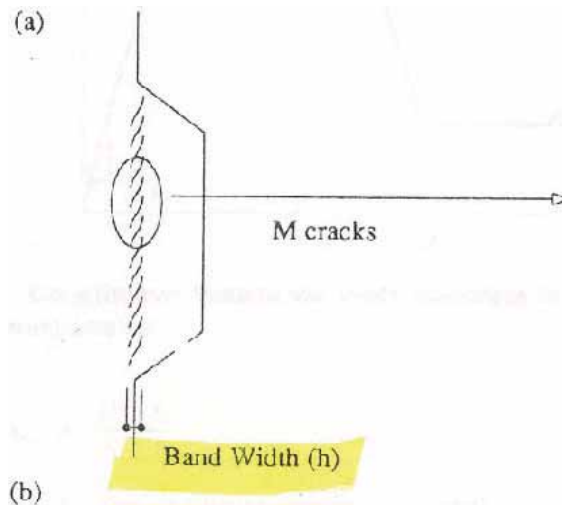


Figure 4.—Band width (Kaneko *et al.*, 1993).

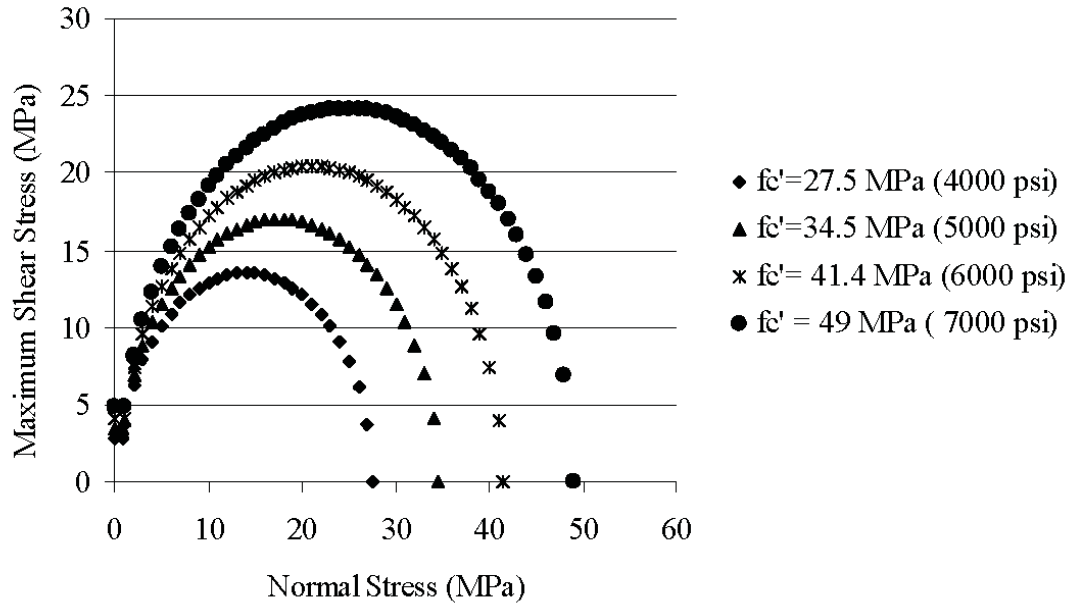
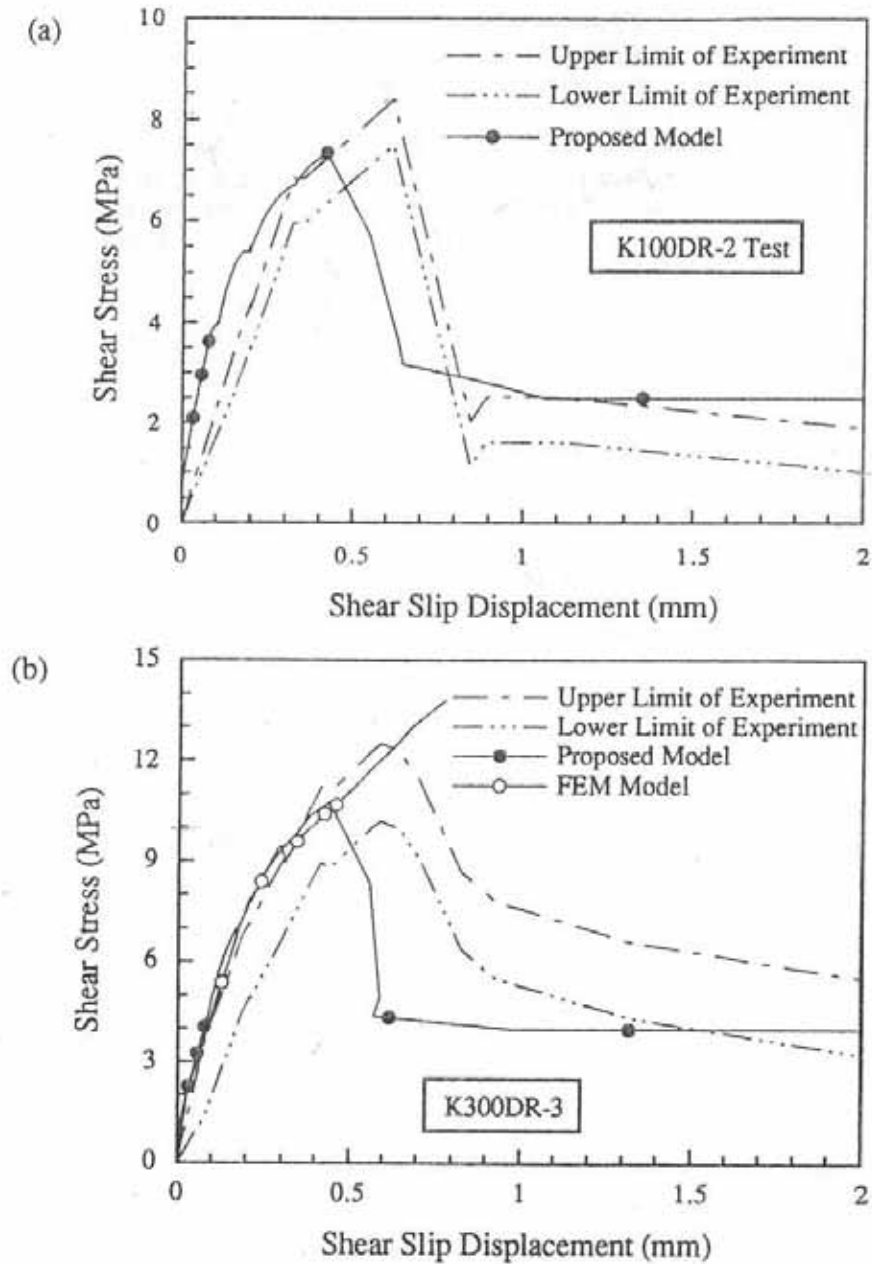


Figure 5.—Shear vs. normal stress for plain concrete shear key based on equations from Kaneko *et al.*, 1993.



Predicted and Experimental Shear Stress versus Shear Slip Displacement Curves for: (a) K100-DR2 Test; (b) K300-DR3 Test

Figure 6.—Shear stress vs. shear slip displacements from Kaneko *et al.*, 1993.

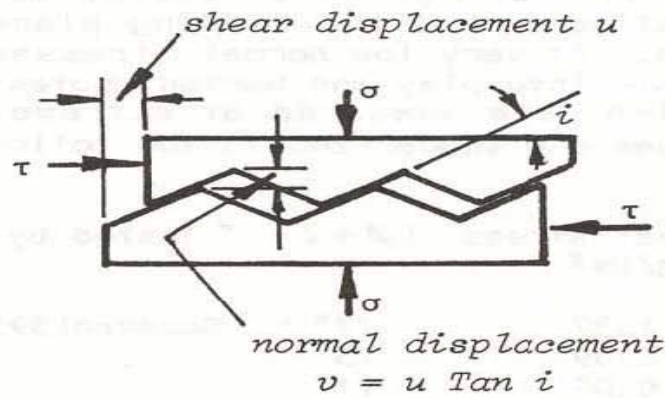


Figure 7.—Rock mechanics—undulating joint.

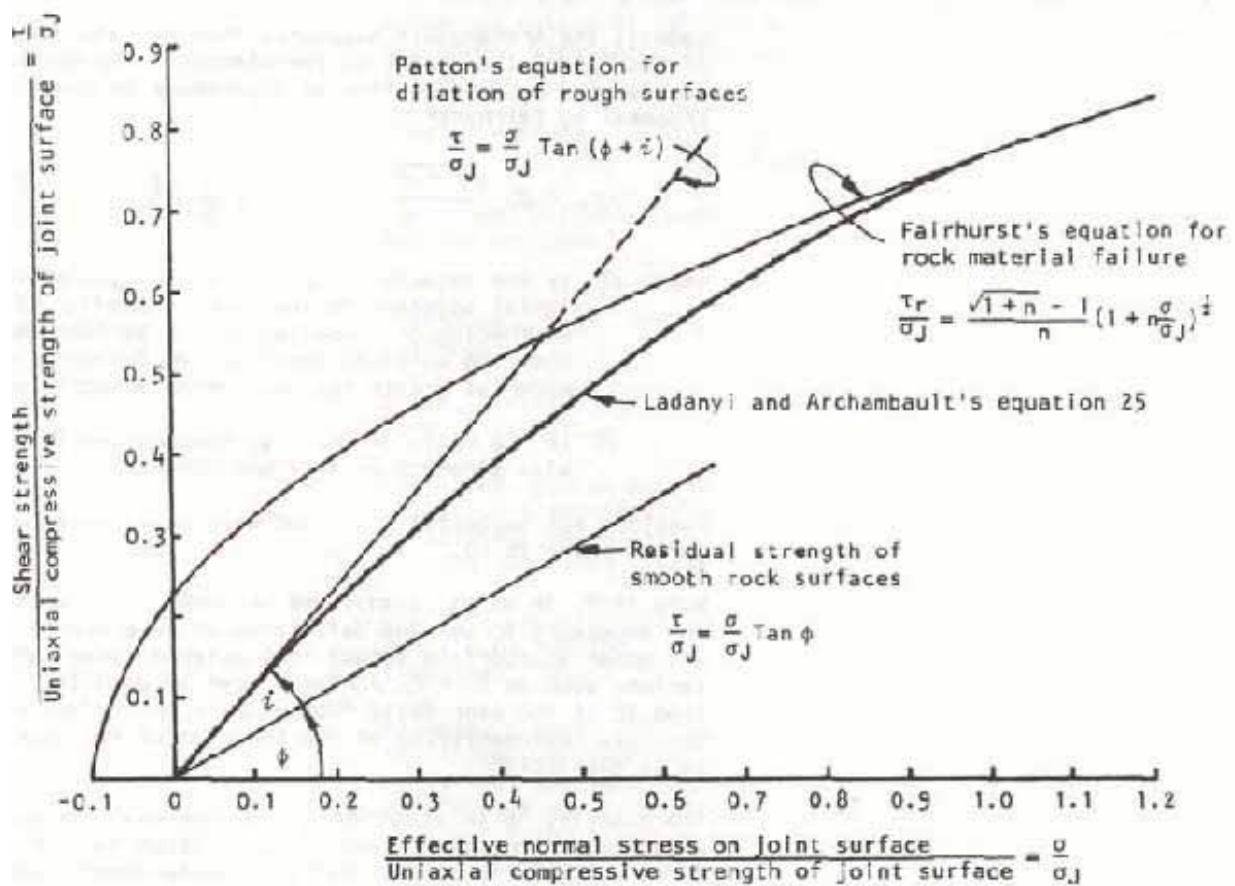


Figure 8.1: Transition from dilation to shearing predicted by Ladanyi and Archambault's equation. Plotted for $i = 20^\circ$ and $\phi = 30^\circ$.

Figure 8.—Shear vs. normal stress in undulating rock joints.

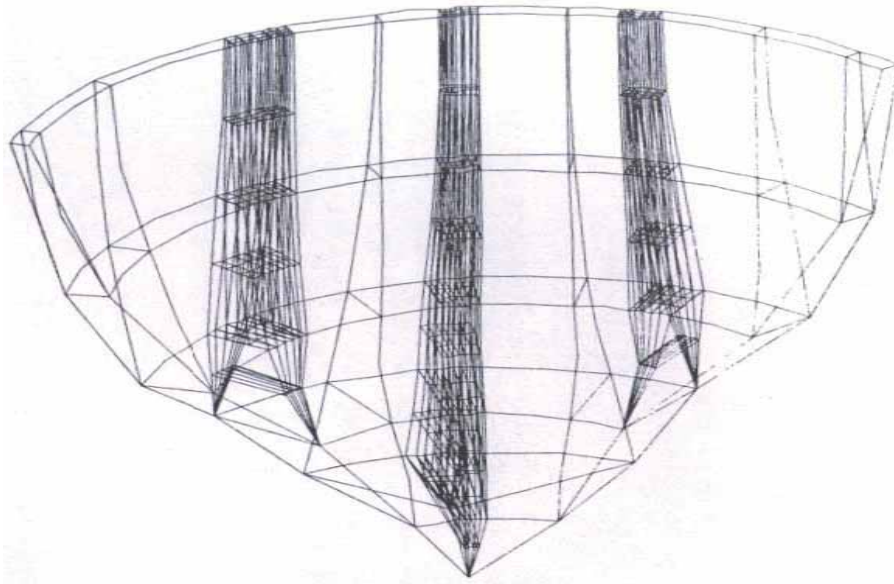


Figure 9.—Finite element mesh of Big Tujunga Dam (Fenves *et al.*, 1992).

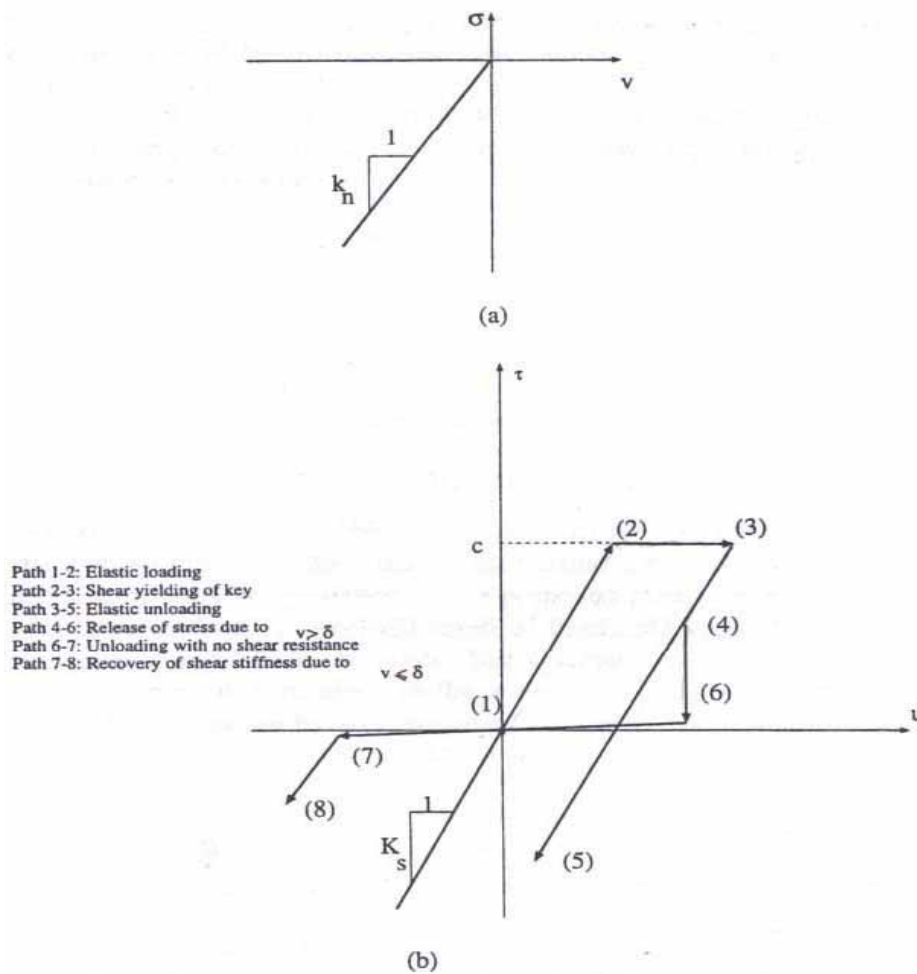
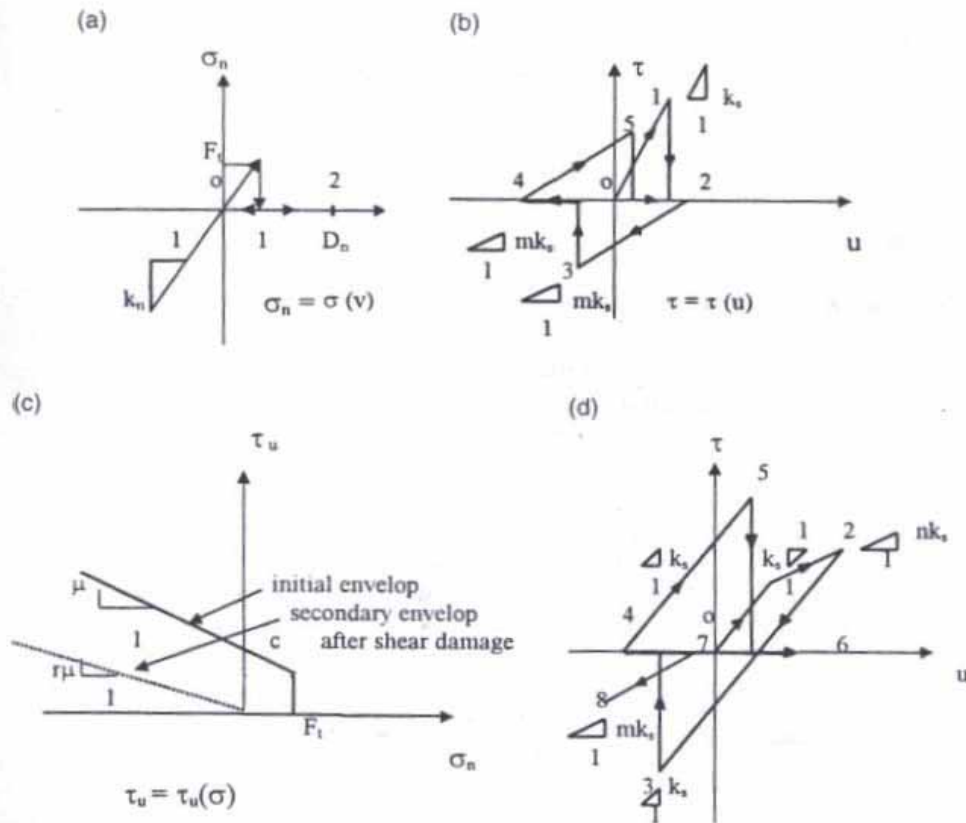
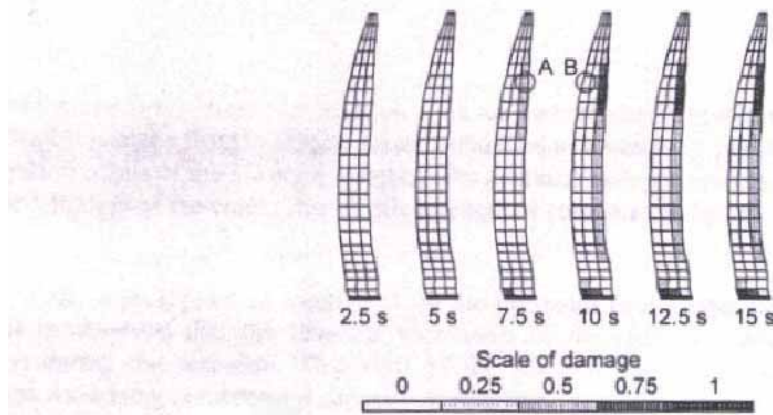


Figure 10.—Constitutive relations of nonlinear joint element (Lau *et al.*, 1998).



Relation between stresses and normal or tangential displacements. (a) Normal displacement: (1) Tensile fracture and (2) joint opening exceeding the shear key height. (b) Constitutive law for joint in shear: (0) loading, (1) shear fracture, (2) shear unloading, (3) new shear fracture, (4) new loading and (5) new shear fracture. (c) Subsequent yield surface for joint damage. (d) Shear and tensile fractures with coupling: (0) shear loading in tension, (1) reduction of shear stiffness with partial joint opening, (2) shear unloading in compression, (3) complete joint opening, (4) shear loading in compression, (5) shear fracture, (6) shear loading, (7) complete slip in tension and (8) shear unloading.

Figure 11.—Relation between stresses and normal or tangential displacements (Ahmadi *et al.*, 2001).



Evolution of the crack pattern in the crown cantilever.

shows the evolution of the crack pattern in the crown cantilever of the dam. It is noted that crushing of concrete is not observed in the dam. The cracking process begins in a limited zone at the heel area of the dam. Between 5 and 7.5 seconds from the beginning of the earthquake excitation, the cracking in the heel area intensifies and cracking initiates on the downstream face in the upper part of the dam. Between 7.5 and 10 seconds, the cracking on the downstream face intensifies and the cracks spread toward the lower parts of the dam. Thereafter, no significant change to the crack pattern is observed.

Figure 12.—Cracking and crushing in Morrow Point Dam (Tzenkov and Lau, 2002).

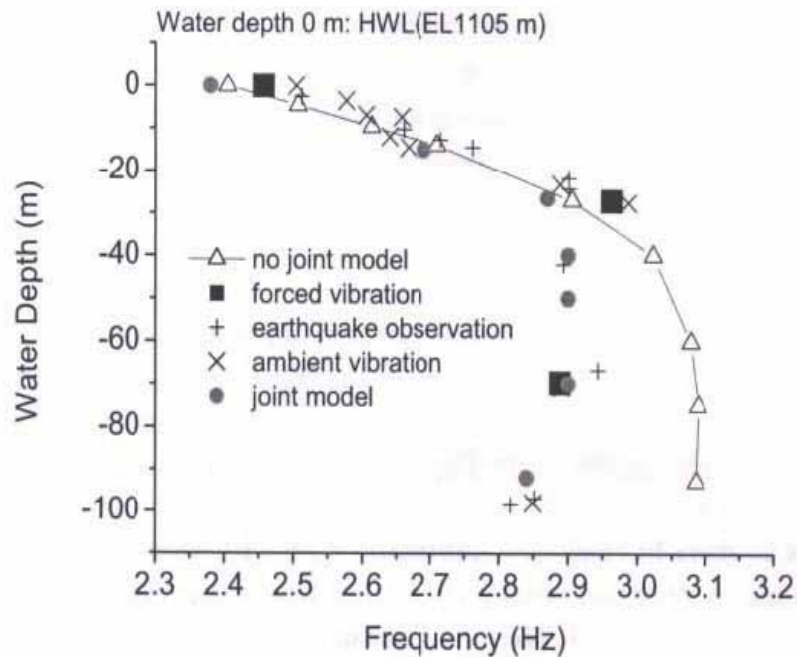


Figure 13.—Effect of reservoir water level (Toyoda *et al.*, 2002).

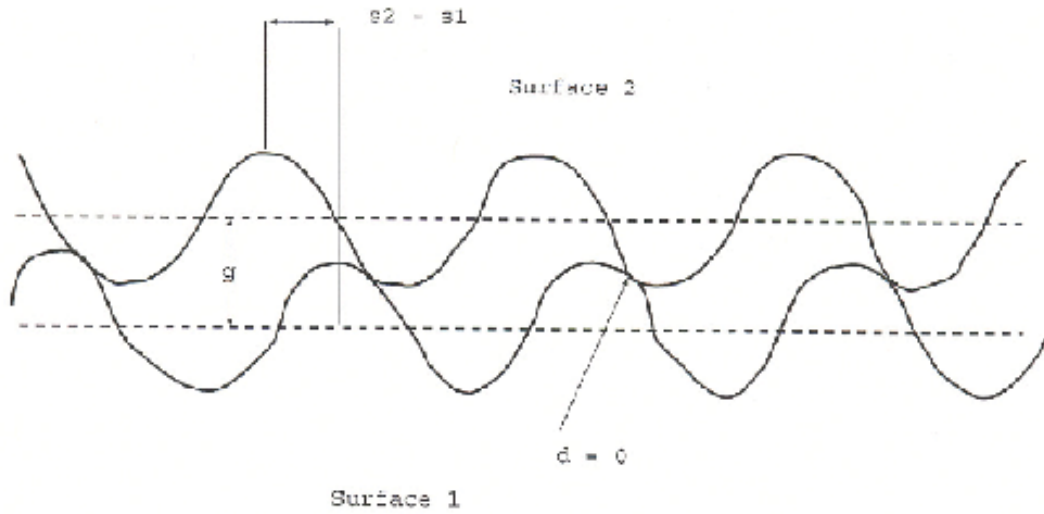


Figure 14.—Sinusoidal contraction joint from Noble and Solberg (2004).

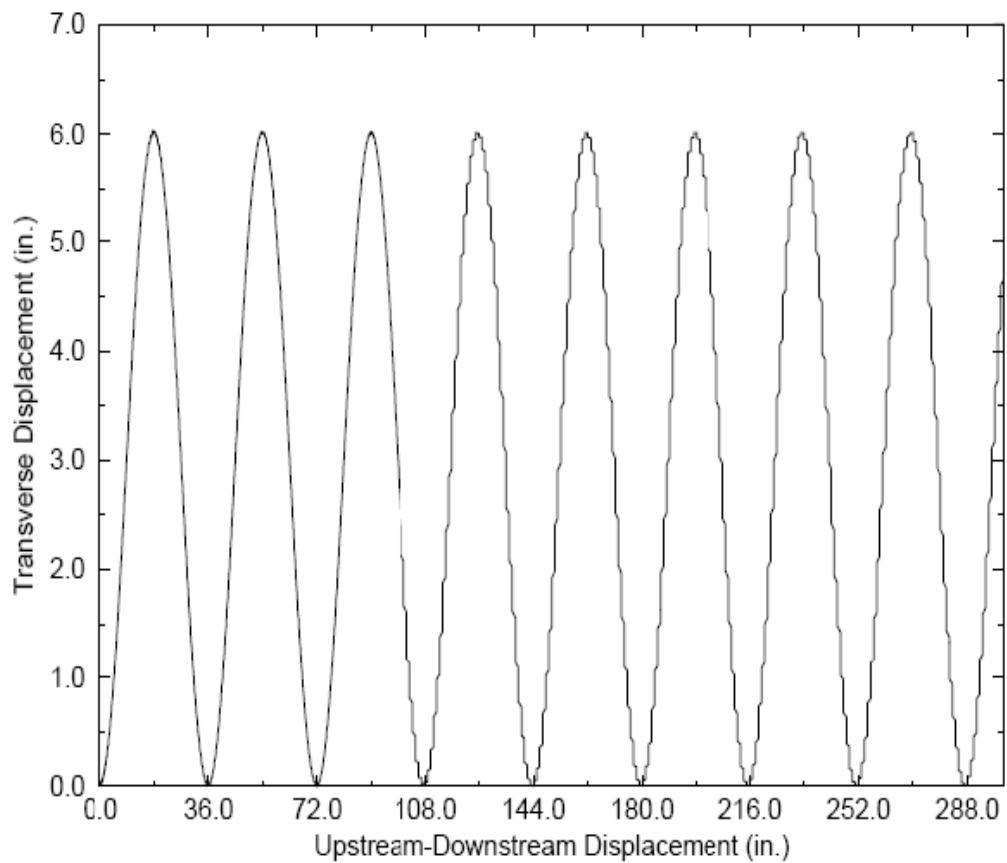


Figure 15.—Transverse displacements vs. upstream/downstream displacements (Noble and Solberg, 2004).

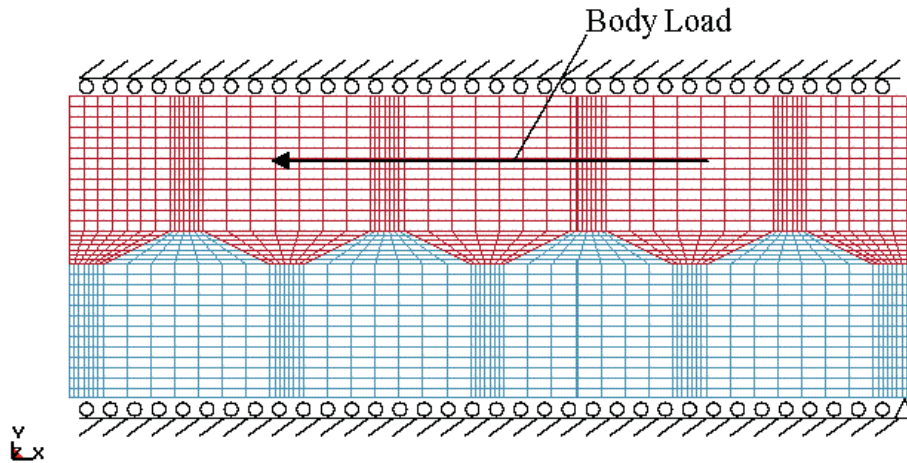


Figure 16.—FEM model with loads and boundary conditions.

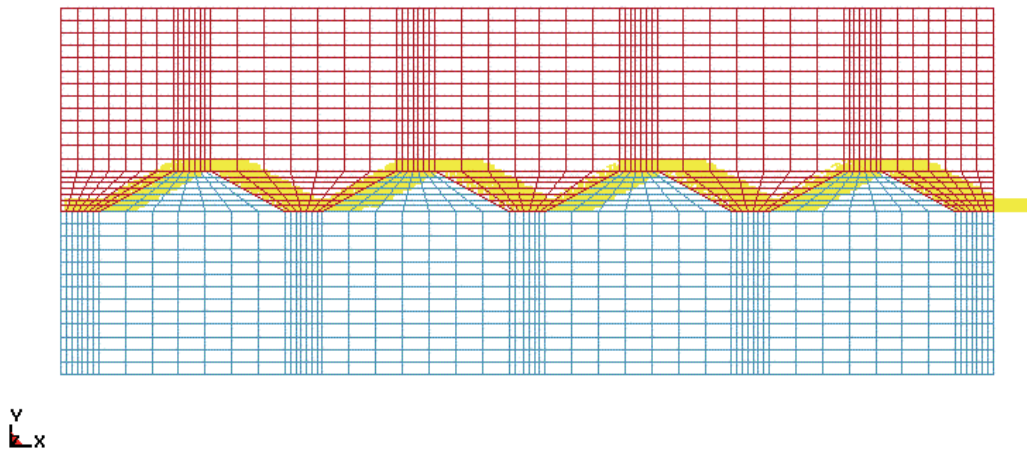


Figure 17.—Contact surface locations in yellow.

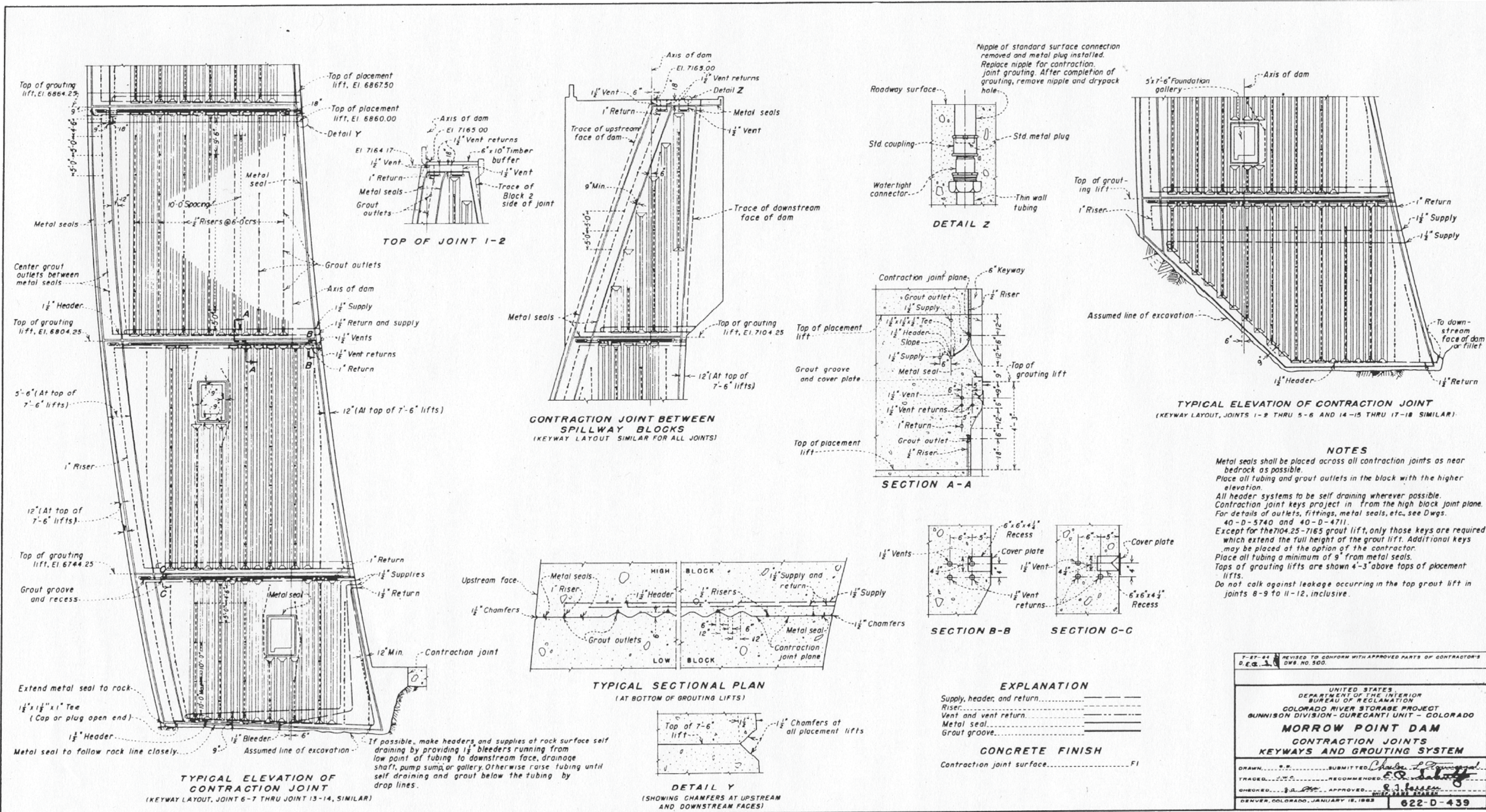
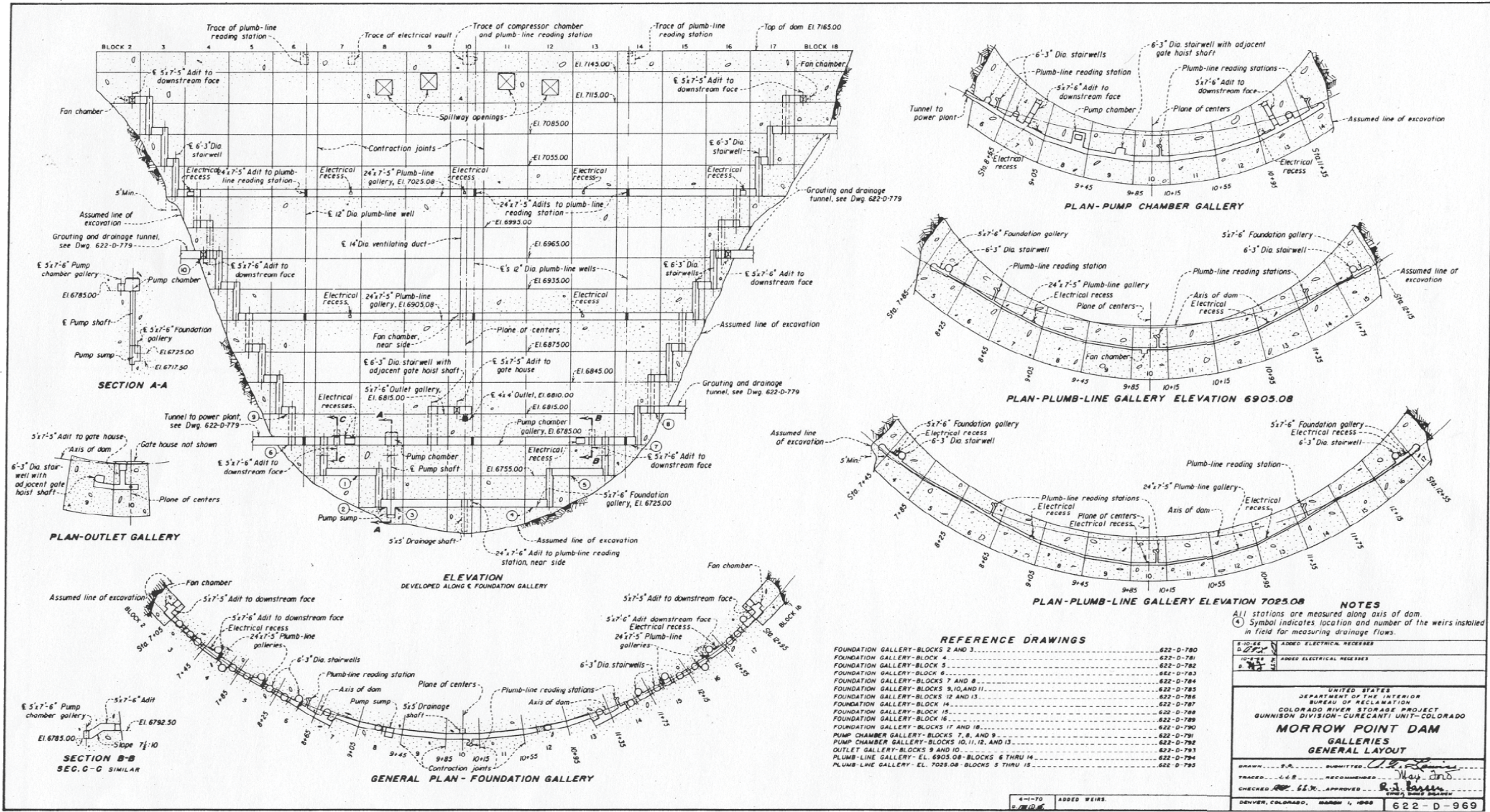


Figure 18.—Morrow Point Dam contraction joints keyways and grouting system.



REFERENCE DRAWINGS

FOUNDATION GALLERY-BLOCKS 2 AND 3.....	622-D-780
FOUNDATION GALLERY-BLOCK 4.....	622-D-781
FOUNDATION GALLERY-BLOCK 5.....	622-D-782
FOUNDATION GALLERY-BLOCK 6.....	622-D-783
FOUNDATION GALLERY-BLOCKS 7 AND 8.....	622-D-784
FOUNDATION GALLERY-BLOCKS 9,10,AND 11.....	622-D-785
FOUNDATION GALLERY-BLOCKS 12 AND 13.....	622-D-786
FOUNDATION GALLERY-BLOCK 14.....	622-D-787
FOUNDATION GALLERY-BLOCK 15.....	622-D-788
FOUNDATION GALLERY-BLOCK 16.....	622-D-789
FOUNDATION GALLERY-BLOCKS 17 AND 18.....	622-D-790
PUMP CHAMBER GALLERY-BLOCKS 7, 8, AND 9.....	622-D-791
PUMP CHAMBER GALLERY-BLOCKS 10, 11, 12, AND 13.....	622-D-792
OUTLET GALLERY-BLOCKS 9 AND 10.....	622-D-793
PLUMB-LINE GALLERY-EL. 6905.08-BLOCKS 6 THRU 16.....	622-D-794
PLUMB-LINE GALLERY-EL. 7025.08-BLOCKS 5 THRU 15.....	622-D-795

NOTES
 All stations are measured along axis of dam.
 (4) Symbol indicates location and number of the weirs installed in field for measuring drainage flows.

2-10-46	ADDED ELECTRICAL RECESSES
10-1-48	ADDED ELECTRICAL RECESSES
2-1-48	

UNITED STATES
 DEPARTMENT OF THE INTERIOR
 BUREAU OF RECLAMATION
 COLORADO RIVER STORAGE PROJECT
 GUNNISON DIVISION-CURECANTI UNIT-COLORADO
MORROW POINT DAM
GALLERIES
GENERAL LAYOUT

BRAWN.....S.E. SUBMITTED.....*U.L. Lewis*
 TRACED.....C.E.R. RECOMMENDED.....*May and*
 CHECKED.....S.S. APPROVED.....*R.J. Bassen*
 DENVER, COLORADO, MARCH 1, 1968

Figure 19.—Morrow Point Dam galleries general layout.

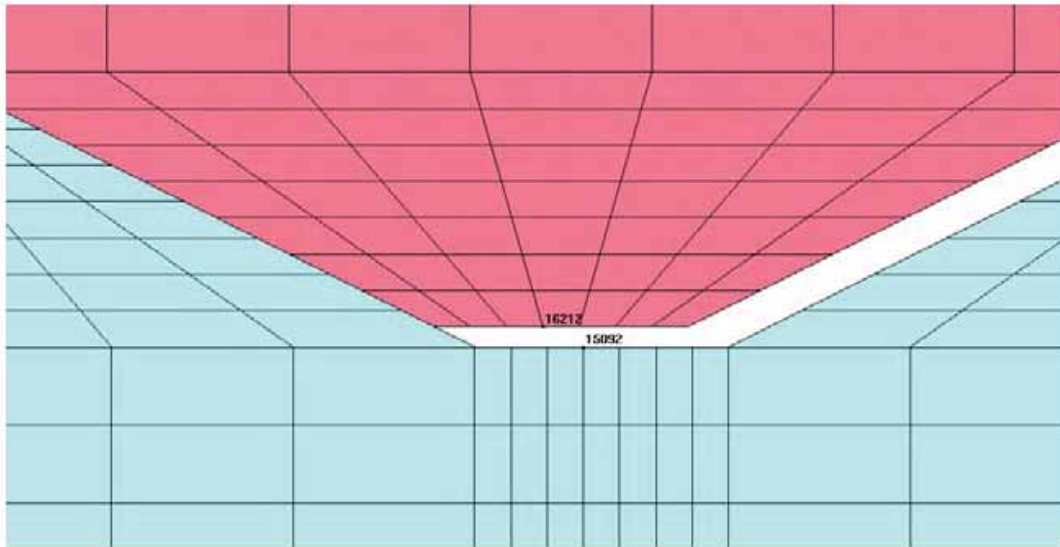


Figure 20.—Node locations for y-displacement plot in figure 21. Analysis I.

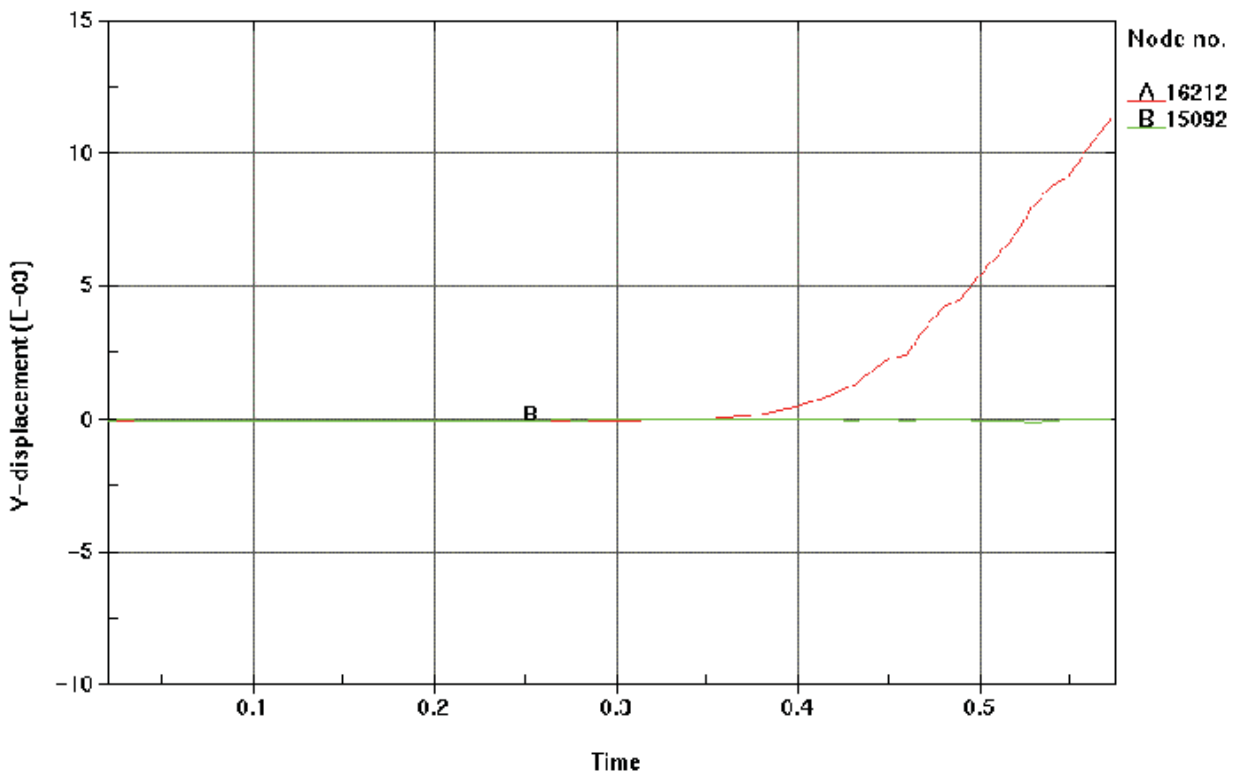
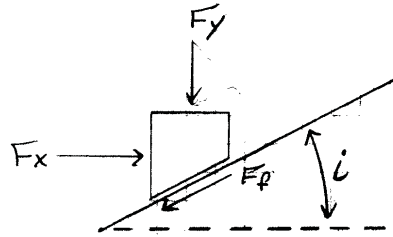
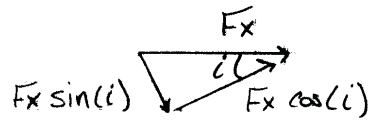
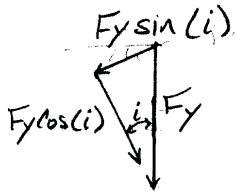


Figure 21.—Y-displacement for nodes shown in figure 20. Analysis I.



F_x and F_y components parallel and perpendicular to sliding plane:



Sum of Forces Parallel to Sliding Plane:

$$\sum F_{\text{parallel}} = 0; \rightarrow \oplus$$

$$-F_t + F_x \cos i - F_y \sin i = 0$$

Sum of Forces Perpendicular to Sliding Plane:

$$\sum F_{\text{perpendicular}} = 0; \uparrow \oplus$$

$$F_n - F_y \cos i - F_x \sin i = 0$$

$$F_n = F_y \cos i + F_x \sin i$$

Force of Friction:

$$F_t = F_n \cdot \tan(\phi) = (F_y \cos i + F_x \sin i) \tan \phi$$

Combining $F_t = (F_y \cos i + F_x \sin i) \tan \phi$ and

$$-F_t + F_x \cos i - F_y \sin i = 0 :$$

$$-(F_y \cos i + F_x \sin i) \tan \phi + F_x \cos i - F_y \sin i = 0$$

$$F_y (-\cos i \tan \phi + \sin i) + F_x (-\sin i \tan \phi + \cos i) = 0$$

$$\frac{F_x}{F_y} = \frac{\sin i + \cos i \tan \phi}{\cos i - \sin i \tan \phi}$$

Figure 22.—Sliding initiation formulation.

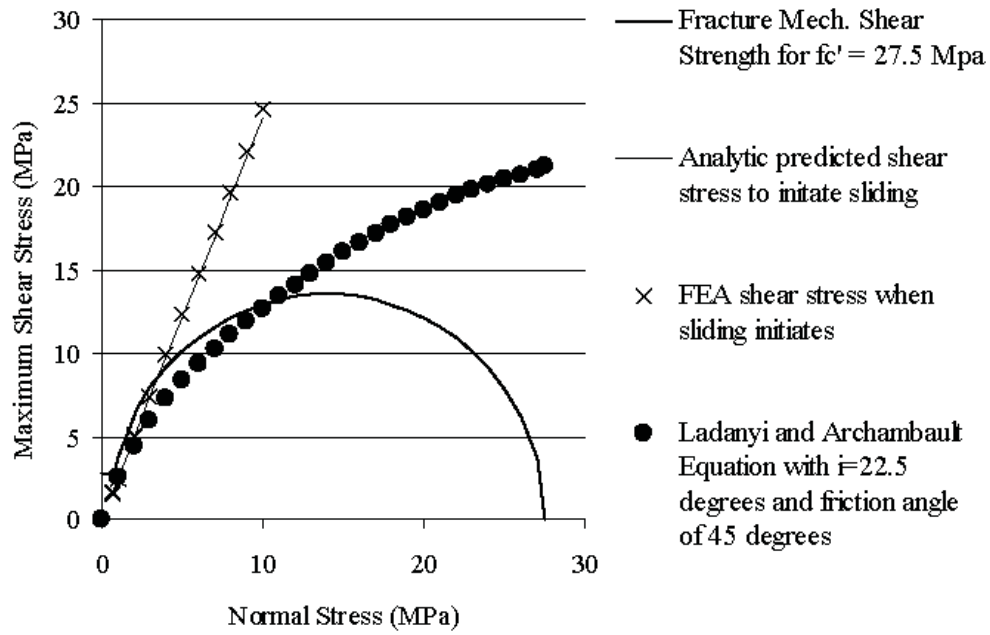


Figure 23.—Plot of shear strengths and sliding initiation.

Time = 3
max displacement factor=400

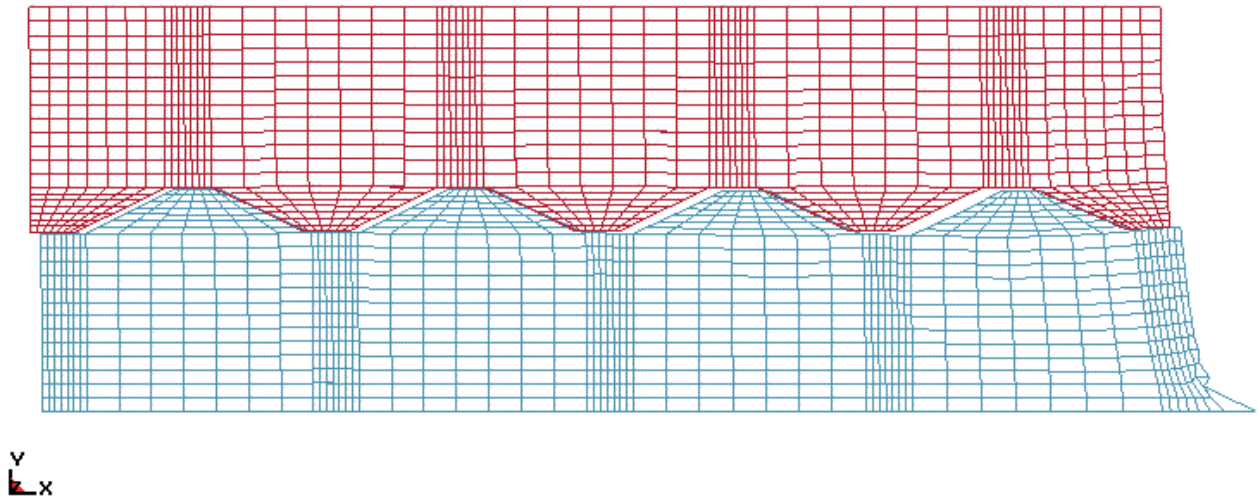


Figure 24.—Deformed shape with body load of 15,000 in/s² at end of 3 seconds.

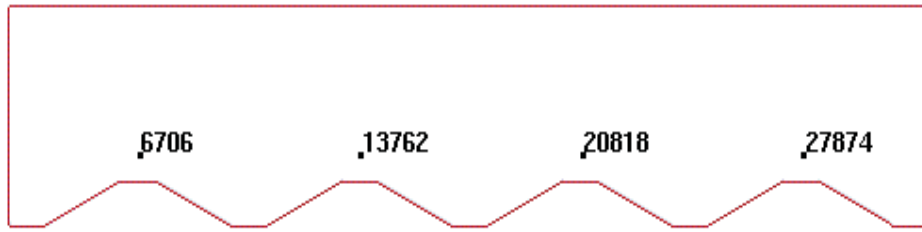


Figure 25.—Node locations for displacement plots.

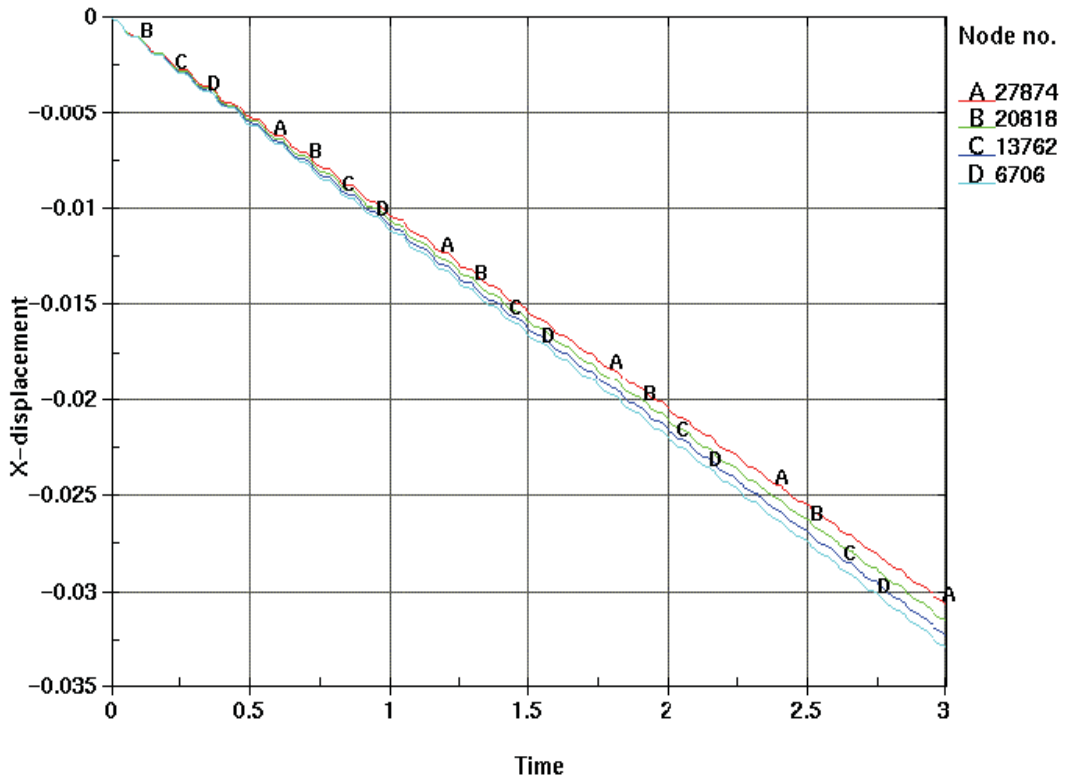


Figure 26.—X-displacements. Analysis II.

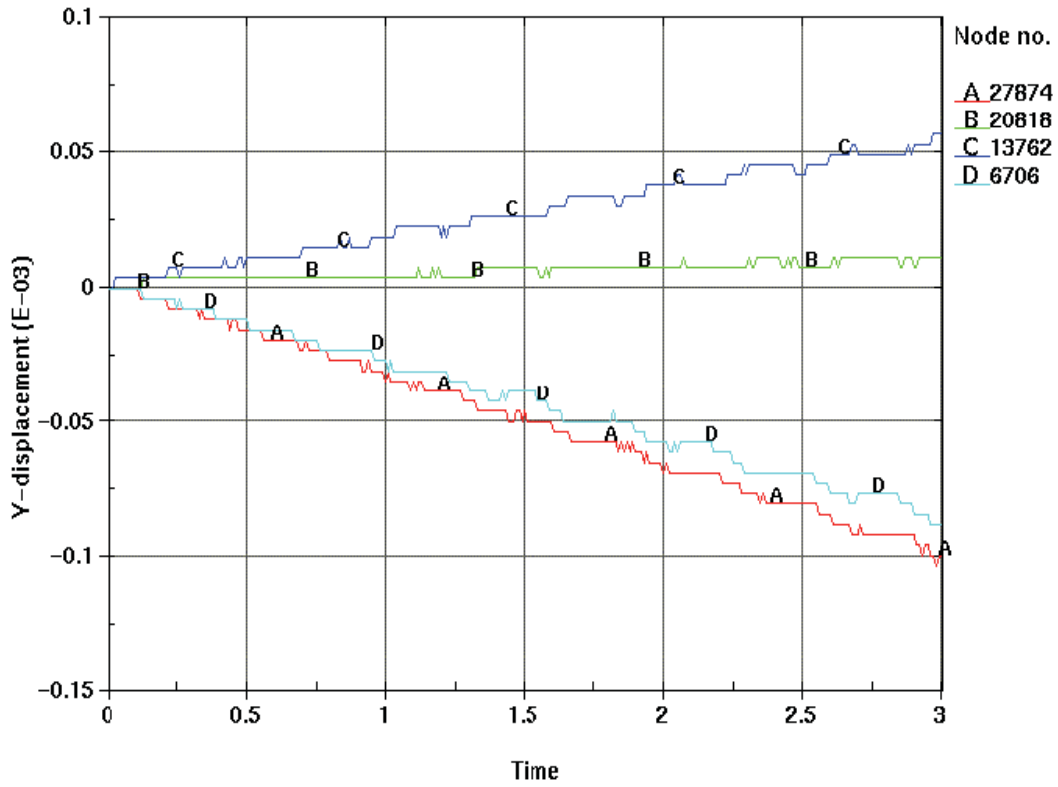


Figure 27.—Y-displacements. Analysis II.

Time = 3
 Contours of Y-stress
 min=-405.628, at elem# 24129
 max=6334.1, at elem# 25032

Fringe Levels

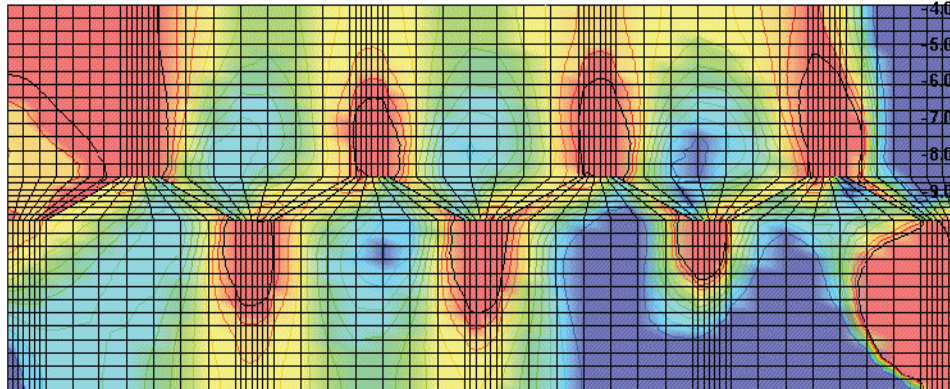
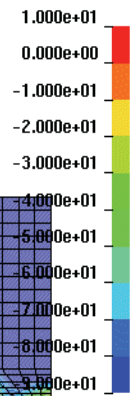


Figure 28.—Y-stress fringe plot. Analysis II.

Time = 3
Contours of XY-stress
min=-5673.44, at elem# 25123
max=1846.16, at elem# 24220

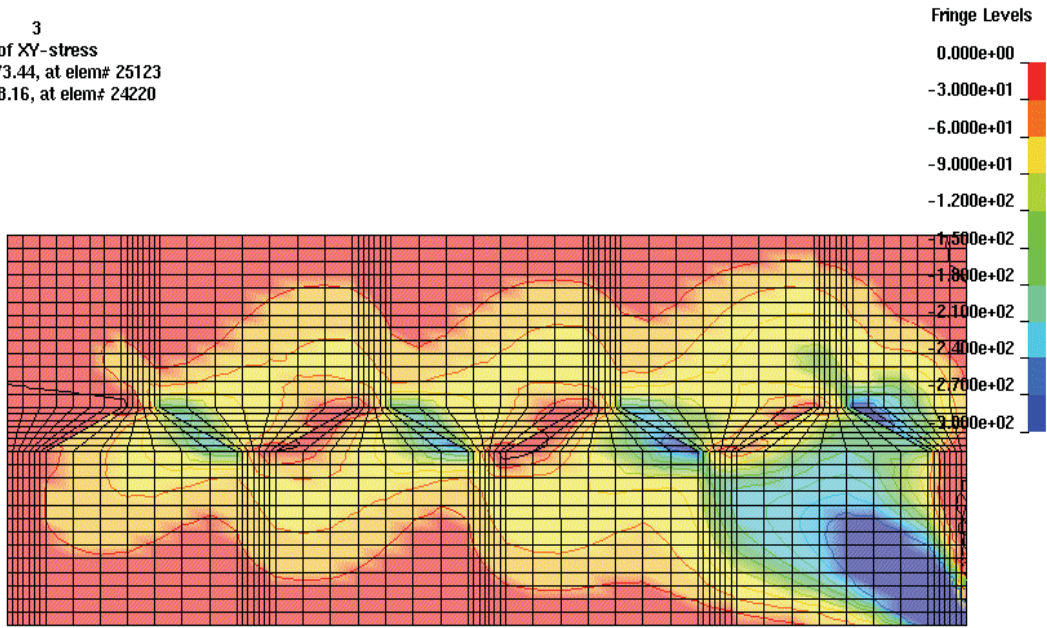


Figure 29.—XY-stress fringe plot. Analysis II.

Time = 3
Contours of Maximum Principal Stress
min=-51.8046, at elem# 22252
max=14821.3, at elem# 25123

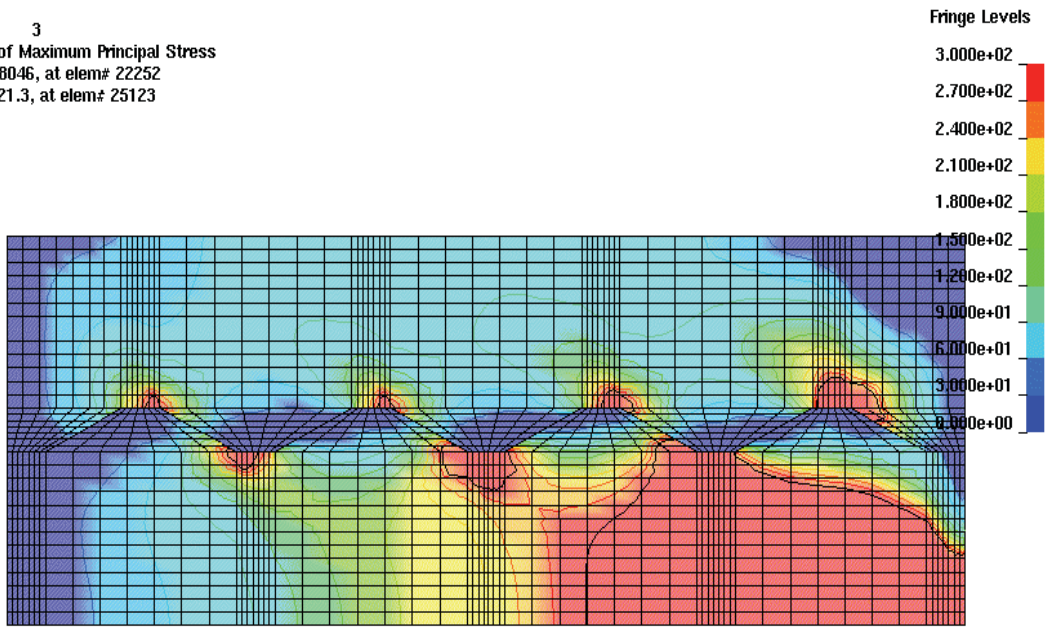


Figure 30.—Maximum principal stress fringe plot. Analysis II.

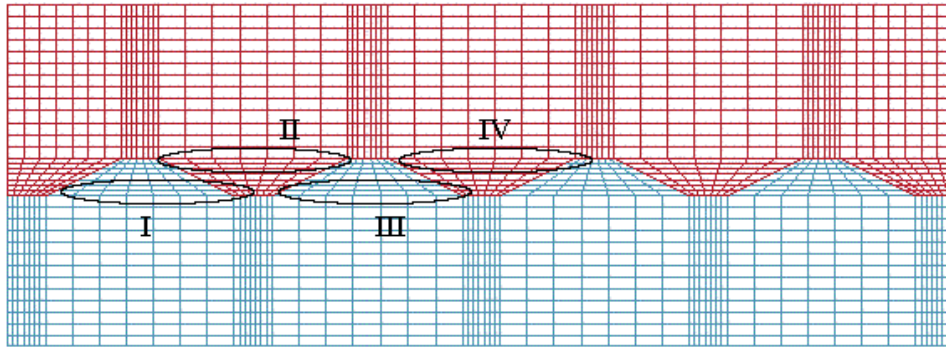


Figure 31.—Regions I through IV for element stress results.

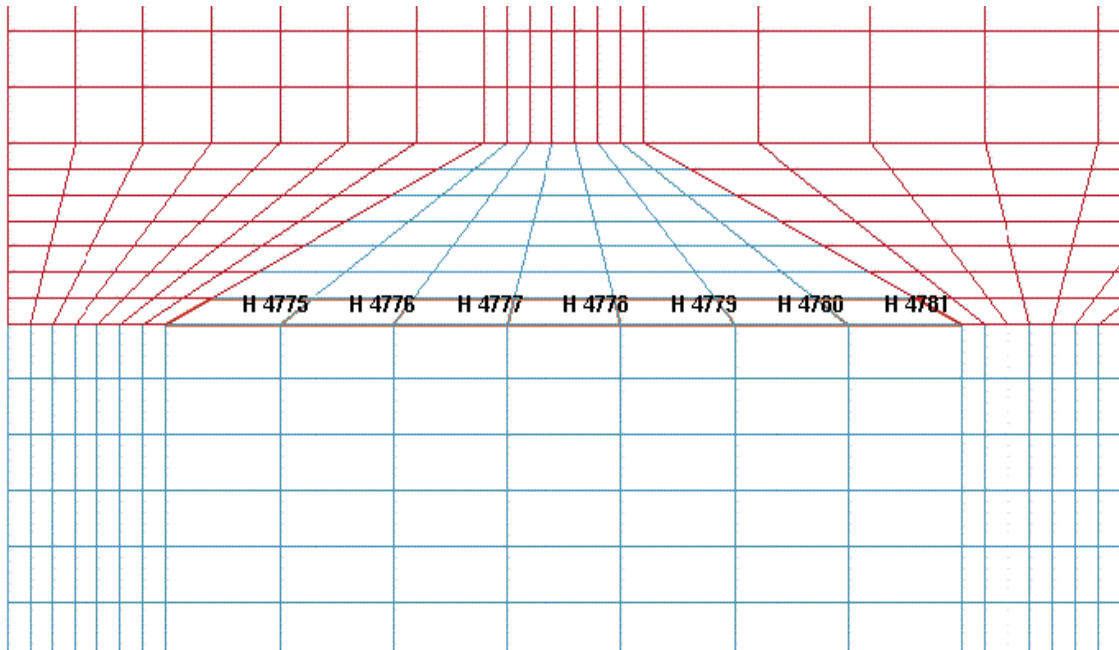


Figure 32.—Element locations for stress results in region I.

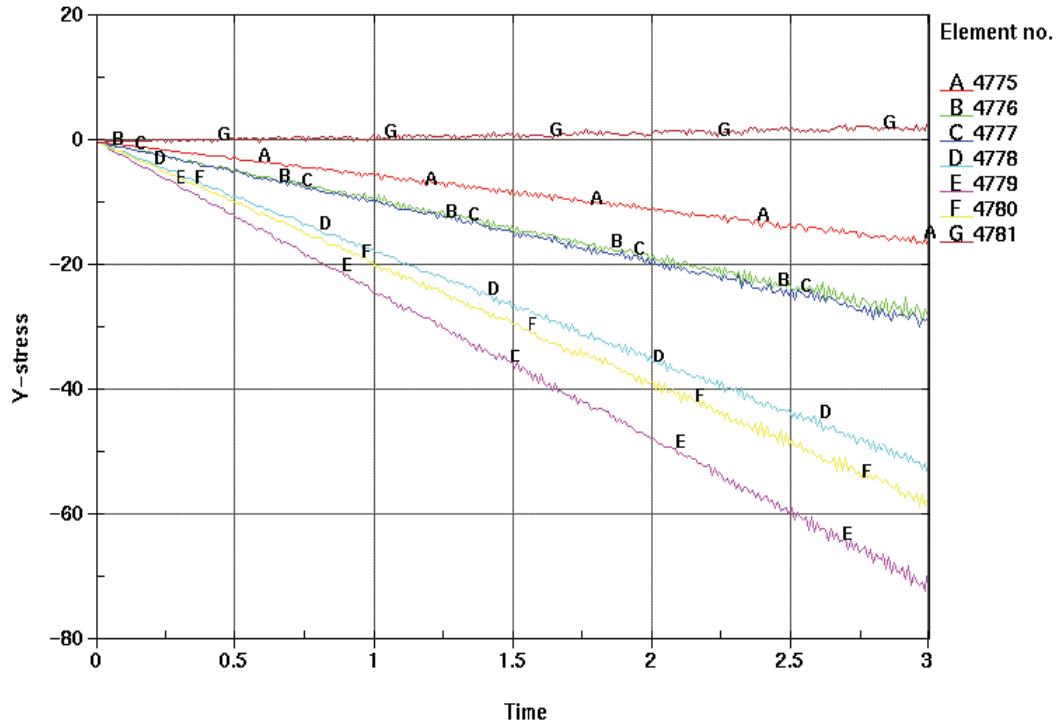


Figure 33.—Y-stress: elements in region I. Analysis II.

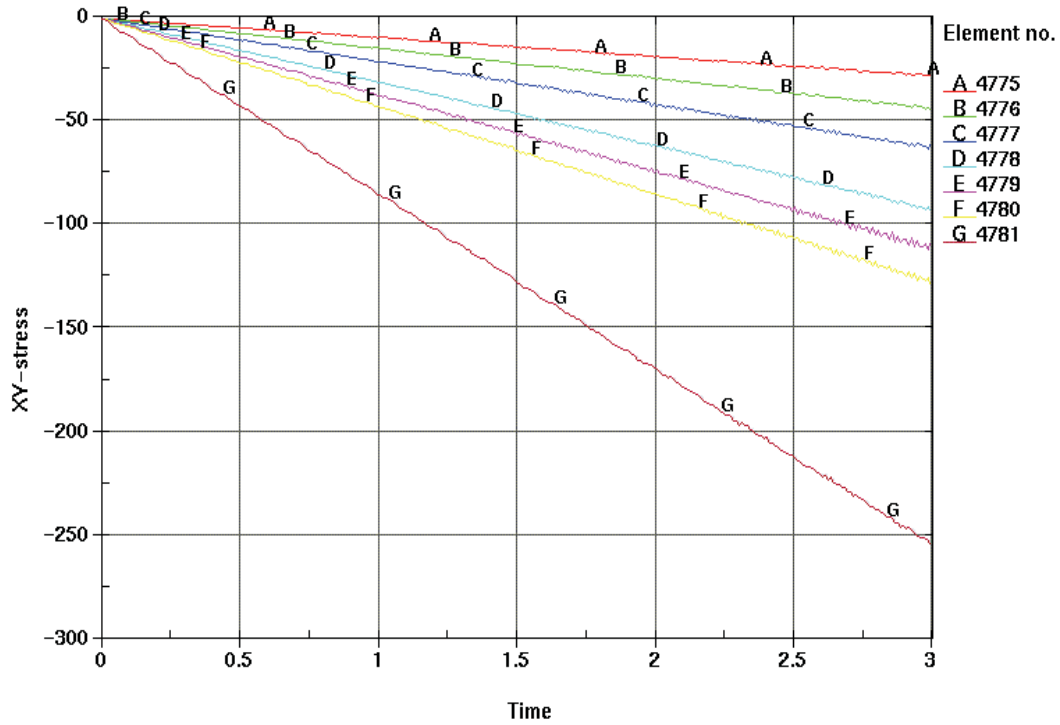


Figure 34.—XY-stress: elements in region I. Analysis II.

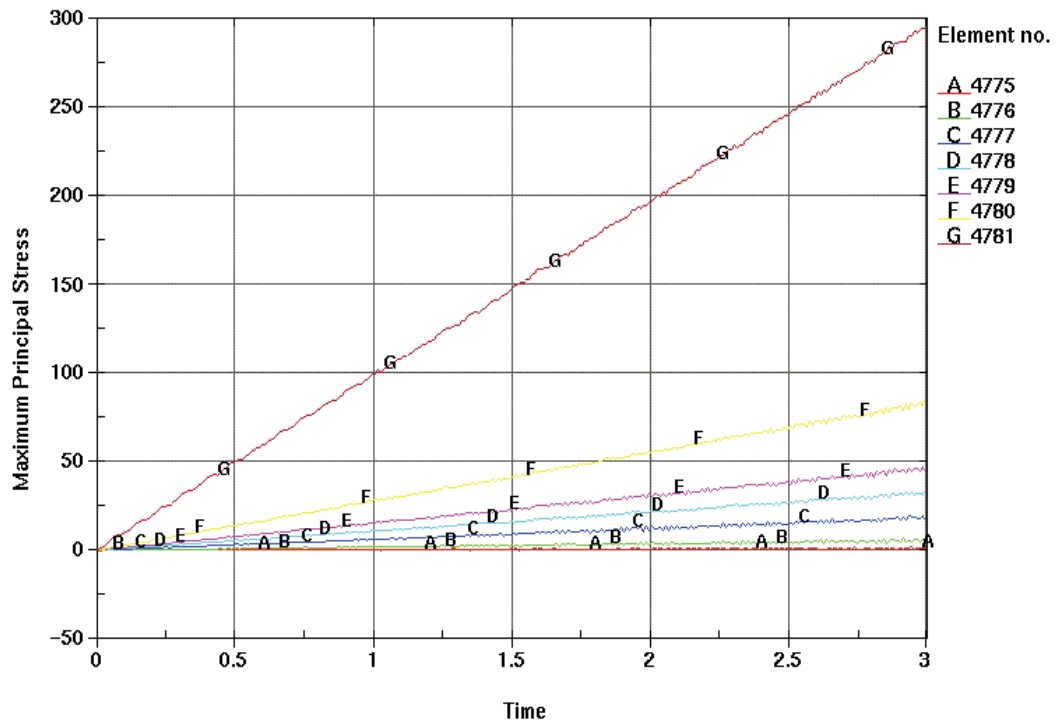


Figure 35.—Maximum principal stress: elements in region I. Analysis II.

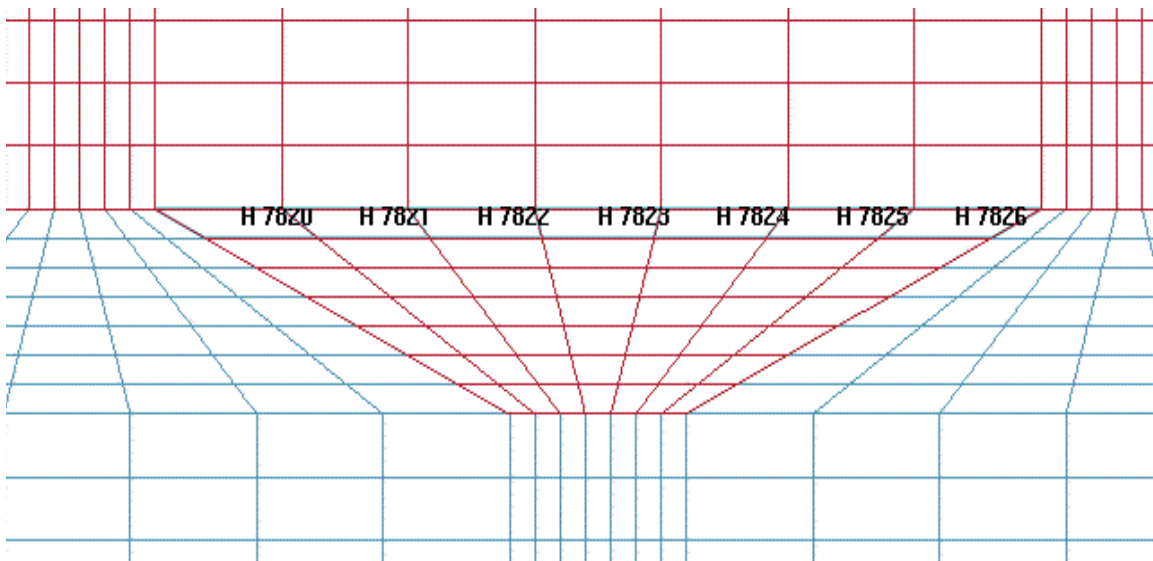


Figure 36.—Element locations for stress results in region II.

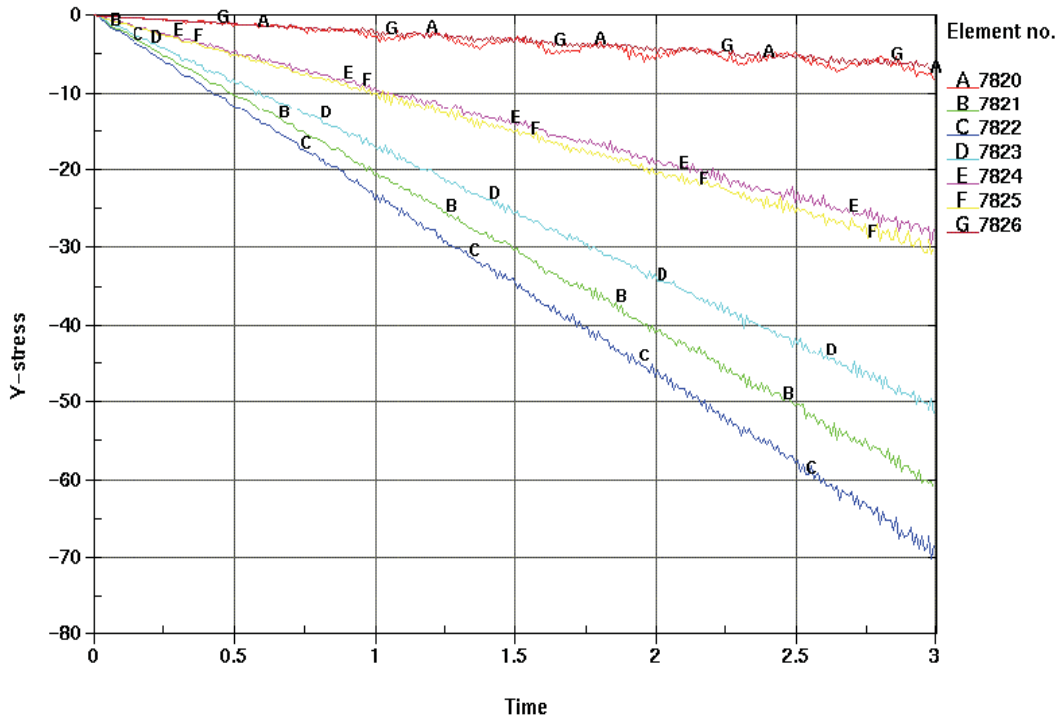


Figure 37.—Y-stress: elements in region II. Analysis II.

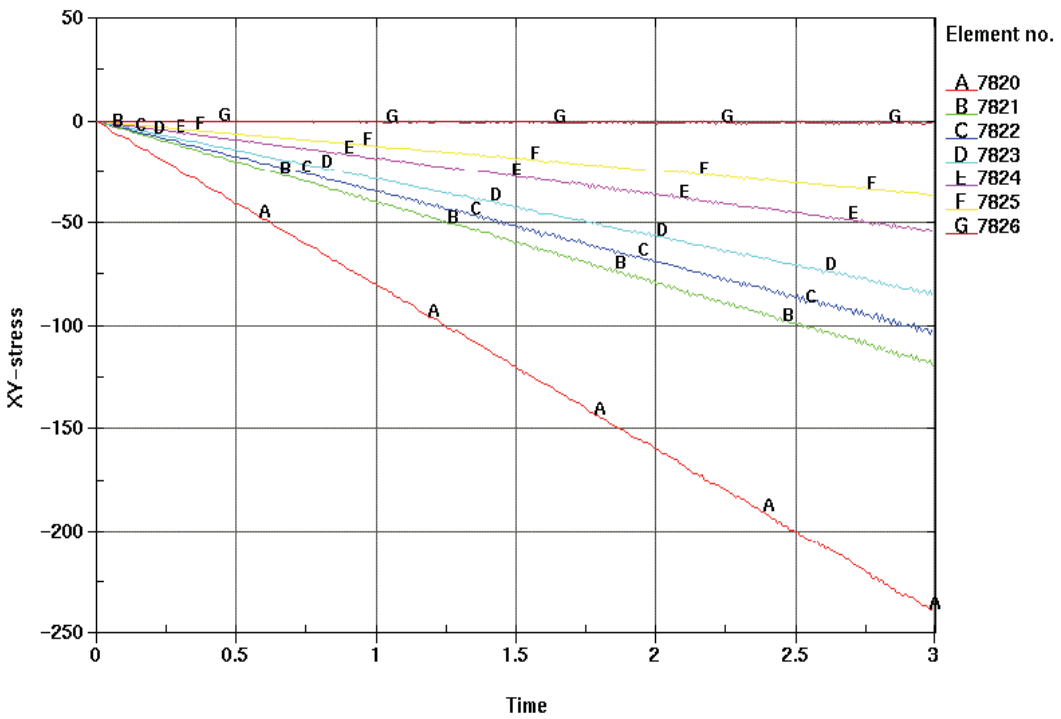


Figure 38.—XY-stress: elements in region II. Analysis II.

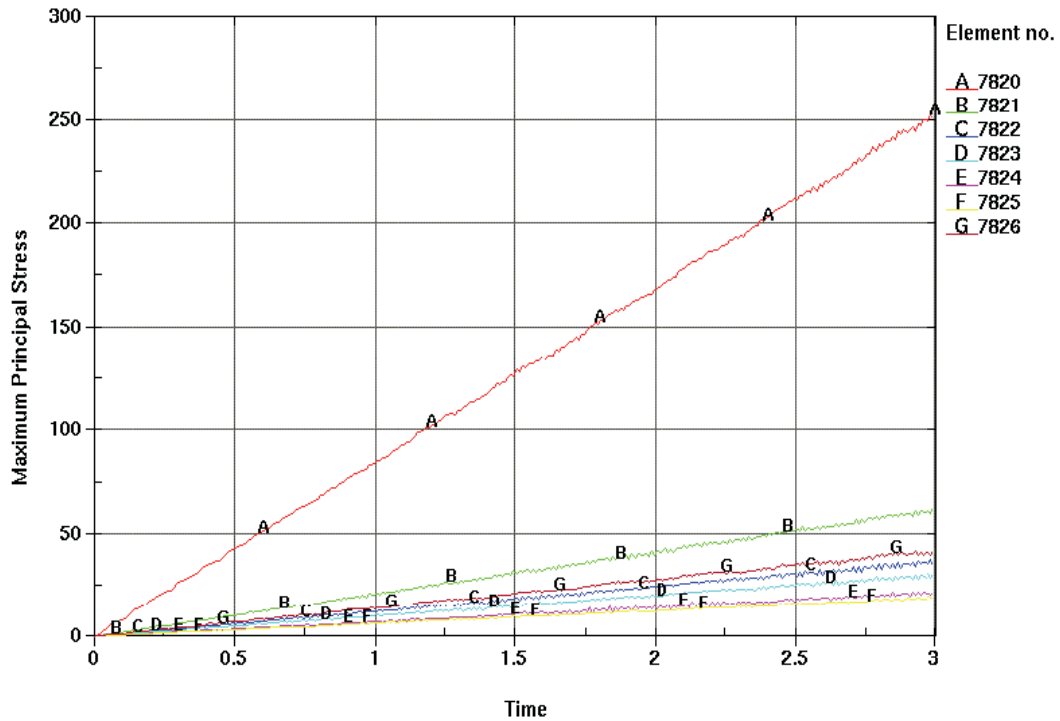


Figure 39.—Maximum principal stress: elements in region II. Analysis II.

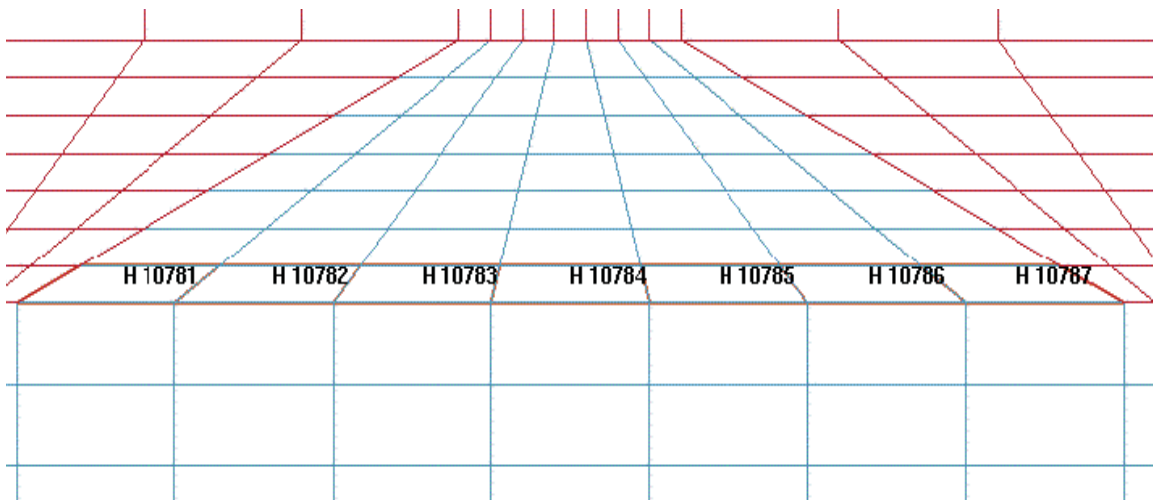


Figure 40.—Element locations and labels for stress results in region III. Analysis II.

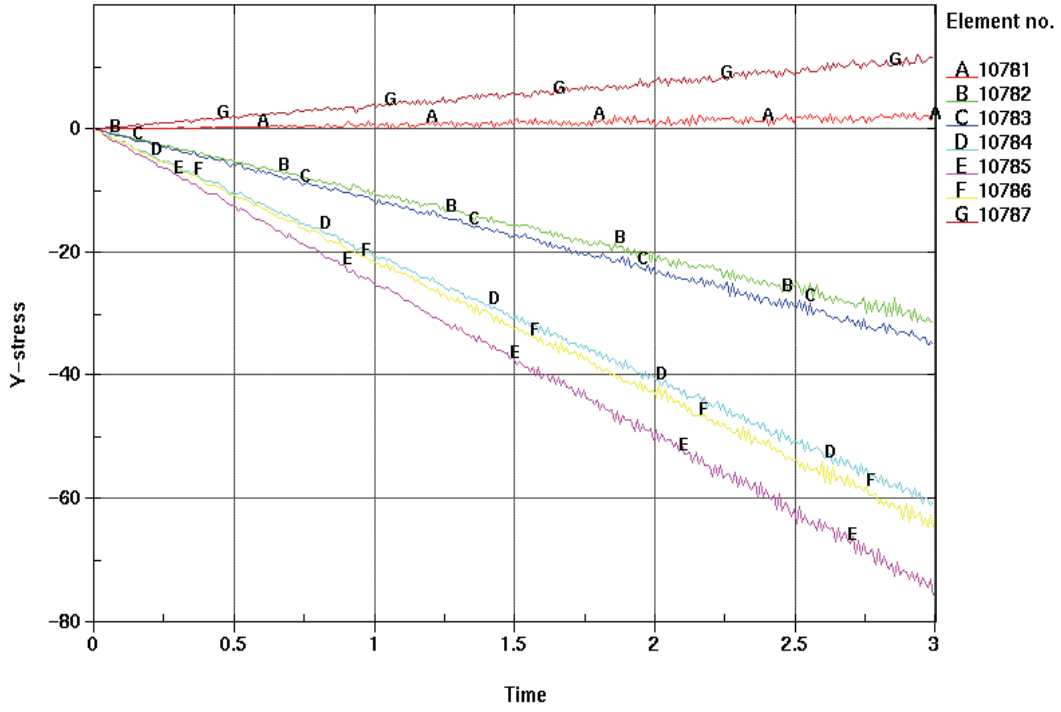


Figure 41.—Y-stress: elements in region III. Analysis II.

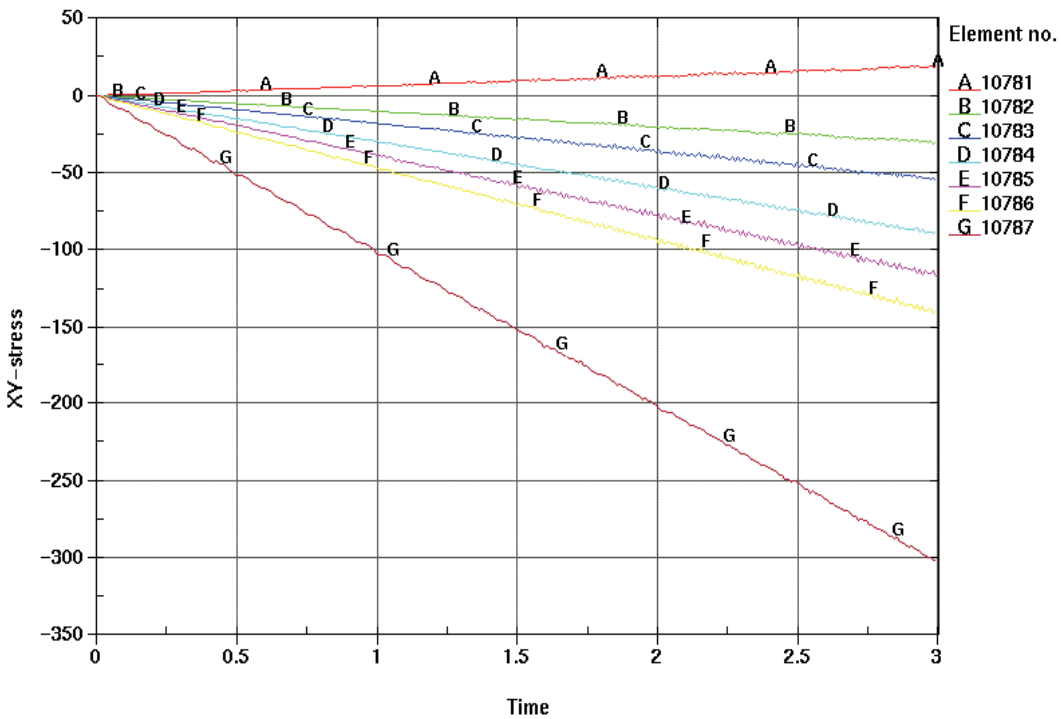


Figure 42.—XY-stress: elements in region III. Analysis II.

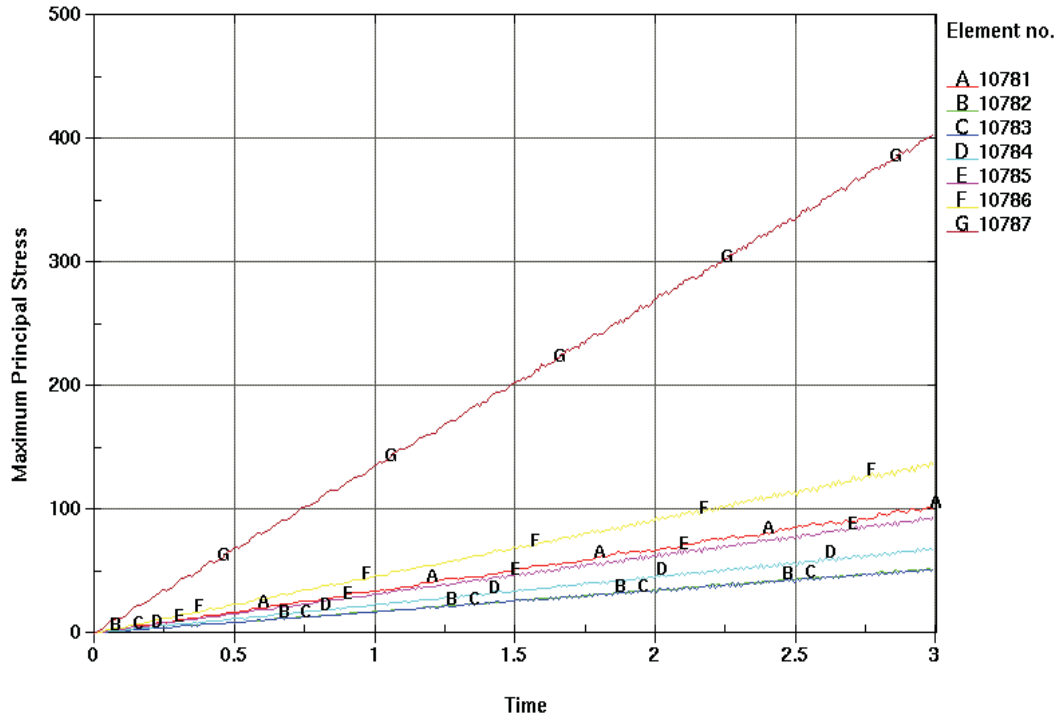


Figure 43.—Maximum principal stress: elements in region III. Analysis II.

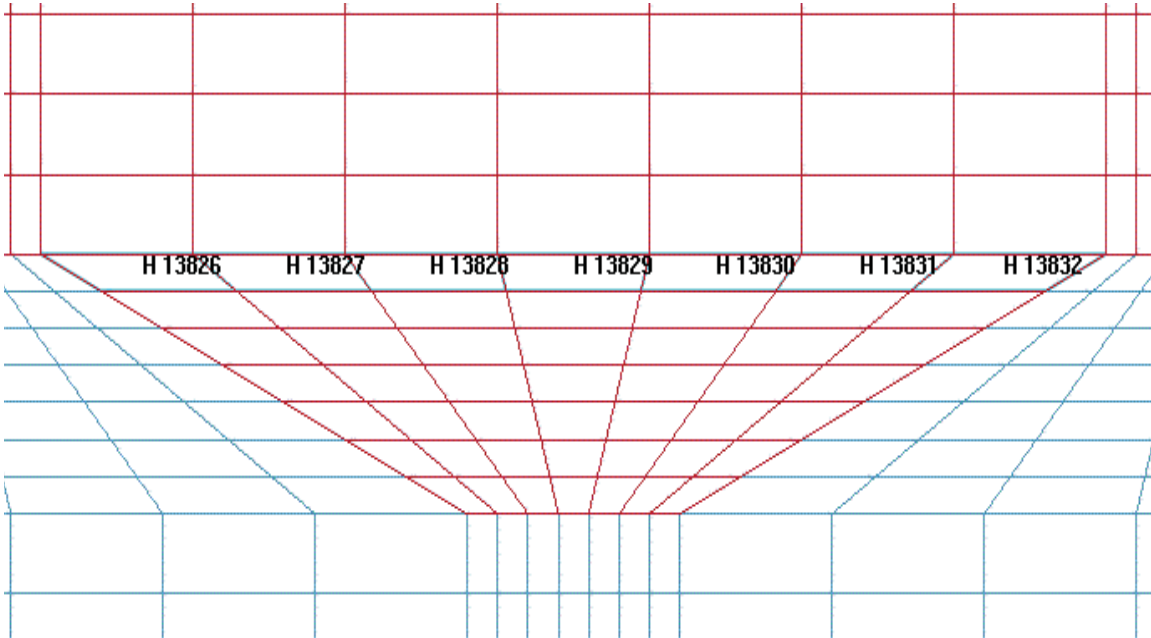


Figure 44.—Element locations and labels for stress results in region IV.

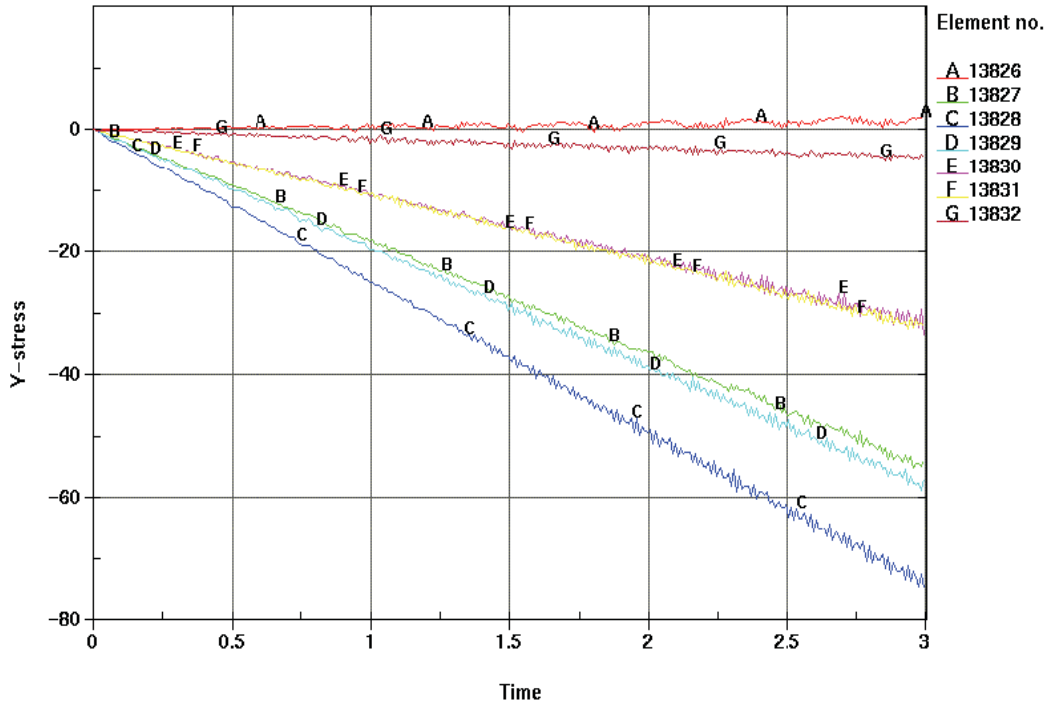


Figure 45.—Y-stress: elements in region IV. Analysis II.

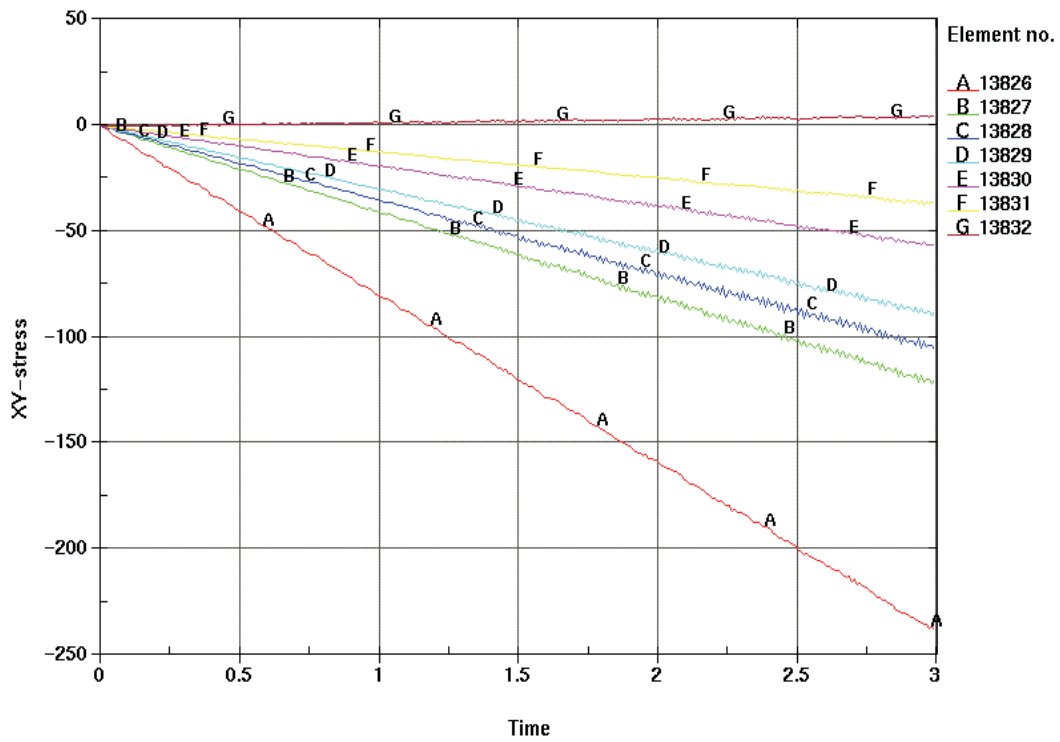


Figure 46.—XY-stress: elements in region IV. Analysis II.

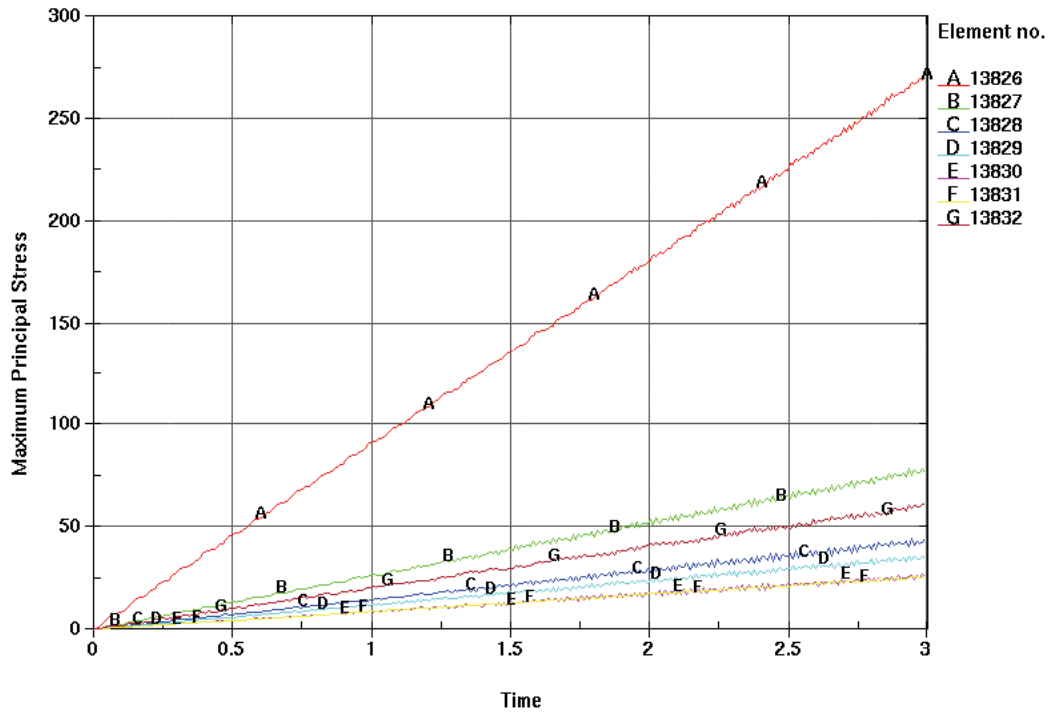


Figure 47.—Maximum principal stress: elements in region IV. Analysis II.

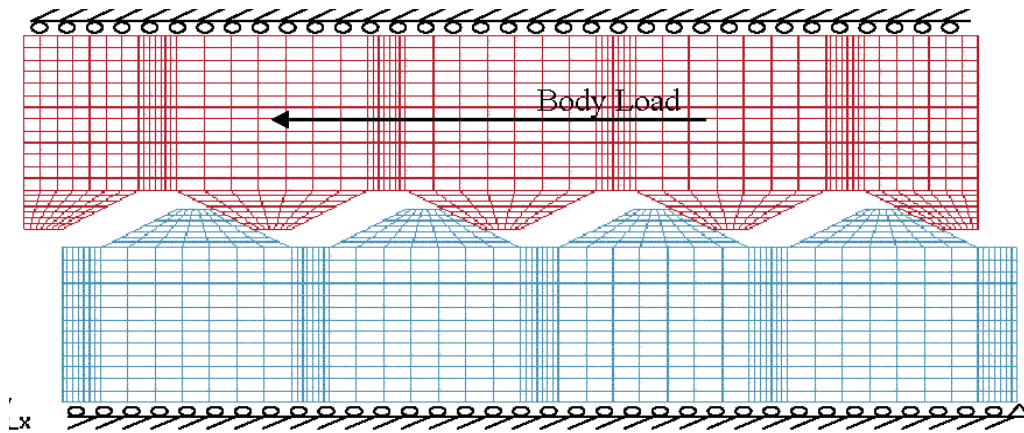


Figure 48.—FEM model, initial condition with-3 inch gap. Analysis III.

Time = 3
max displacement factor=400

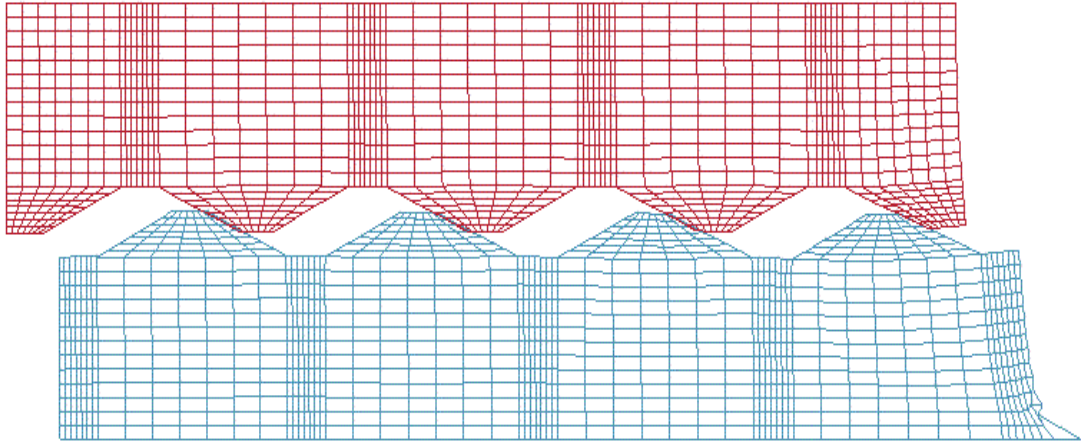


Figure 49.—Deformed shape with body load of $15,000 \text{ in/s}^2$ at end of 3 seconds. Analysis III.

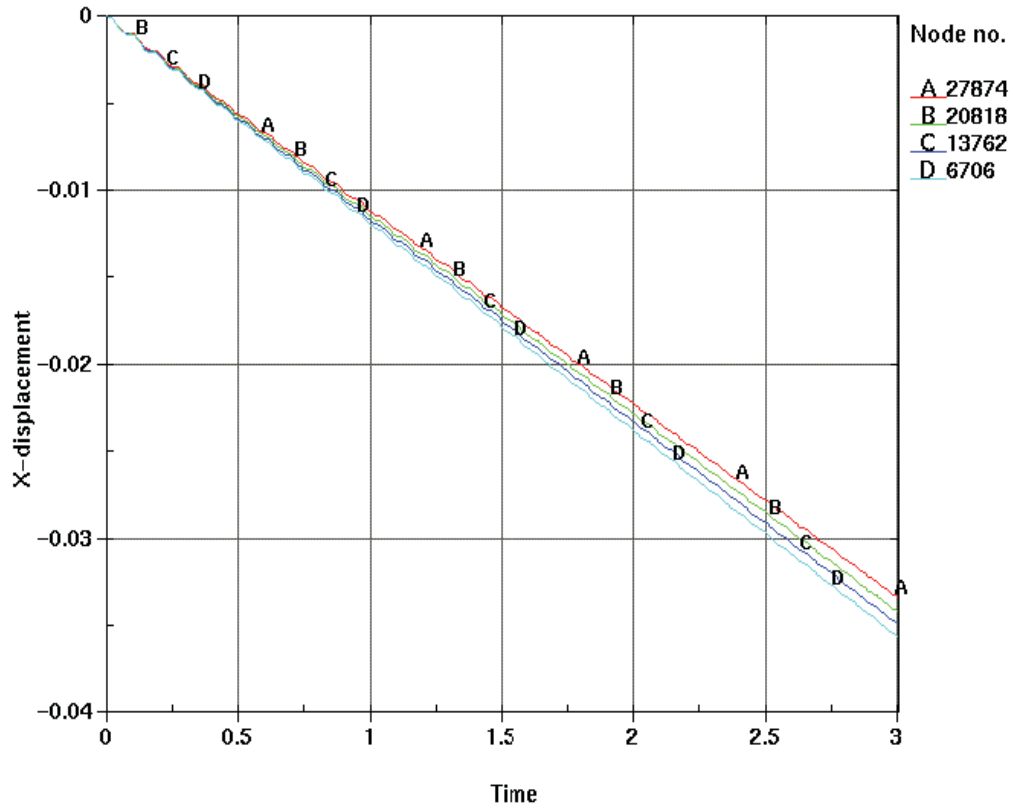


Figure 50.—X-displacements. Analysis III.

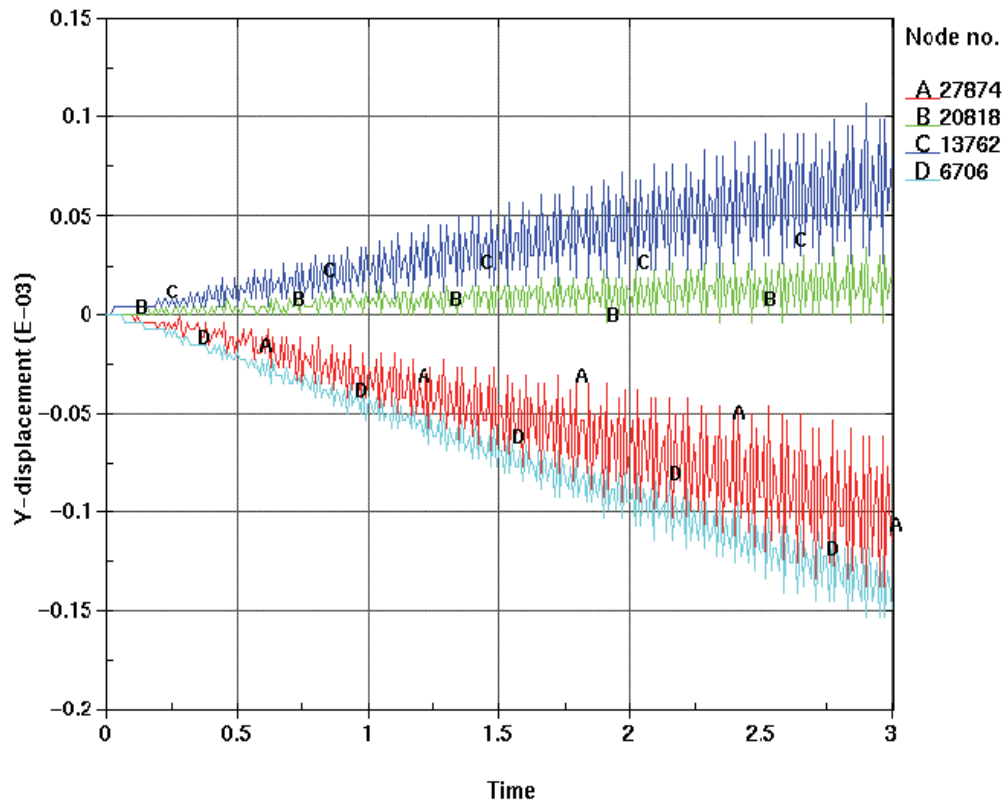


Figure 51.—Y-displacements. Analysis III.

Time = 3
 Contours of Y-stress
 min=-416.886, at elem# 25130
 max=6321.67, at elem# 24304

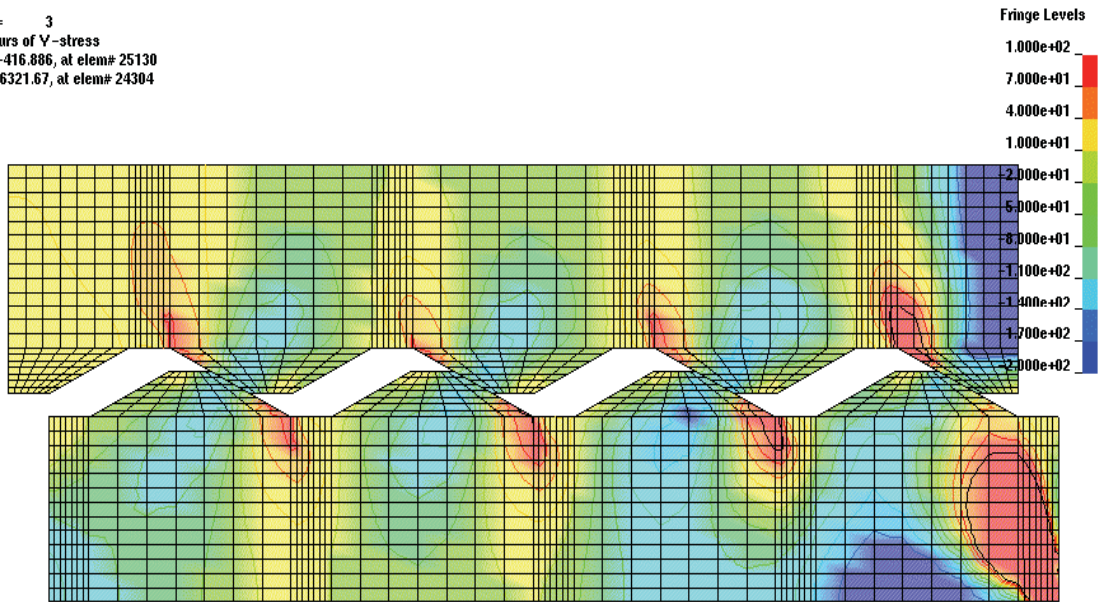


Figure 52.—Y-stress fringe plot. Analysis III.

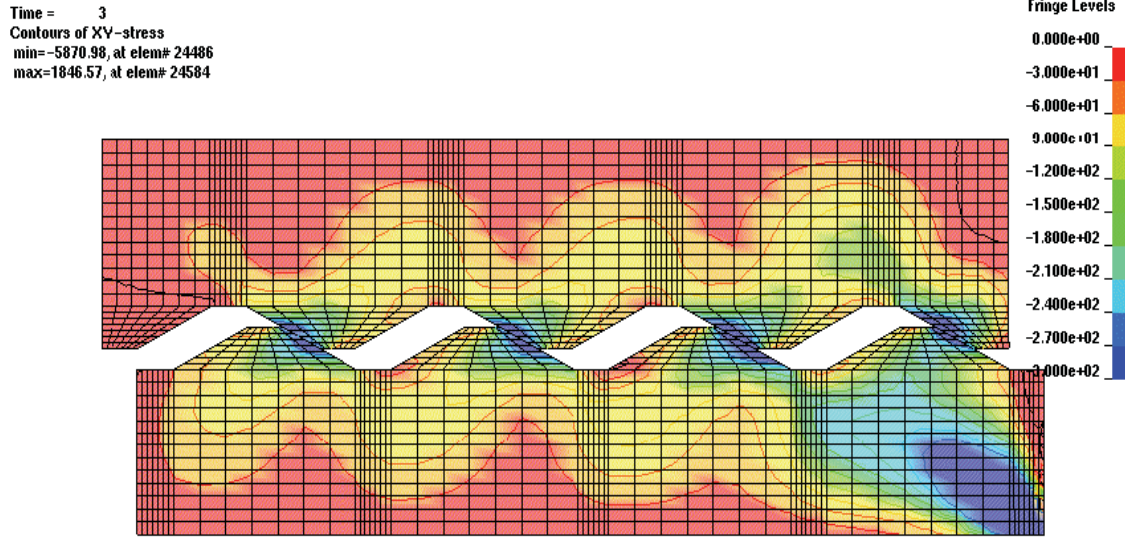


Figure 53.—XY-stress fringe plot for region I elements. Analysis III.

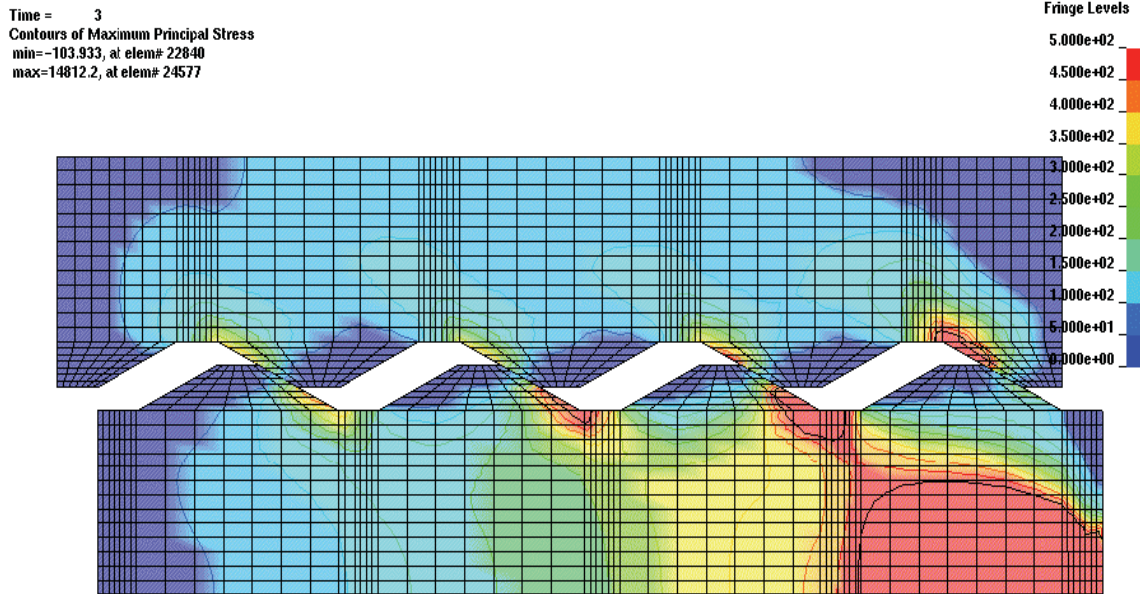


Figure 54.—Maximum principal stress fringe plot. Analysis III.

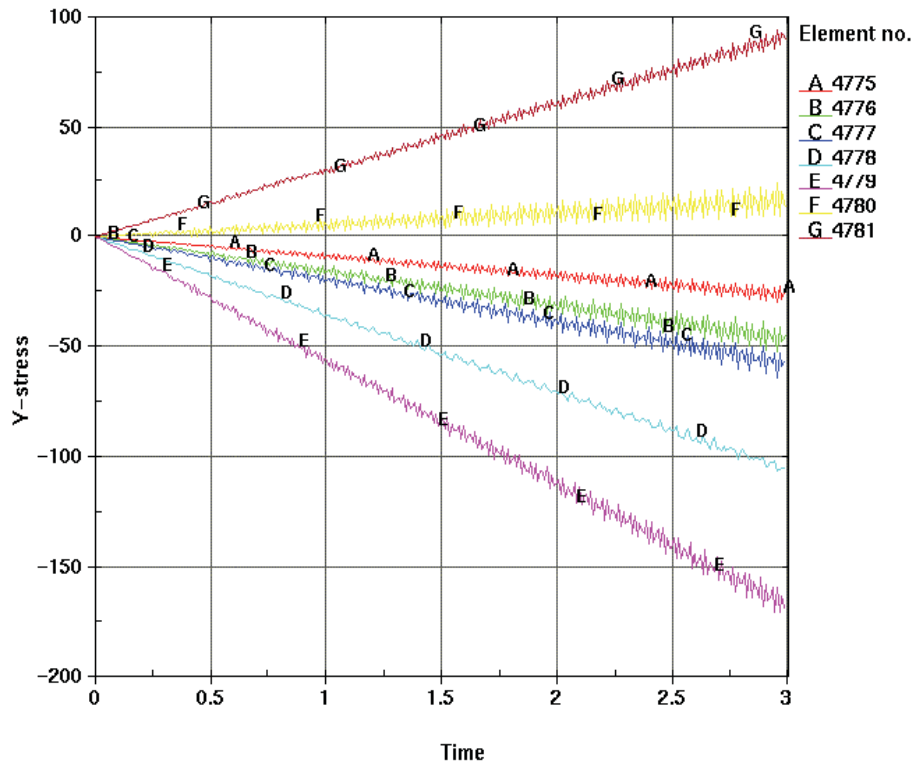


Figure 55.—Y-stress: elements in region I. Analysis III.

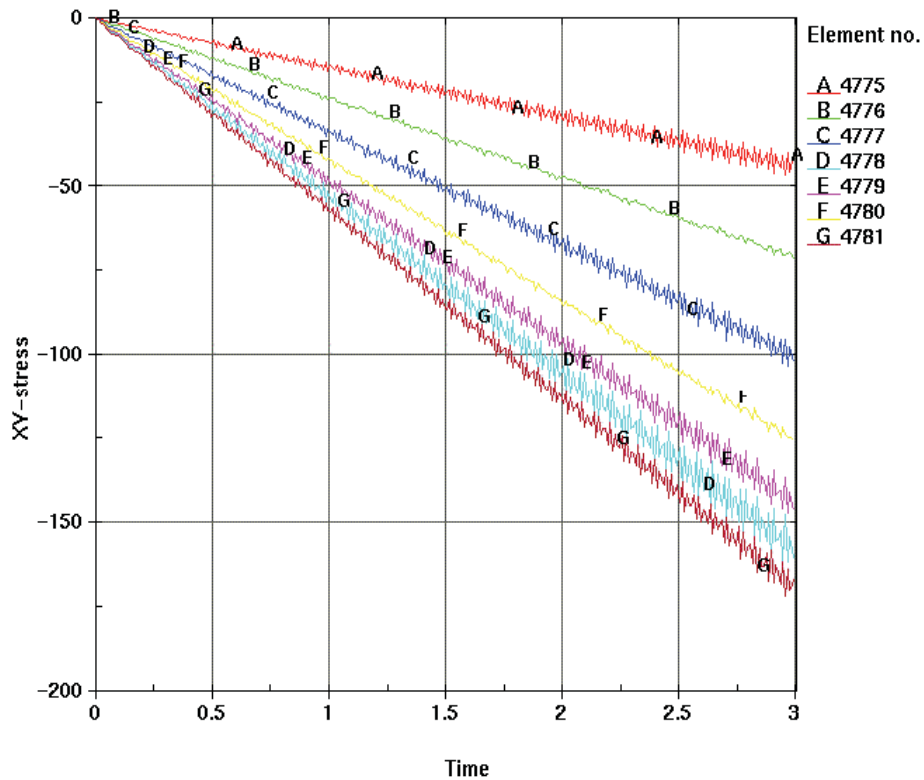


Figure 56.—XY-stress for elements in region I. Analysis III.

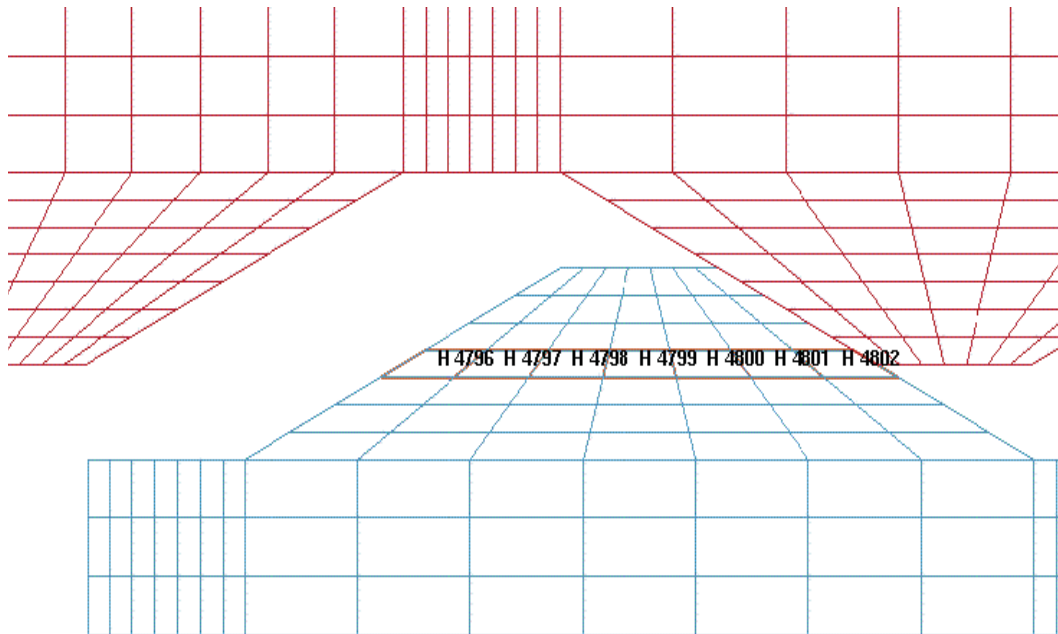


Figure 57.—Element location and labels for XY-stress of partially open joint.

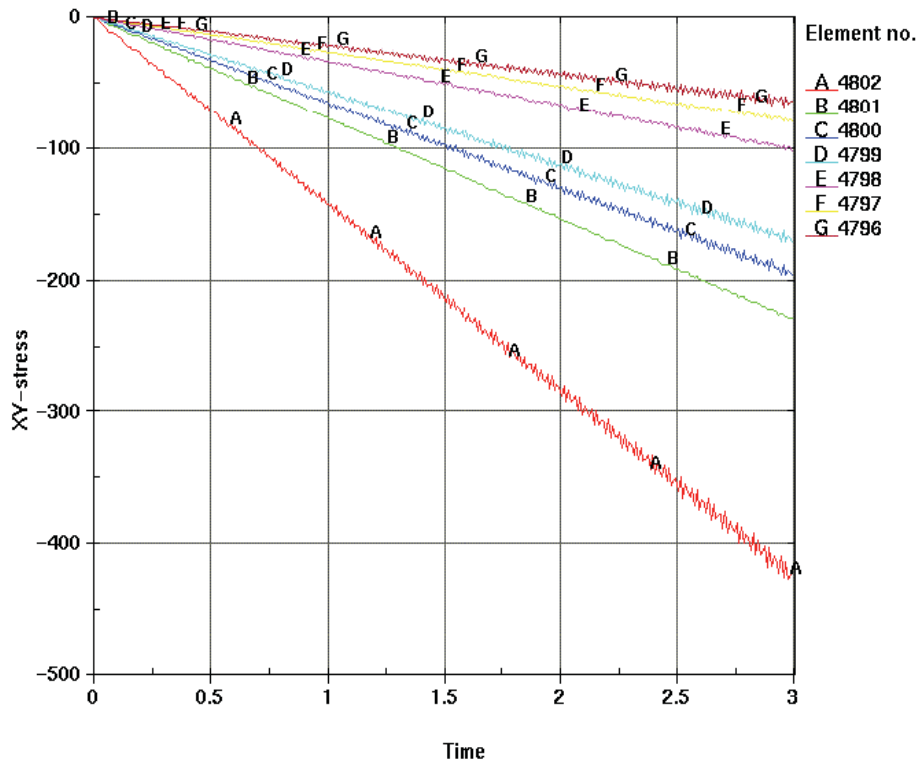


Figure 58.—XY-stress for elements shown in figure 56. Analysis III.

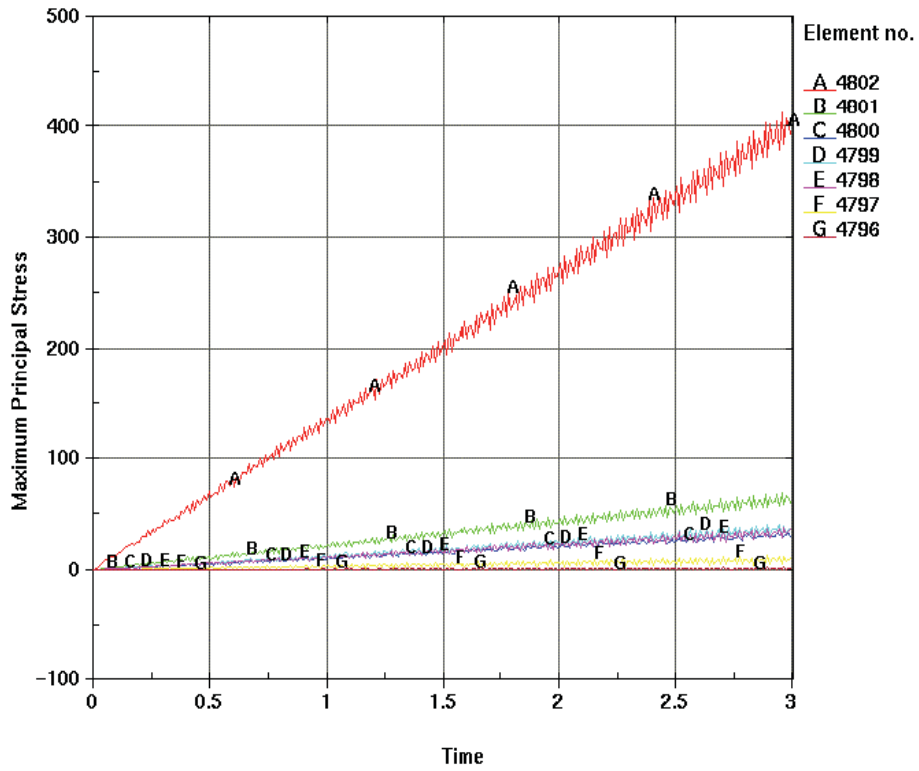


Figure 59.—Maximum principal stress for elements shown in figure 56. Analysis III.

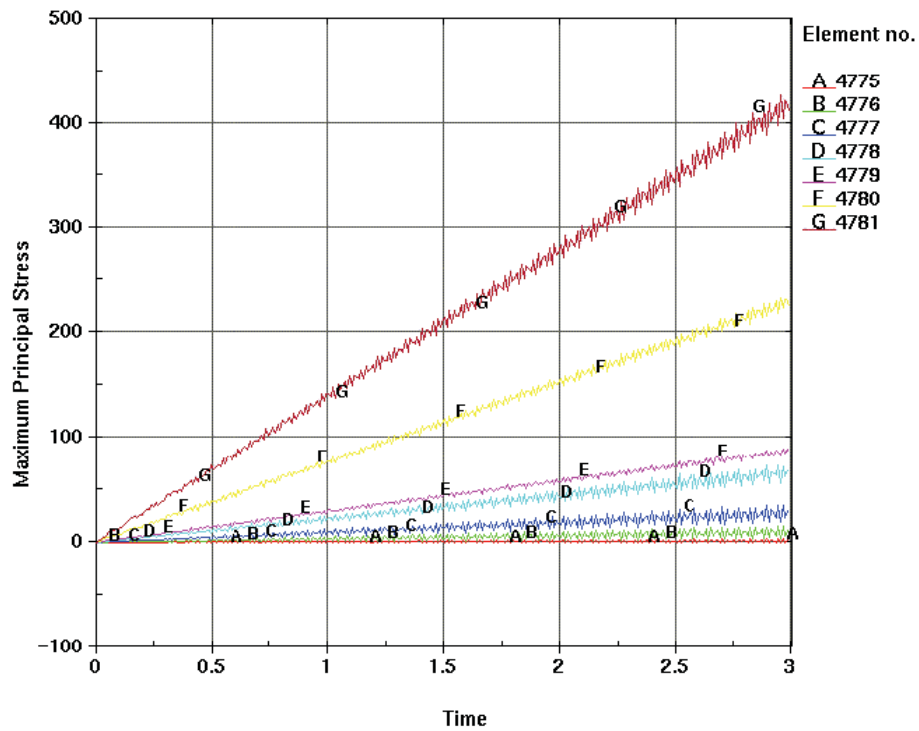


Figure 60.—Maximum principal stress for elements in region I. Analysis III.

Time = 3
max displacement factor=400

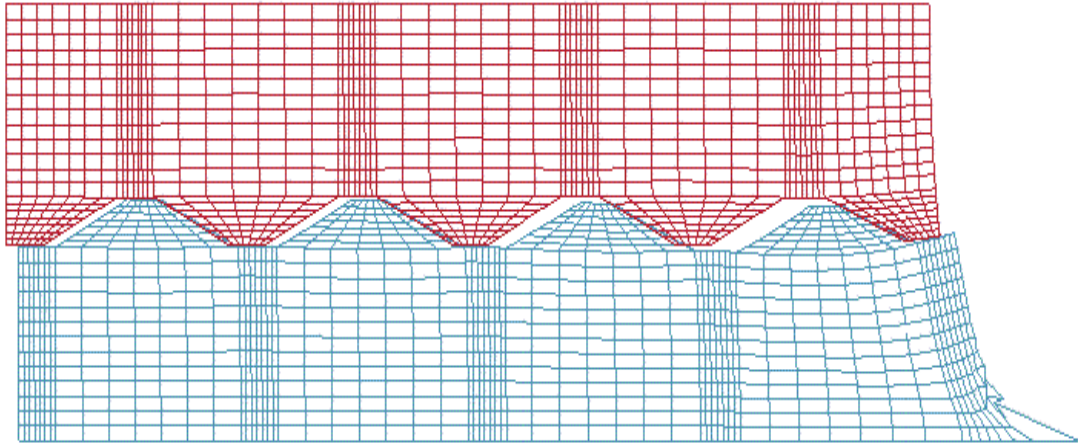


Figure 61.—Deformed shape with body load of $15,000 \text{ in/s}^2$ at end of 3 seconds. Bottom part has degraded material properties ($2 \text{ million lb/in}^2$ modulus). Analysis IV.

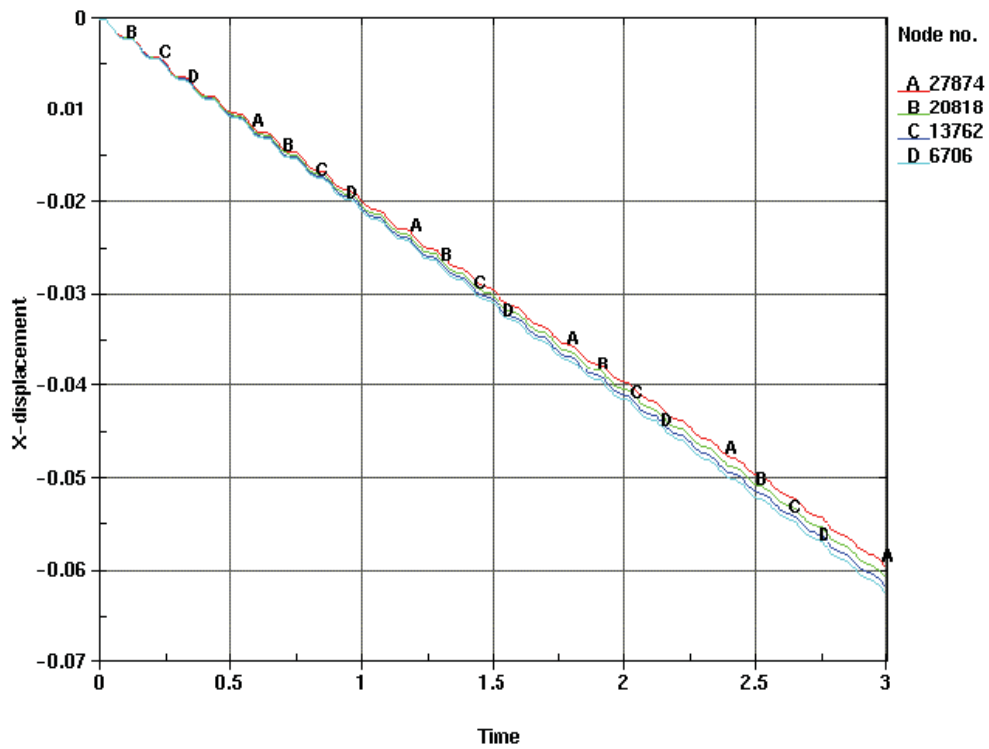


Figure 62.—X-displacements. Analysis IV.

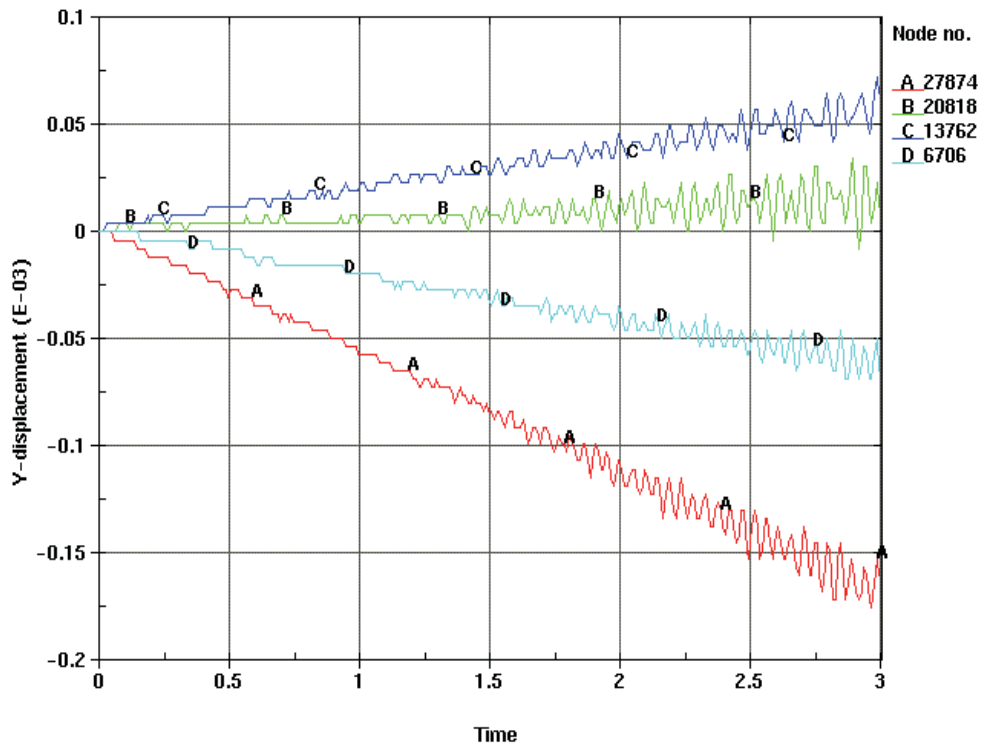


Figure 63.—Y-displacements. Analysis IV.

Time = 3
 Contours of Y-stress
 min=-438.995, at elem# 26082
 max=6324.04, at elem# 24668

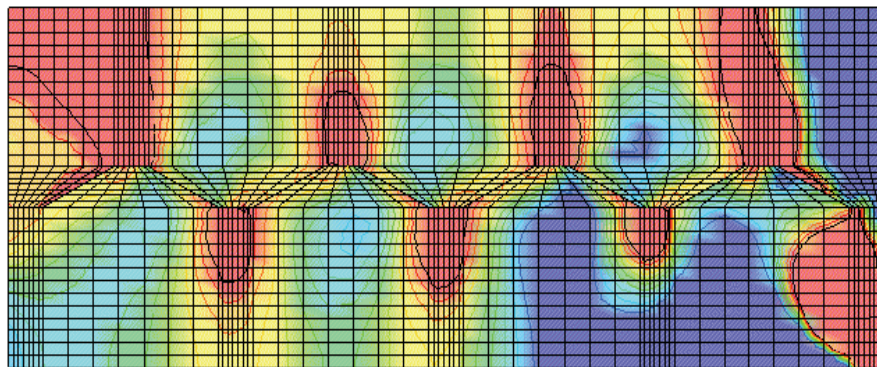


Figure 64.—Y-stress fringe plot. Analysis IV.

Time = 3
Contours of XY-stress
min=-5879.18, at elem# 24213
max=1829.56, at elem# 25039

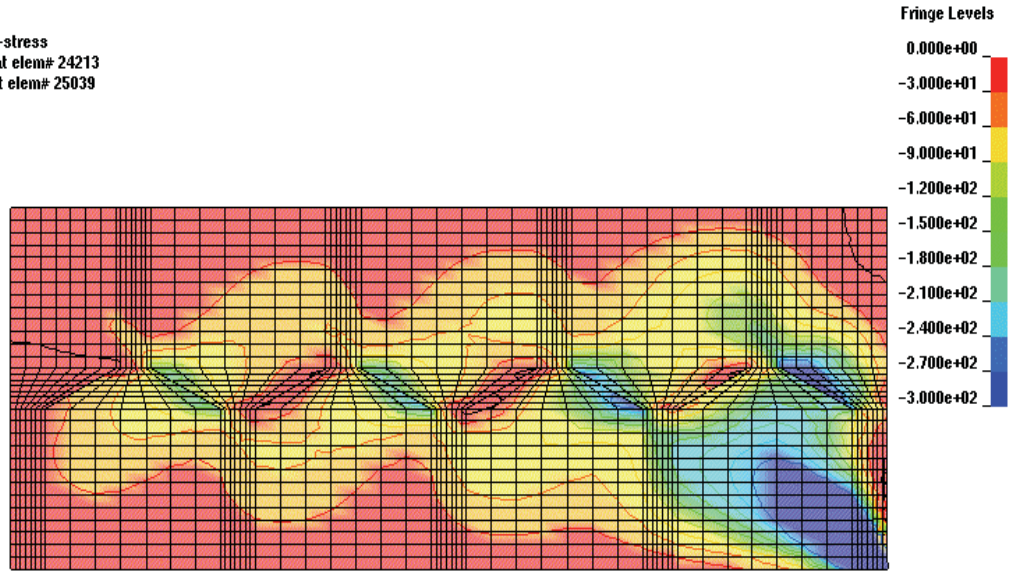


Figure 65.—XY-stress fringe plot. Analysis IV.

Time = 3
Contours of Maximum Principal Stress
min=-53.3765, at elem# 22245
max=14860.1, at elem# 24213

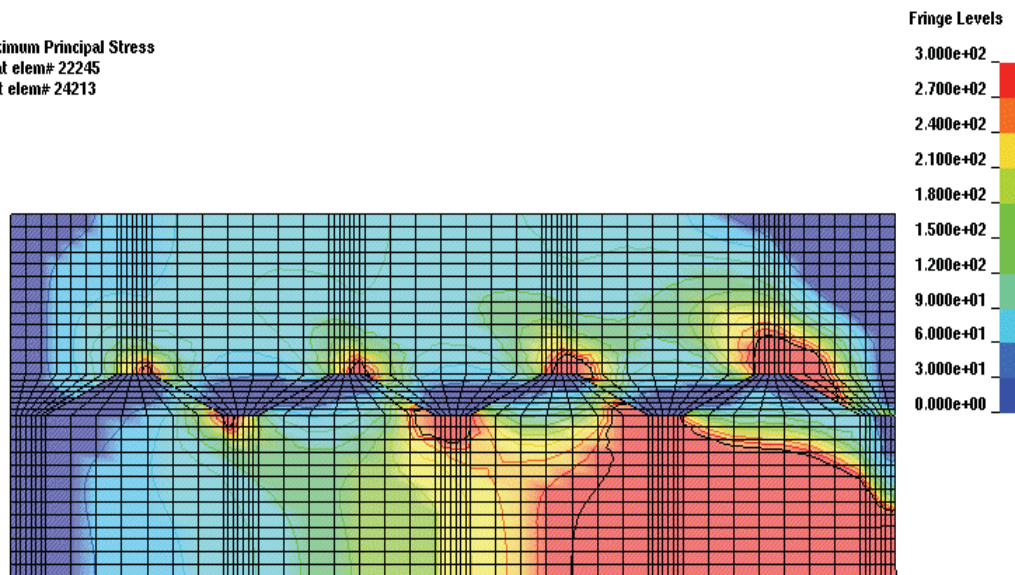


Figure 66.—Maximum principal stress fringe plot. Analysis IV.

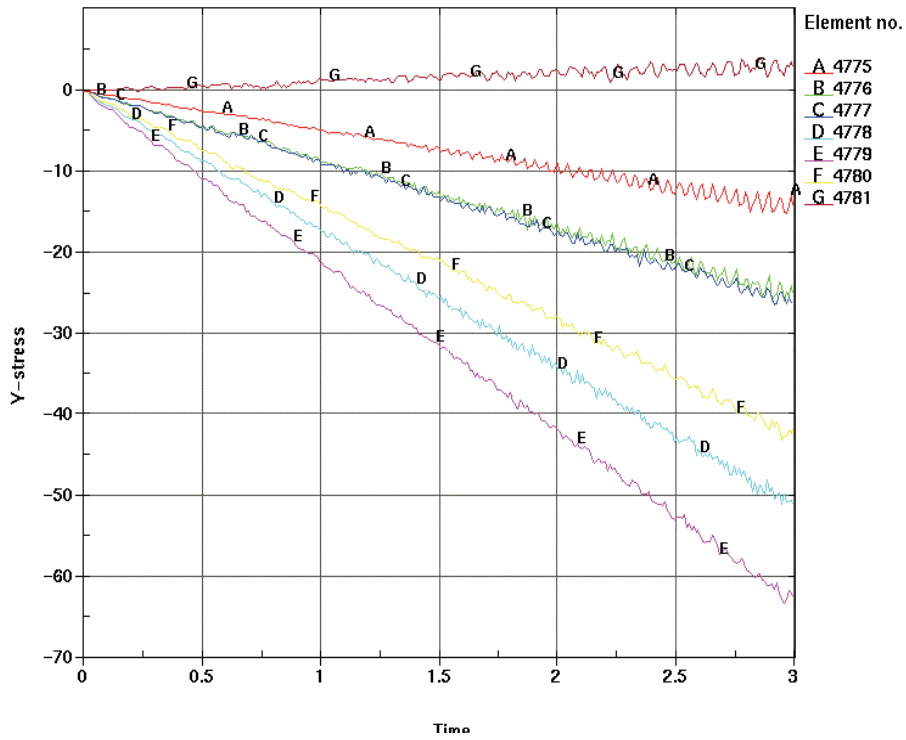


Figure 67.—Y-stress: elements in region I. Analysis IV.

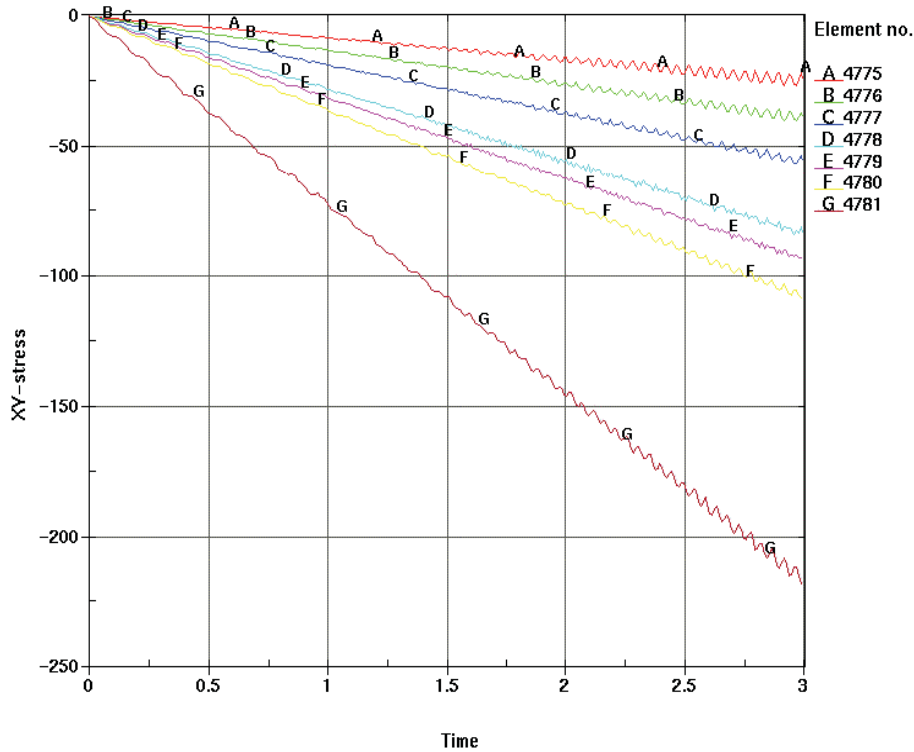


Figure 68.—XY-stress for elements in region I. Analysis IV.

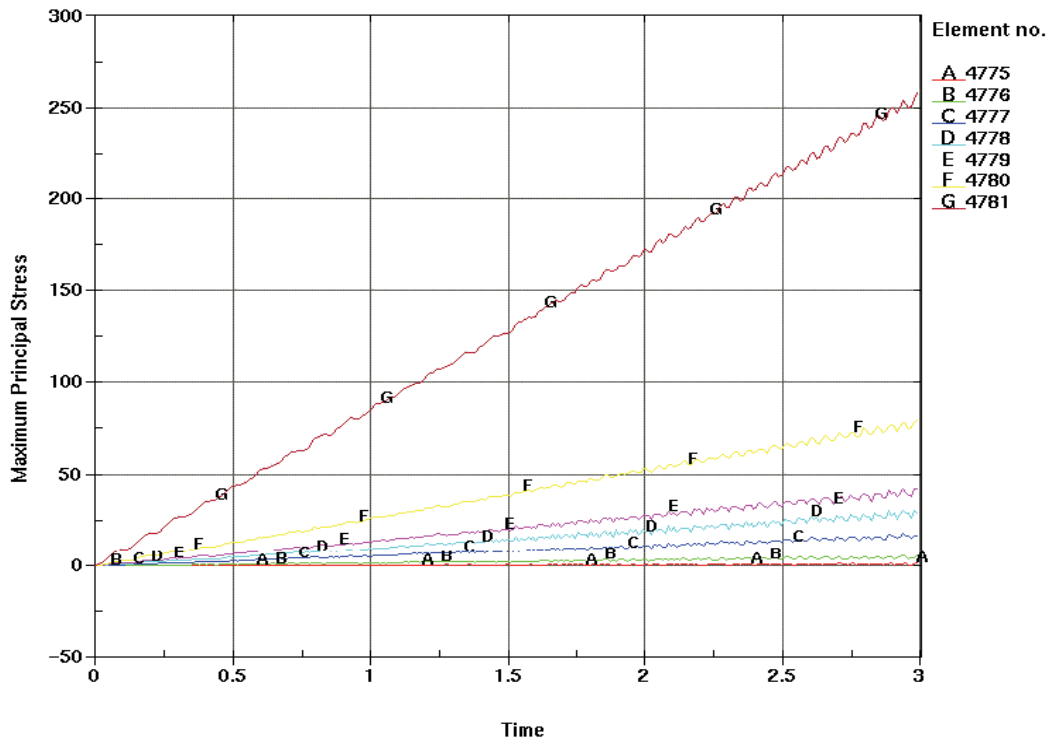


Figure 69.—Maximum principal stress for elements in region I. Analysis IV.

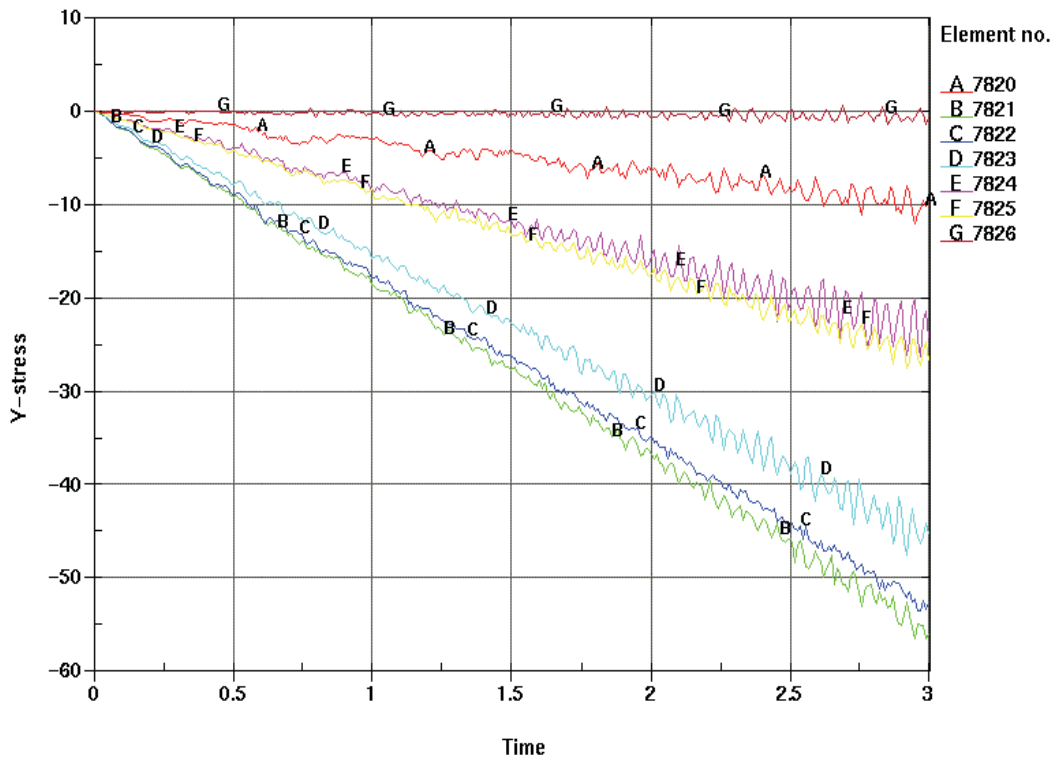


Figure 70.—Y-stress for elements in region II. Analysis IV.

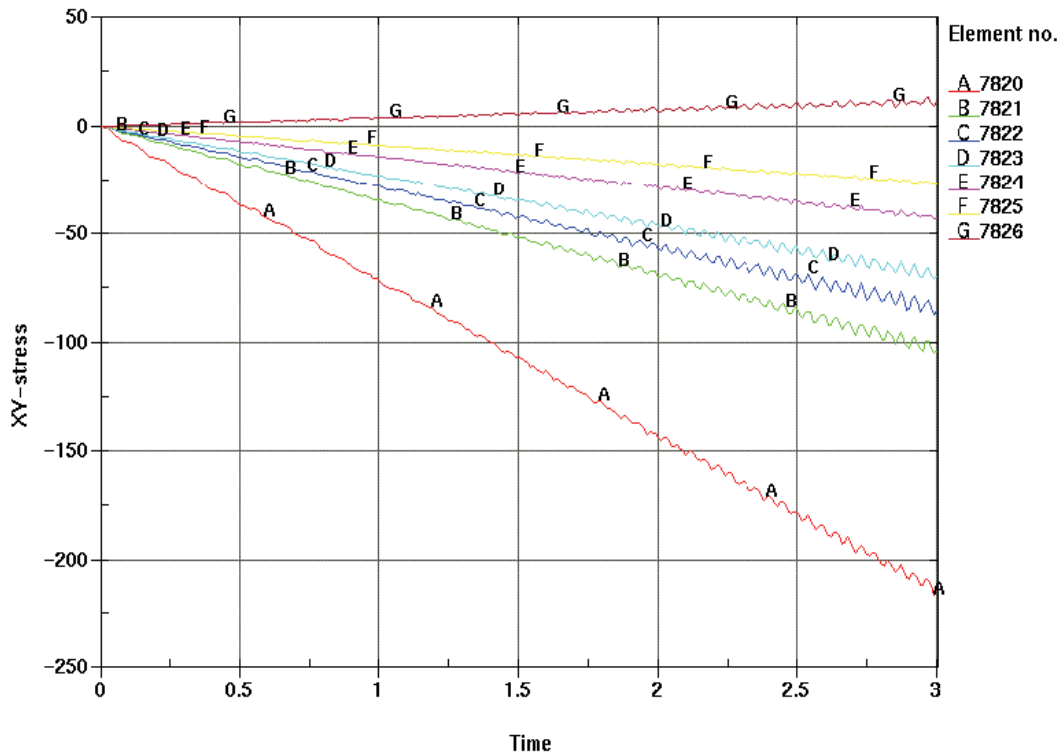


Figure 71.—XY-stress for elements in region II. Analysis IV.

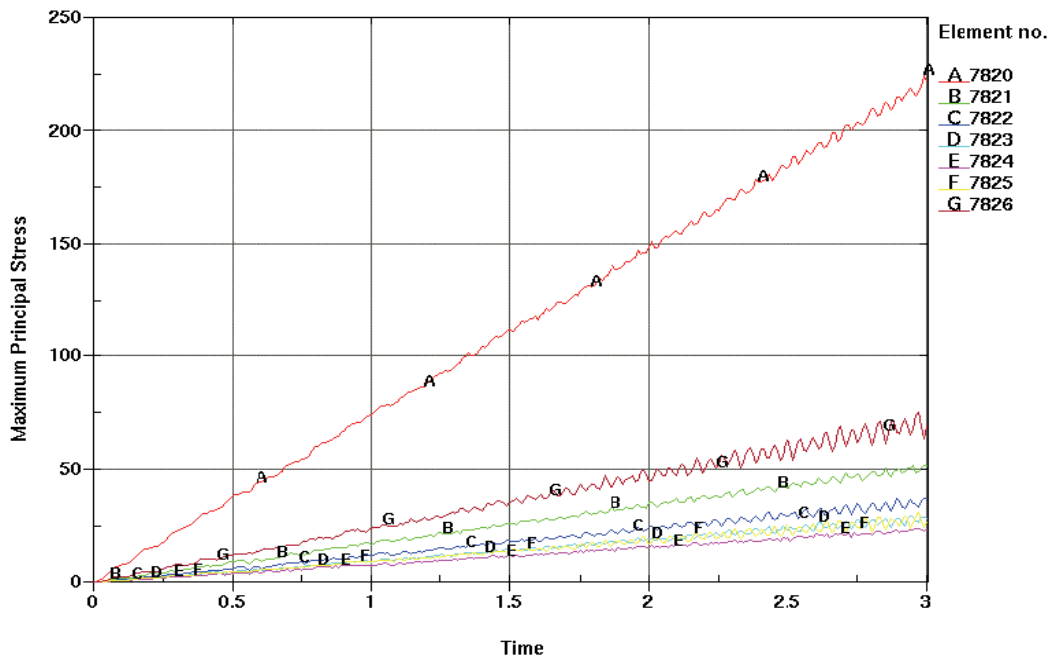
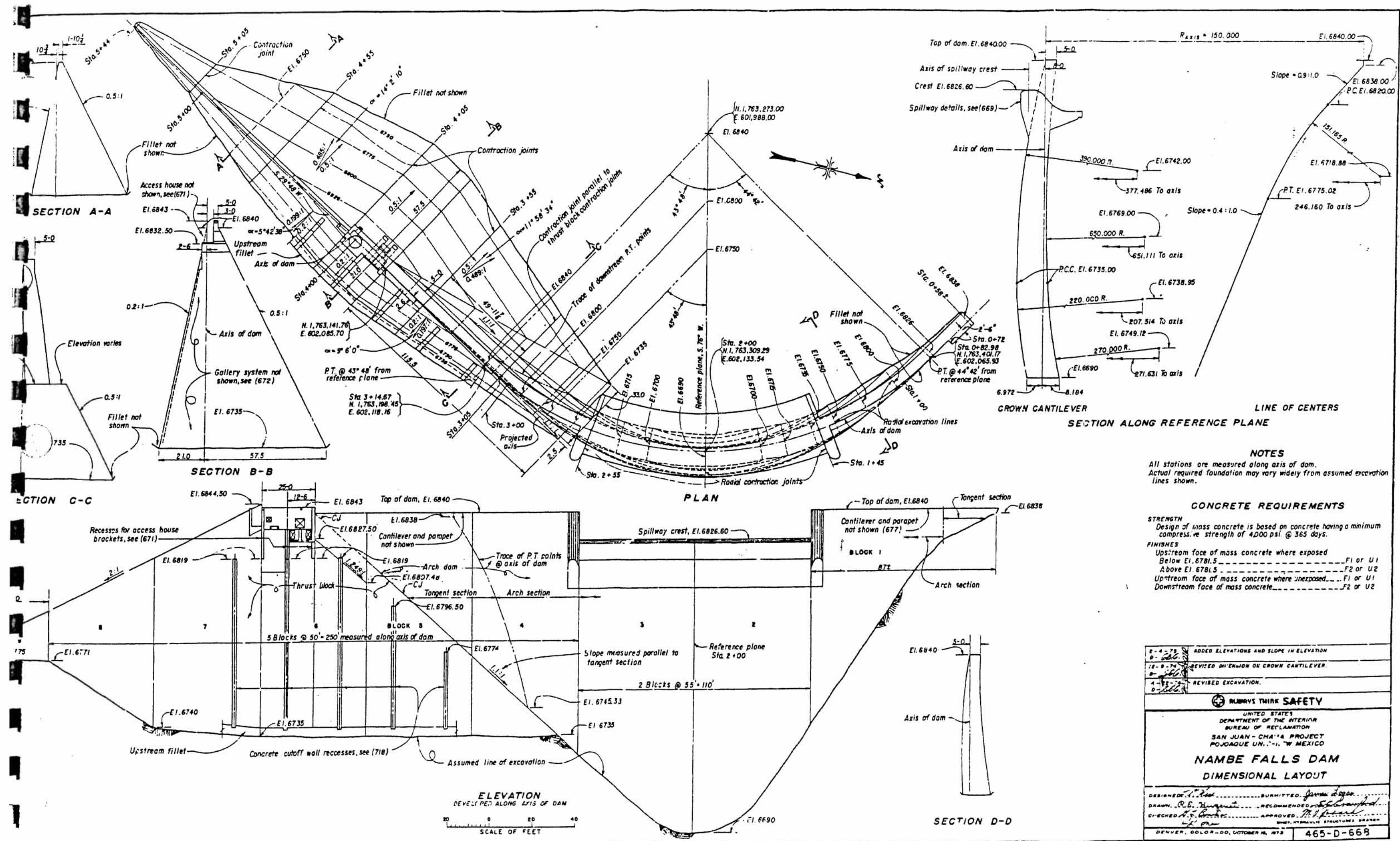


Figure 72.—Maximum principal stress for elements in region II. Analysis IV.



NOTES
 All stations are measured along axis of dam.
 Actual required foundation may vary widely from assumed excavation lines shown.

CONCRETE REQUIREMENTS

STRENGTH
 Design of mass concrete is based on concrete having a minimum compressive strength of 4000 psi @ 365 days.

FINISHES
 Upstream face of mass concrete where exposed F1 or U1
 Below El. 6781.5 F2 or U2
 Above El. 6781.5 F1 or U1
 Upstream face of mass concrete where unexposed F1 or U1
 Downstream face of mass concrete F2 or U2

2-4-78	ADDED ELEVATIONS AND SLOPE IN ELEVATION
9-1-78	REVISED DIMENSION ON CROWN CANTILEVER.
4-12-78	REVISED EXCAVATION.
ALWAYS THINK SAFETY	
UNITED STATES DEPARTMENT OF THE INTERIOR BUREAU OF RECLAMATION SAN JUAN - CHA'AA PROJECT POJOAQUE UNIT - N. MEXICO	
NAMBE FALLS DAM DIMENSIONAL LAYOUT	
DESIGNED: J. L. ...	SUBMITTED: James Logan
DRAWN: R. C. ...	RECOMMENDED: ...
CHECKED: A. S. ...	APPROVED: M. J. ...
DENVER, COLORADO, OCTOBER 14, 1978	
465-D-668	

Figure 73.—Nambe Falls Dam dimensional layout

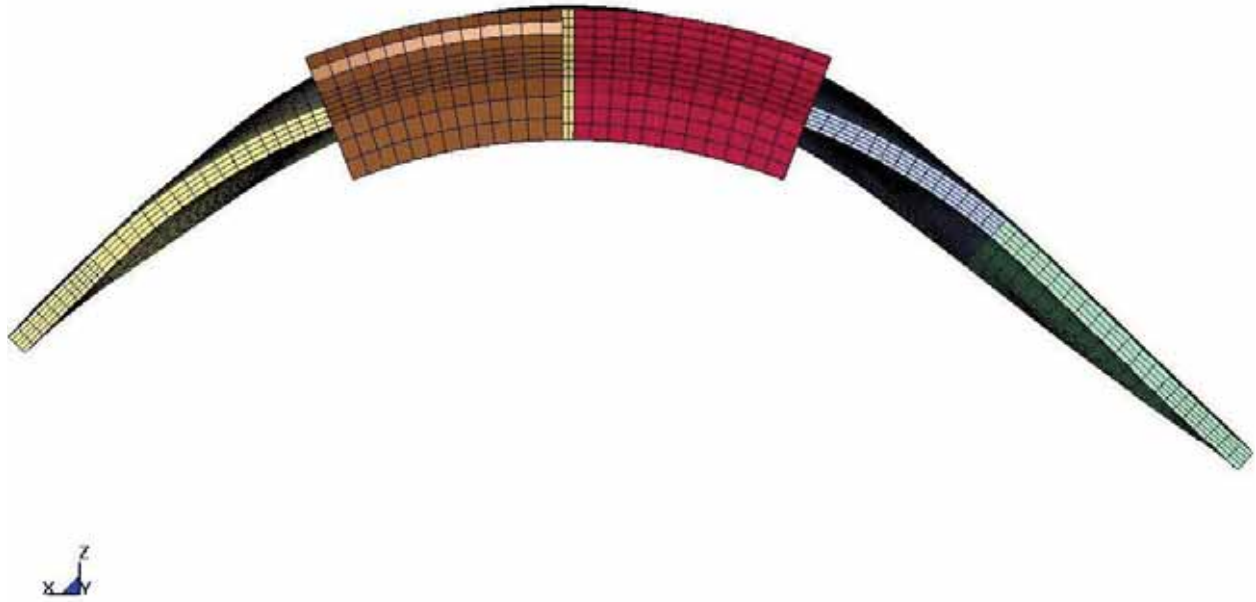


Figure 74.—Plan view, Nambe Falls Dam 3-dimensional finite element model.

Nambe Falls Dam
NF_MEAN_50 Records

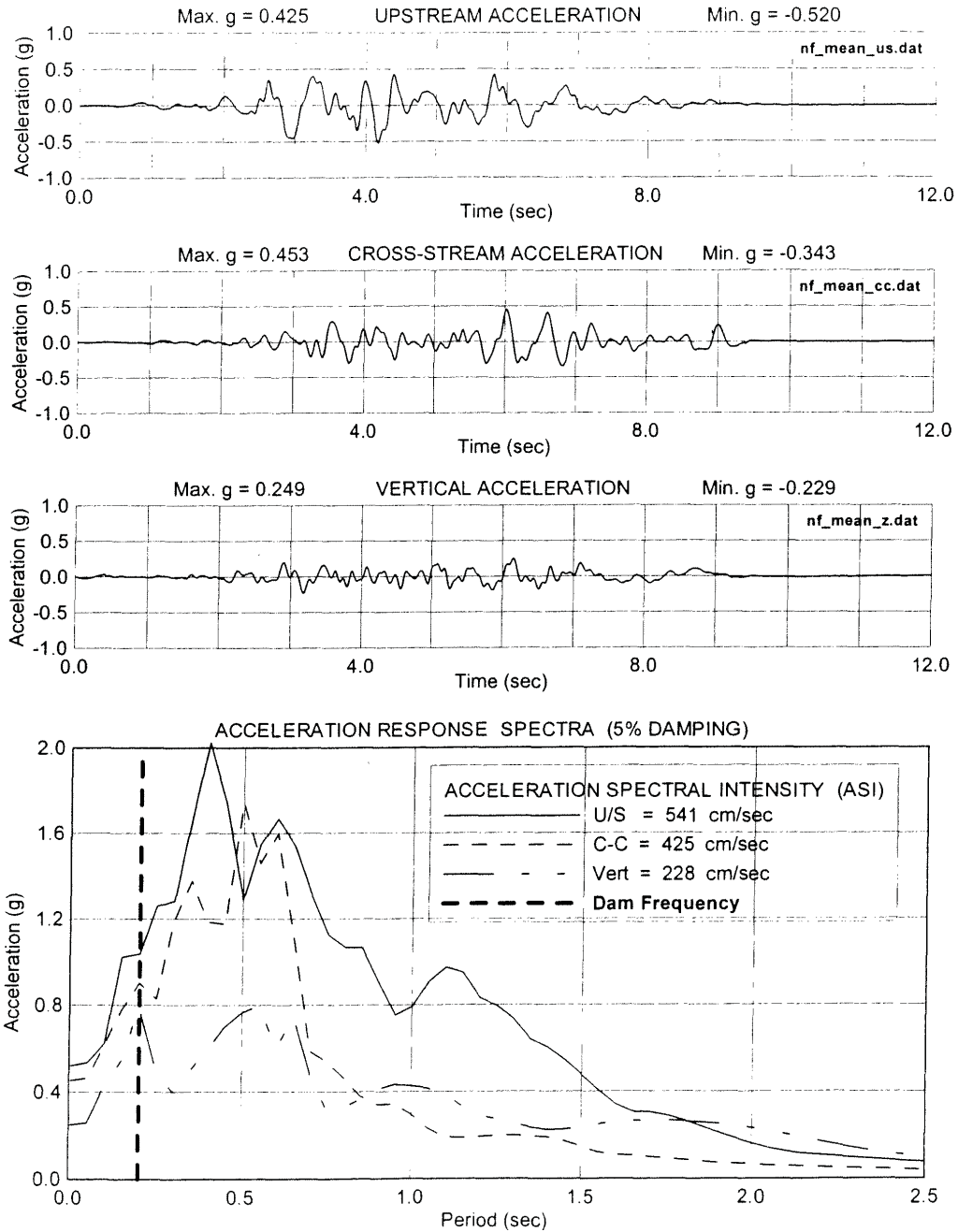


Figure 75a.—Nambe Falls Dam $1/50,000$ AEP earthquake acceleration time histories and acceleration response spectra.

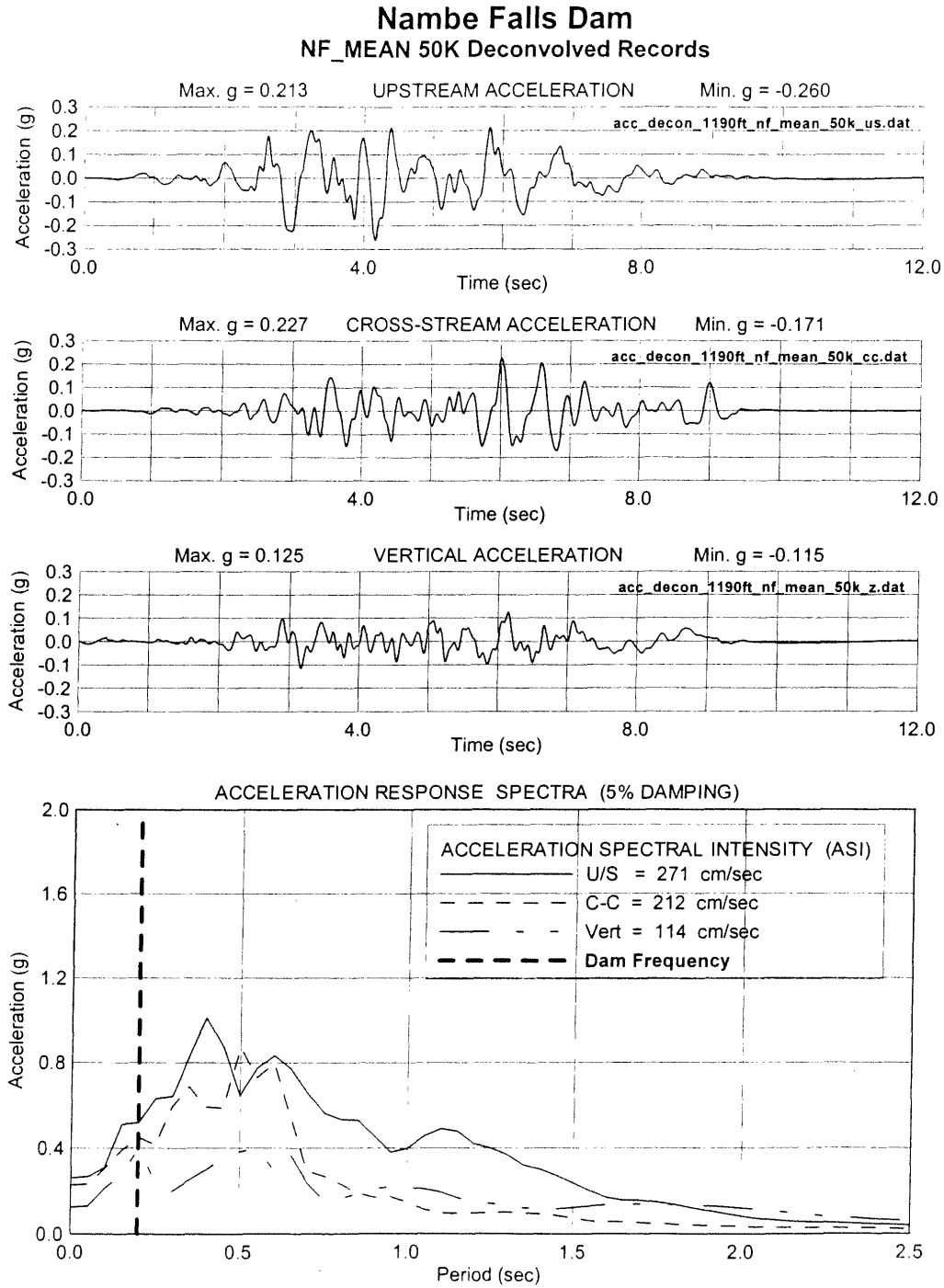


Figure 75b.—Deconvolved Nambe Falls Dam $1/50,000$ AEP earthquake acceleration time histories and acceleration response spectra.

Time = 7.44
max displacement factor=100

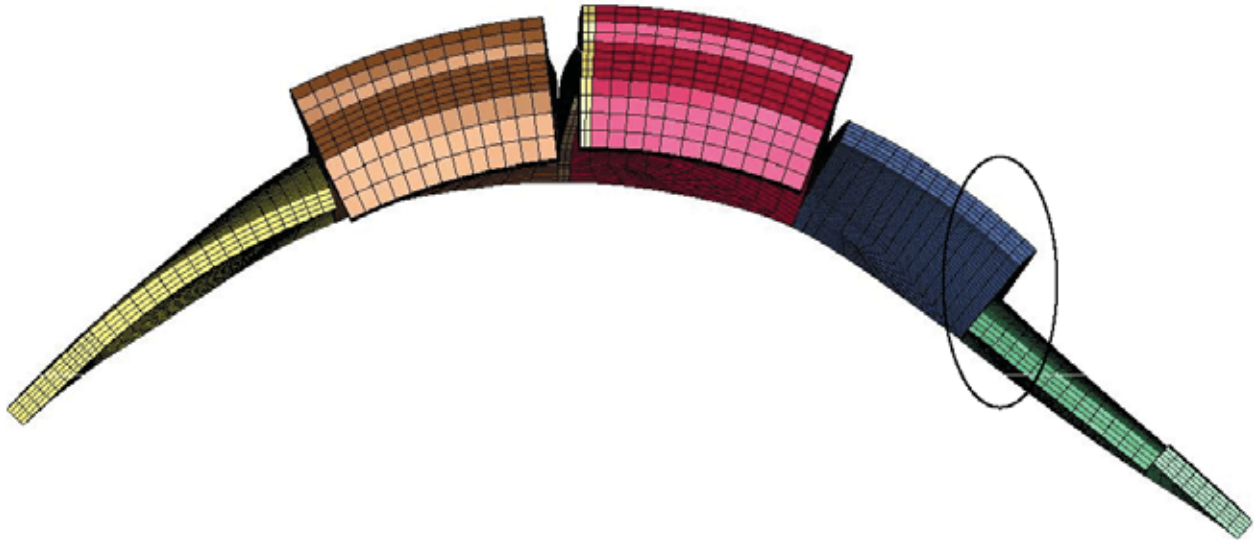


Figure 76.—Plan view at time of large openings in the contraction joints (displacement magnification factor of 100).

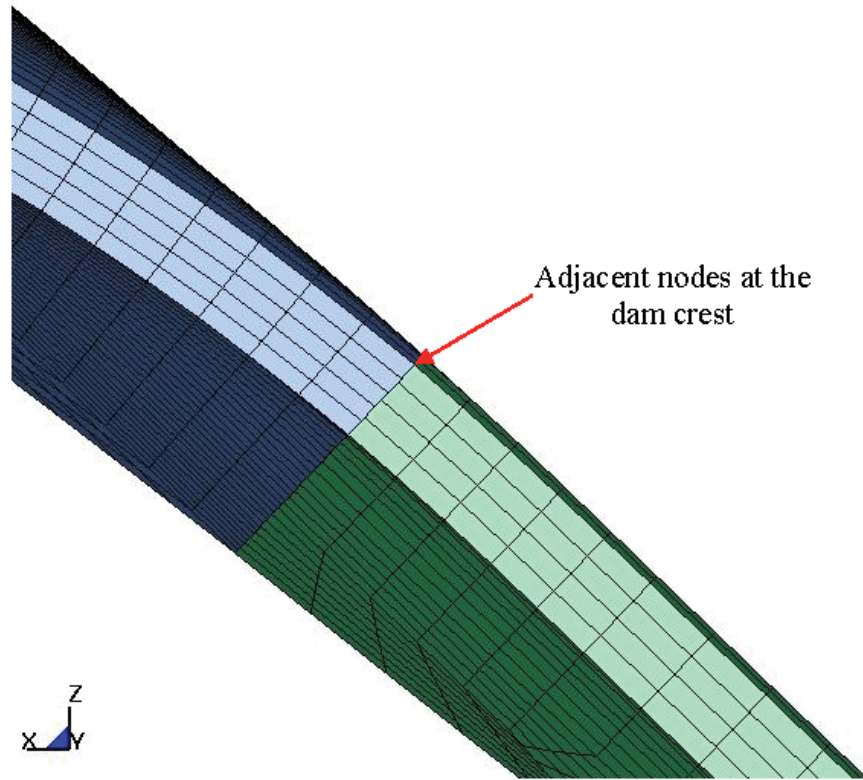


Figure 77.—Plan view of contraction joint circled in figure 76 at time = 0 seconds.

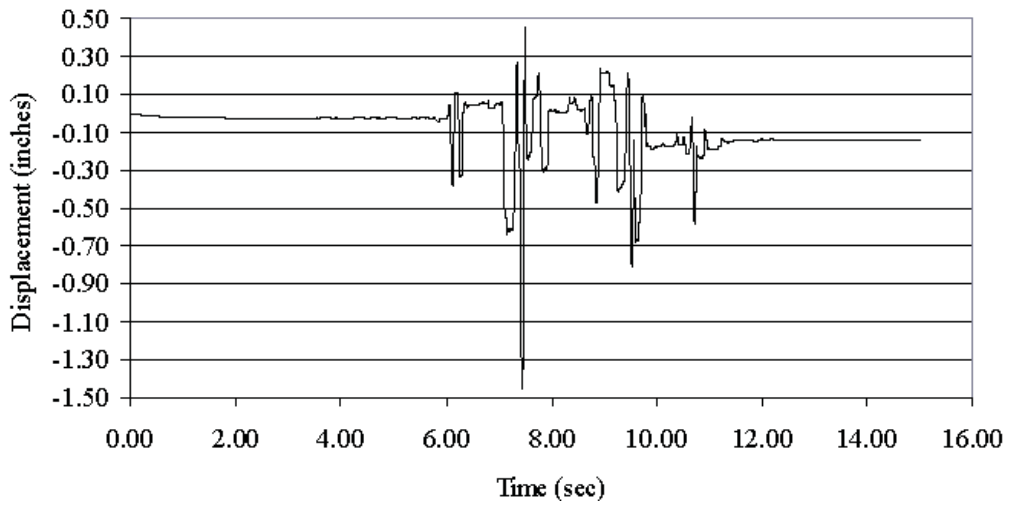


Figure 78.—Relative x-displacement between adjacent nodes.

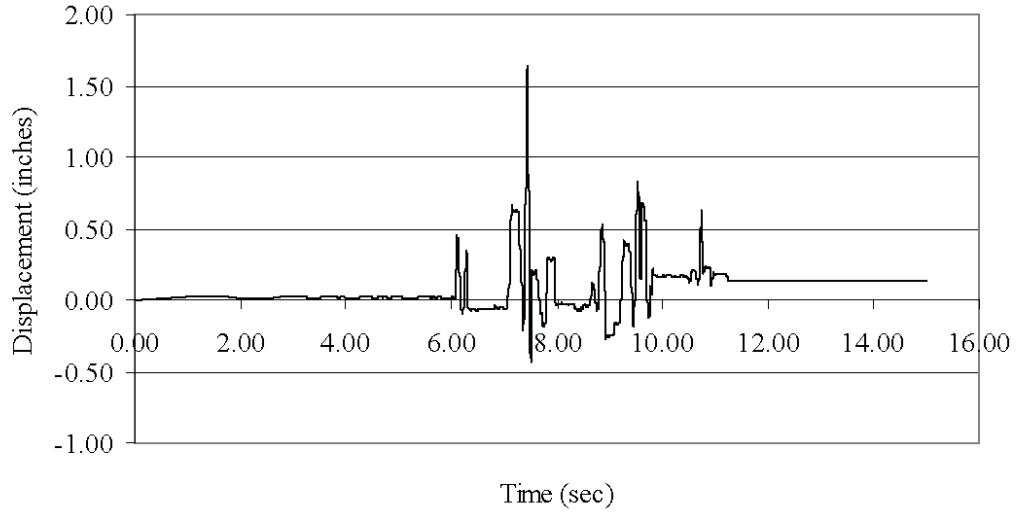


Figure 79.—Relative z-displacement between adjacent nodes.

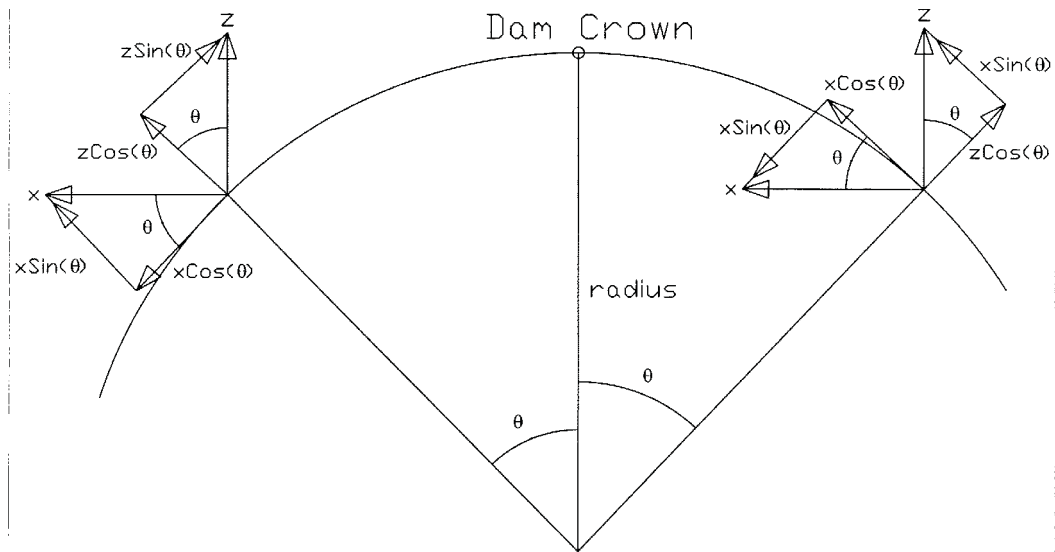


Figure 80.—Illustration of radial and tangential components to the left and right of crown of dam.

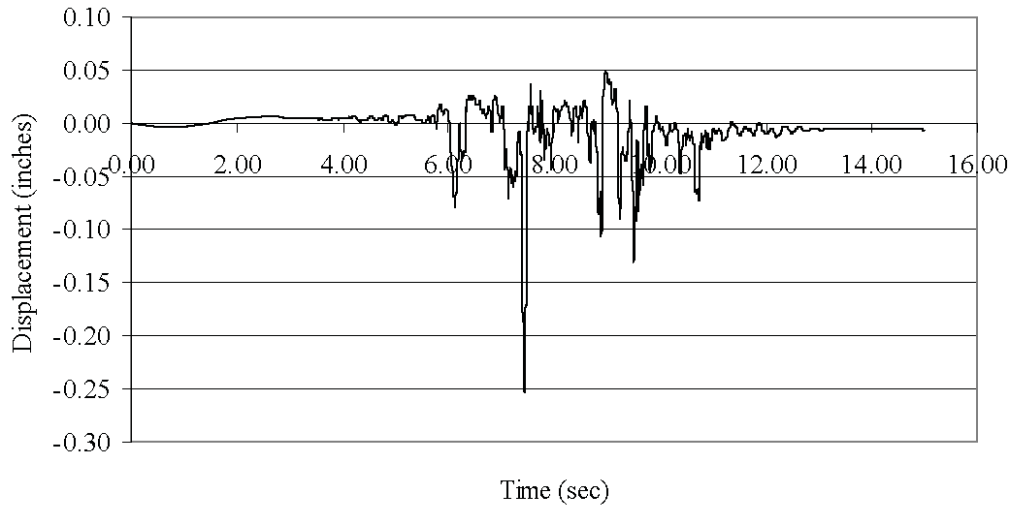


Figure 81.—Relative radial displacements between adjacent nodes.

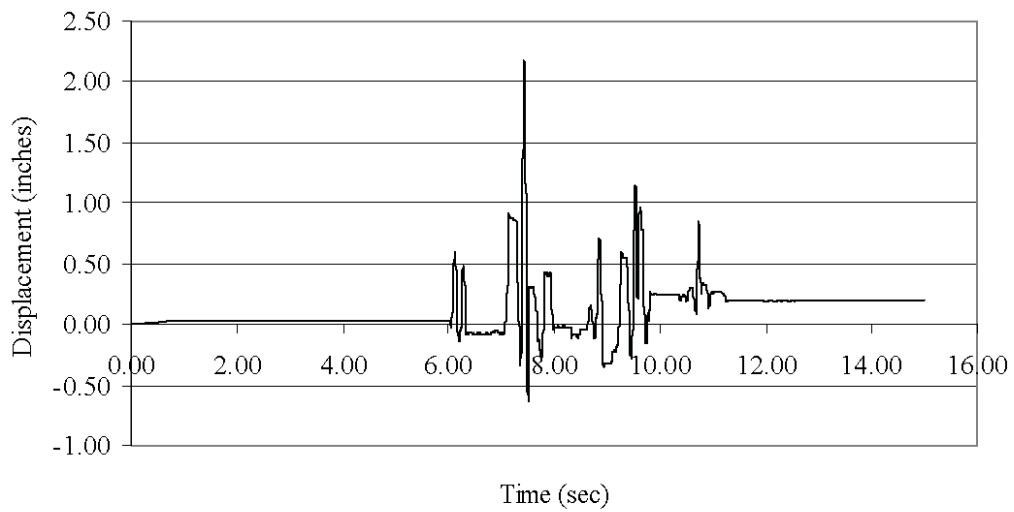


Figure 82.—Relative tangential displacement between adjacent nodes.

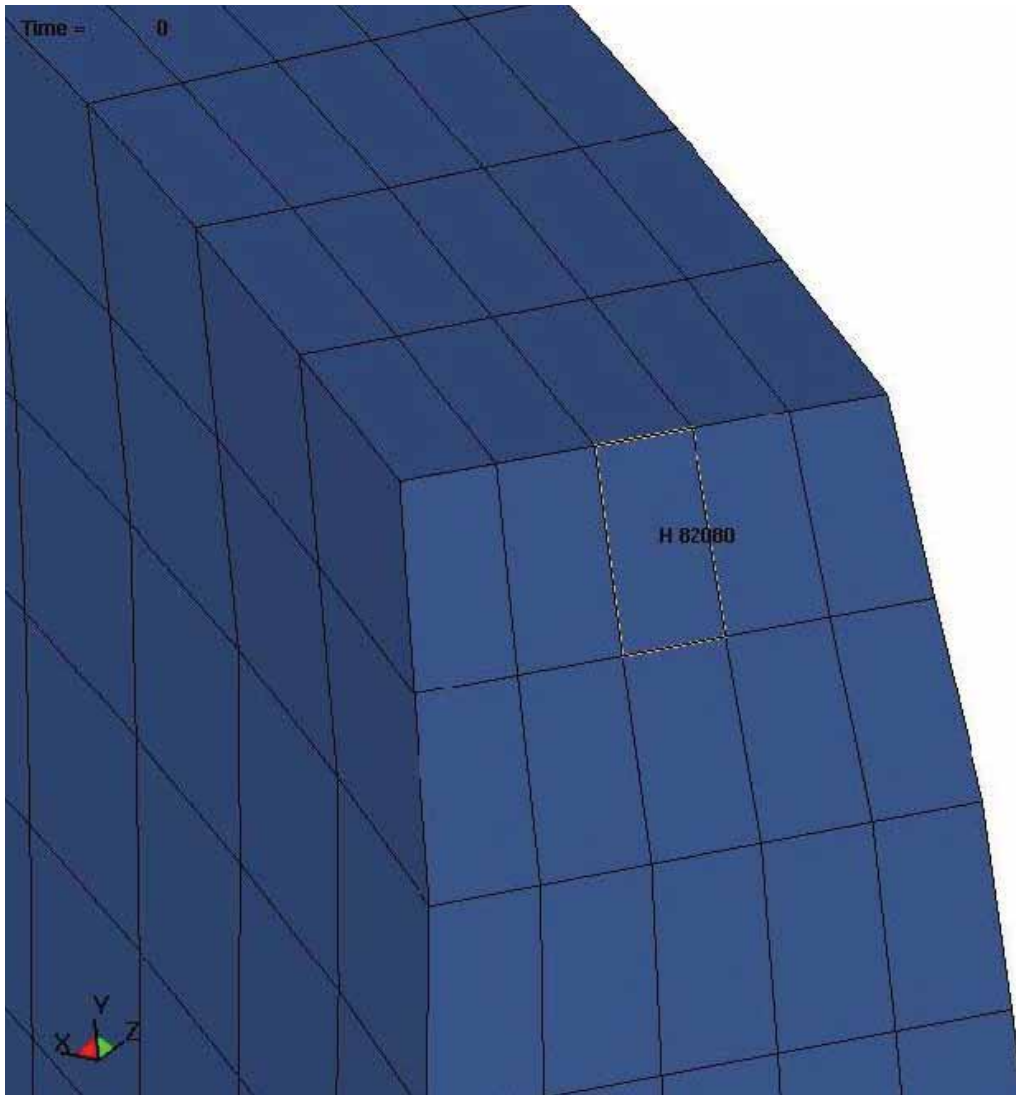


Figure 83.—Illustration of element 82080 used for stress time history data.

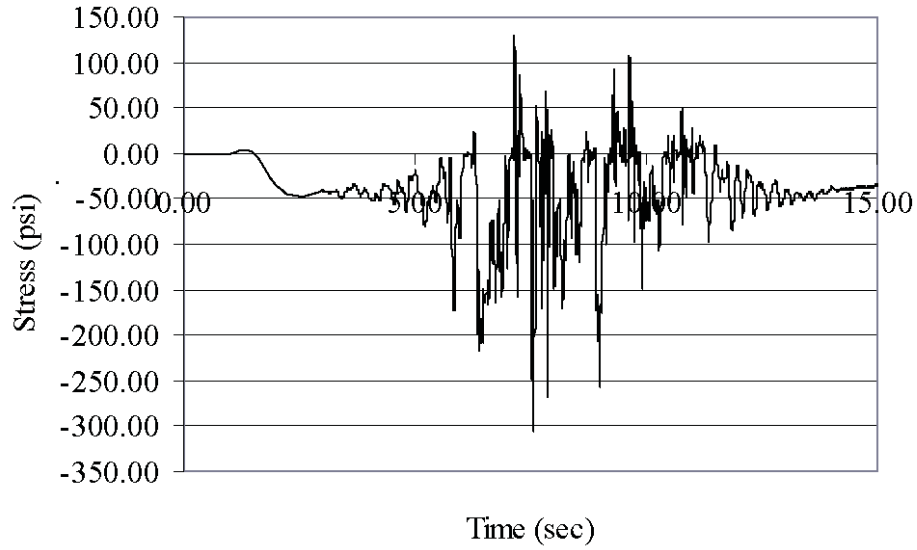


Figure 84.—X-stress in the joint at element 82080.

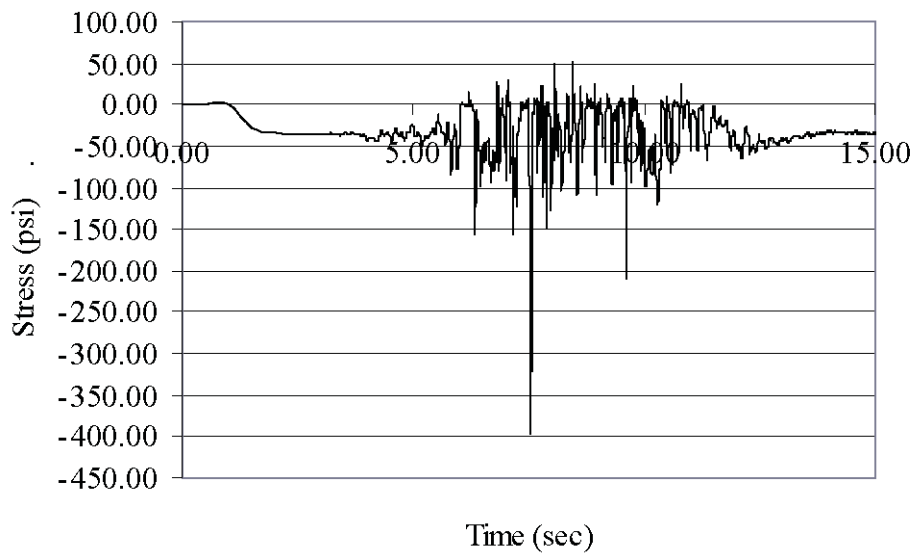


Figure 85.—Z-stress in the joint at element 82080.

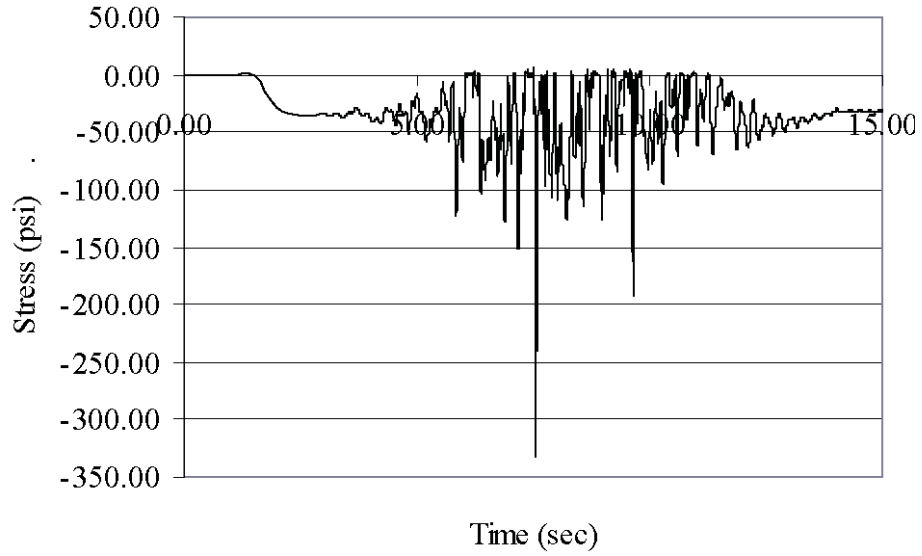


Figure 86.—ZX-stress in the joint at element 82080.

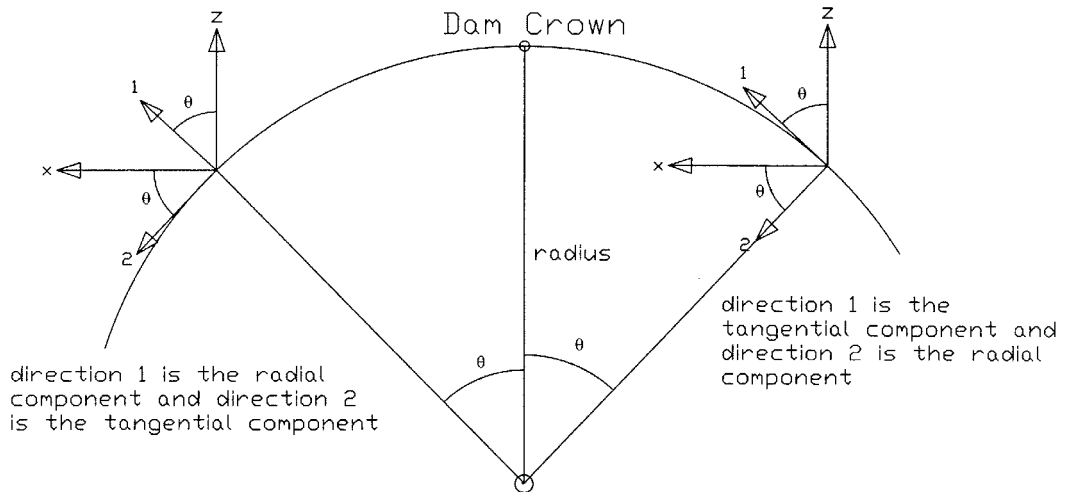


Figure 87.—Illustration of positive rotation from x-z axes to 1-2 axes.

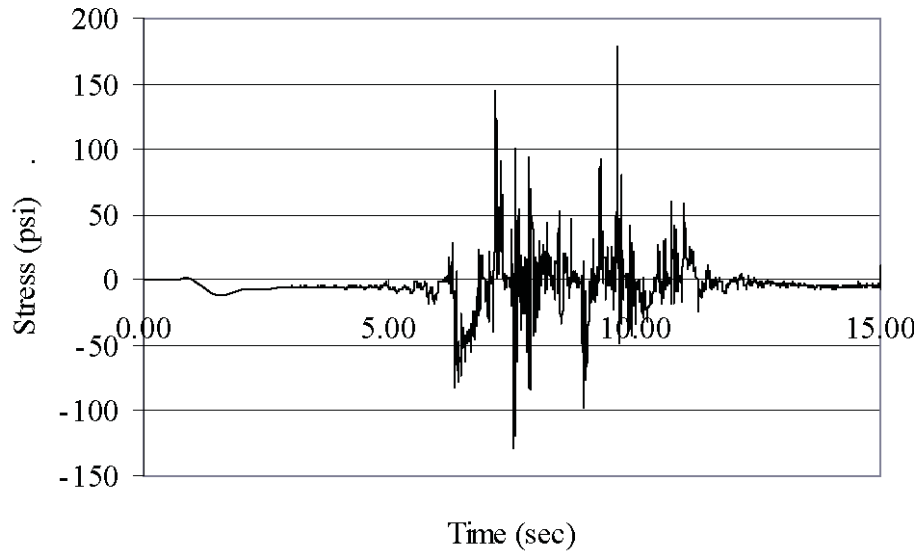


Figure 88.—Radial stress in the joint at element 82080.

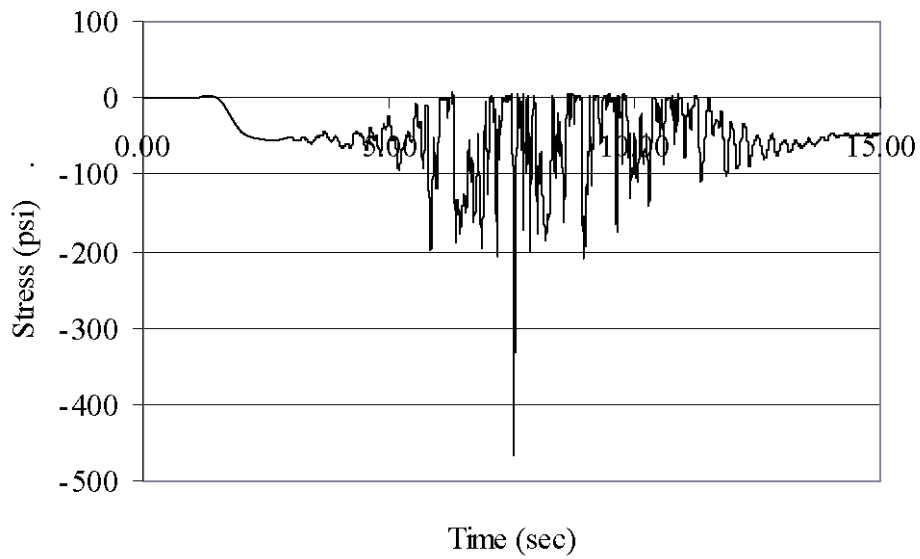


Figure 89.—Tangential stress in the joint at element 82080.

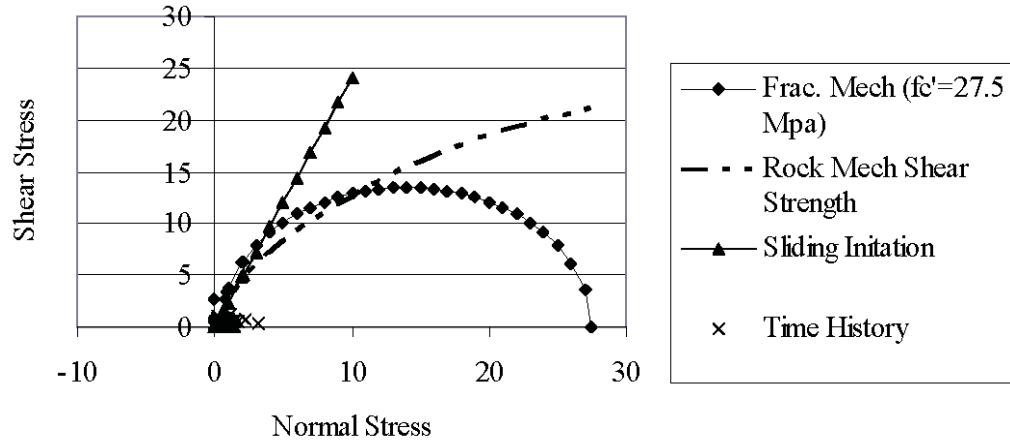


Figure 90.—Shear key interaction diagram with time history shear and normal stress pairs.

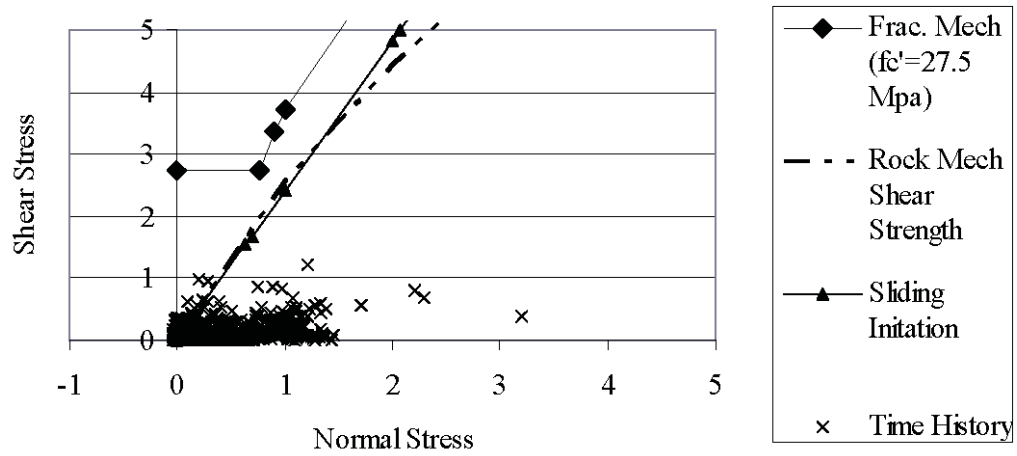


Figure 91.—Close up of shear key interaction diagram with time history shear and normal stress pairs.